INVESTIGATION OF NON-TRADITIONAL ROLES OF THE NEURAL GUT-BRAIN AXIS

BY

ELIZABETH A. DAVIS

DISSERTATION

Submitted in partial fulfillment of the requirements
for the degree of Doctor of Philosophy in Neuroscience
in the Graduate College of the
University of Illinois at Urbana-Champaign, 2018

Urbana, Illinois

Doctoral Committee:

Assistant Professor Megan J. Dailey, Chair
Associate Professor Lori T. Raetzman
Associate Professor Daniel A. Llano
Assistant Professor Catherine A. Christian

ABSTRACT

The neural gut-brain axis is an important bidirectional pathway through which the gastrointestinal (GI) tract communicates with the central nervous system (CNS). This axis includes sensory nerves that send information from the GI tract to the brain and motor nerves that transmit descending information from the brain to the GI tract. Traditional research has focused on nutrient-induced changes in sensory neural signaling and the subsequent motor response altering muscular and secretory functions. These nerves, though, may also play novel, non-traditional roles in the function of the gut-brain axis. Just as nutrients have been shown to induce neuroplasticity of CNS neurons, long-term alterations in nutrition may do more than just change signaling, and ultimately lead to modifications in fiber density, branching, and terminal morphology. These neuroplastic changes may underlie aberrant signaling and could be associated with GI diseases, as has been found with CNS-associated neuroplasticity and disease. The GI tract also has to perform many functions beyond muscular contraction/relaxation and secretion. One essential function in maintaining GI homeostasis is the constant renewal of the cells lost due to normal apoptosis, a process whereby entire GI tissues can be replaced every few days. Because loss of the motor nerves of the gut-brain axis results in changes in the rate of tissue renewal and the location of the nerves are in close contact with the GI stem cells responsible for cell renewal, these motor nerves may play a direct role in inducing proliferation and differentiation of the GI tissue. I hypothesized that there are indeed new, non-traditional roles of the sensory and motor nerves of the gut-brain axis in neuroplasticity and tissue regeneration and tested the mechanisms underlying these processes. Specifically, I used rodents and swine mammalian models to develop new methods by which to investigate multiple hypotheses about nutrient-induced vagal sensory neuroplasticity and found a direct mechanism by which the autonomic motor nerves induce changes in intestinal epithelial renewal. The results of the experiments included in this dissertation establish roles for the neural gut-brain axis that are outside those that are traditionally studied, which can expand the available methods to manipulate gut-brain system for therapeutic purposes.

In loving memory of my indescribable mother.

TABLE OF CONTENTS

CHAPTER 1: LITERATURE REVIEW

1.1 The gut-brain axis

The neural gut-brain axis allows for bidirectional communication between the gastrointestinal (GI) tract and the brain (Fig. 1). Sensory information from the gastrointestinal tract to the brain is communicated through afferent fibers. These afferent fibers travel in two distinct pathways: the vagal afferent pathway (with fibers in the vagus nerve, or cranial nerve X), and the spinal afferent pathway (with fibers in spinal afferent nerves). These sensory pathways allow the central nervous system (CNS) to monitor GI function and integrate GI sensory information with the sensory information from other peripheral organs. In turn, motor signals are sent from the brain to the GI tract via efferent nerves that are sympathetic (SNS) and parasympathetic (PNS) fibers of the autonomic nervous system (ANS). The SNS fibers travel in thoracolumbar nerve tracts, while PNS fibers travel in craniosacral nerve tracts. Together, these SNS and PNS efferent fibers are responsible for effecting changes in GI function. Overall, the gut-brain axis provides a critical link for information to be exchanged between the CNS and the GI tract.

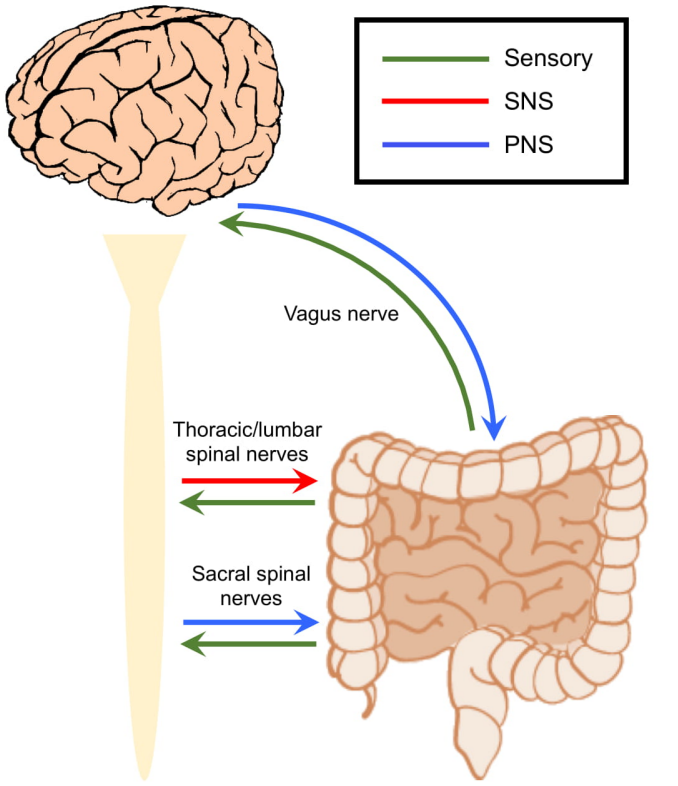

Figure 1. **Sensory and motor pathways of the neural gut-brain axis.**

1.2 The small intestine

Among the GI organs that receive gut-brain neural innervation is the small intestine. The sensory and motor nerves of the gut-brain axis facilitate the main functions of the small intestine, including

digestion, propulsion, and absorption of all macronutrients. These nerves innervate the three distinct segments (i.e., duodenum, jejunum, and the ileum) and all but the outer serosal layer of the small intestine (i.e., mucosa, submucosa, muscularis externa; Brookes *et al.*, 2013). The anatomy and traditional functional roles of the these sensory and motor nerves have largely been identified and found to coordinate the actions of the small intestine along its axis and between other physiological systems of the body (i.e., cardiovascular, respiratory).

1.3 Vagal afferent innervation of the small intestine

Vagal afferent terminals sense stimuli in the small intestine and transmit this sensory information to the CNS (Fig. 2). Nerve fibers travel in the vagus nerve (cranial nerve X), and neuronal cell bodies of these vagal afferent fibers are located in the nodose ganglia at the level of the superior cervical spinal cord. From the nodose ganglia, vagal afferent fibers project centrally toward the caudal brainstem, where they make synaptic connections with neurons in the nucleus of the solitary tract (NTS). The NTS is a major sensory integration center, receiving neural signals from many peripheral organs and bloodborne information. The NTS makes synaptic projections with a variety of other central nuclei (e.g., the dorsal motor nucleus of the vagus, the rostroventrolateral medulla, and the paraventricular nucleus of the hypothalamus). It is through this pathway that intestinal stimuli is able to be transmitted to the brain and integrated with other visceral/peripheral sensory information and forebrain circuits (Berthoud & Neuhuber, 2000).

The vagal afferent pathway transmits diverse sensory information. This vagal multimodality is achieved through the expression of several different types of receptors on vagal afferent terminals. In the small intestine, these receptors include two specialized types of mechanoreceptors, intraganglionic laminar endings (IGLEs) and intramuscular arrays (IMAs). In addition, a set of vagal afferent terminals within the mucosal layer of the intestine, termed mucosal afferents, sense chemosensory and possibly mechanosensory information within the intestinal mucosa.

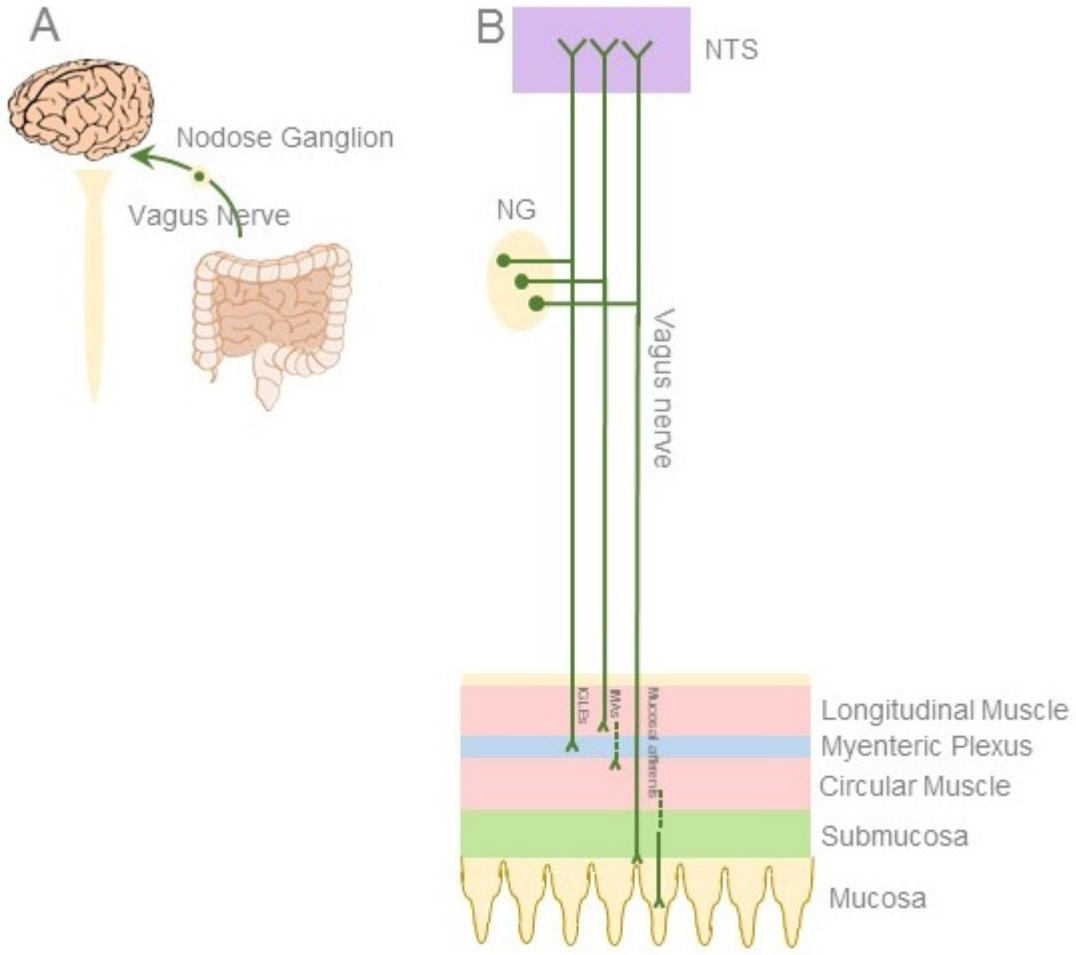

Figure 2. **Vagal afferent innervation of the small intestine. A.** Representation of vagal afferent fibers from the intestinal tract to the brain, with the cell bodies of these nerves located in the nodose ganglia (NG) at the level of the superior cervical spinal cord (only one of the bilateral ganglia is depicted). **B.** Depiction of the three types of vagal afferent terminals and their location of innervation within specific layers of the small intestine. Intraganglionic laminar endings (IGLEs) innervate the myenteric plexus (MP), located between the longitudinal muscle and circular muscle layers of the muscularis externa. Intramuscular arrays (IMAs) innervate muscle fibers of the longitudinal and circular muscle layers. Mucosal afferents innervate intestinal epithelial crypts and villi in the mucosa. The nerve fibers of all terminal types collectively travel in the vagus nerve. The nodose ganglion houses the vagal afferent neuron cell bodies. Vagal afferent fibers synapse within the nucleus of the solitary tract (NTS) in the caudal brainstem.

Intraganglionic laminar endings (IGLEs), are mechanosensitive vagal afferent terminals found throughout the small intestine (Berthoud *et al.*, 1997; Fox *et al.*, 2000; Phillips & Powley, 2000; Wang & Powley, 2000). These mechanoreceptors are located in between the two smooth muscle layers of the muscularis externa, which includes the circular and the longitudinal muscle layers. IGLEs make contact with the myenteric plexus of the enteric nervous system, which is the intrinsic neural network of the GI tract. Functionally, IGLEs have been hypothesized to monitor mechanical movement involved in the contraction of the smooth muscle layers of the small intestine (Powley & Phillips, 2002). Although this

has not been definitively proven in the small intestine, IGLEs have been shown to be electrophysiologically responsive to distension in the stomach (Zagorodnyuk *et al.*, 2001), which supports the hypothesis that they are involved in sensing mechanical movement.

Intramuscular arrays (IMAs) are a type of mechanosensitive vagal afferent mechanoreceptors that directly innervate the circular and longitudinal muscle layers of the small intestine. (Fox *et al.*, 2000; Phillips & Powley, 2000; Powley & Phillips, 2002). IMA arborizations produce the elongated, narrow array of nerve terminals that run parallel to and eventually make contact with smooth muscle fibers (Fox *et al.*, 2000; Wang & Powley, 2000). IMAs are distributed sparsely throughout most of the small intestine, but are found in very high densities in sphincter regions including the pyloric sphincter (located between the stomach and small intestine) and the ileocecal valve (located between the ileum and the cecum; the Fox *et al.*, 2000; Wang & Powley, 2000). Sphincter IMAs are hypothesized to sense stretch based on their dense localization in areas of the stomach that stretch to accommodate meals, but functional studies investigating this have not been performed (Powley & Phillips, 2002; Powley *et al.*, 2011; Powley *et al.*, 2014). In the small intestine, putative stretch signals from IMAs may participate in coordinating sphincter function, allowing food to enter into the next segment of the GI tract and subsequently preventing reflux back into the previous segment (Powley & Phillips, 2002).

Mucosal afferent terminals are free nerve endings that innervate the mucosa (Berthoud *et al.*, 1995; Powley *et al.*, 2011). Throughout the small intestine, mucosal afferent terminals come into close contact with the basal side of intestinal epithelial cells of both the villi and crypts (Powley *et al.*, 2011). The populations of villus and crypt afferents are morphologically distinct, with separate nerves innervating each of these regions. It is important to note that these mucosal afferents do not make direct contact with the lumen of the small intestine (Powley *et al.*, 2011). Functionally, mucosal afferents have been determined to be chemosensitive and mechanosensitive (Powley *et al.*, 2011). Both direct and indirect mechanisms occur for vagal afferents to sense nutrients and send this information to the brain. Direct sensing of absorbed nutrients by vagal afferents has been recently established, specifically

regarding fatty acids (de Lartigue & Diepenbroek, 2016). Vagal afferent neurons express fatty acid receptors, including fatty acid receptor G-protein coupled receptor 40 (Darling *et al.*, 2014) and peroxisome proliferator-activated receptor γ (Liu *et al.*, 2014a). Fatty acids can act directly on vagal afferent neurons *in vitro*, as demonstrated by changes in cytosolic calcium concentrations (Darling *et al*., 2014). This functional evidence and the position of these nerves in close contact with the nutrients absorbed from the intestine makes it likely that they are sensing macronutrients directly, including but not necessarily limited to fatty acids. In addition to sensing nutrients directly, it is well established that vagal afferent fibers sense nutrients indirectly by responding to factors released by epithelial cells in response to nutrients. Specifically, satiety peptides (e.g., cholecystokinin, glucagon-like peptide 1, peptide YY) are released by enteroendocrine cells in response to macronutrients in the intestinal lumen. The level of release may vary with the level and type of specific macronutrients present. Thus, type and amount of macronutrients in the intestinal lumen are sensed indirectly by mucosal vagal afferents (Dockray, 2014). Vagal afferent fibers in the small intestinal mucosa also respond electrophysiologically to mechanical stimulation, the physiological function of which is not entirely clear (Clarke & Davison, 1978). However, it has been postulated that these rapidly adapting mechanoreceptors sense the perturbations of the villi as a bolus of food passes down the intestinal tract (Powley *et al.*, 2011). Overall, these terminals are indeed providing critical sensory information about the small intestinal mucosa to the brain, but the available technology is insufficient to answer many of the specific questions about what and how these afferents are signaling.

1.4 Functional roles of the sensory branch of the gut-brain axis

Traditionally-defined roles of the sensory gut-brain axis

As described above, sensory pathways send information about GI status so that this information can be used to regulate functions of the GI tract and coordinate this activity with other physiological systems in the body. With respect to sensory pathways, previous research has focused on the how these nerves send signals about food intake from the gut to the brain. These nerves have been shown to detect

amount and type of food in the GI tract (Raybould, 2010; Dockray, 2014; de Lartigue & Diepenbroek, 2016). Consequently, these nerves play a crucial role in satiety signaling (Powley & Phillips, 2004; Berthoud, 2008), and it has been hypothesized that dysregulation in this signaling contributes to the development of obesity (de Lartigue, 2016). In addition, a great deal of research has investigated how sensory nerves transmit pain signals from the GI tract, which are thought to contribute to visceral pain in disease states (Grundy, 2002; Christianson & Davis, 2010).

Non-traditional role of the sensory gut-brain axis: Neuroplasticity in aberrant sensory gut-brain signaling

Neuroplasticity is an important adaptive process of the nervous system, and refers to changes in neurons including neuronal excitability, levels of signaling molecules, and/or morphology. Neuroplasticity occurs not only in the CNS, but also in peripheral nerves. Neuroplastic changes of the vagal afferent sensory nerves are of particular interest due to the association of these changes in these nerves with diseases such as obesity and inflammatory bowel disease. On a molecular level, these diseases are associated with environmental changes within the gut (e.g., dietary, inflammatory), which drive neuroplastic alterations in the level or function of protein-kinase and metabolic signaling molecules. Ultimately, these changes lead to aberrant sensory signaling in the gut-brain axis. Another consequence of these disease-associated neuroplastic changes in signaling molecules is the initiation of morphological neuroplastic changes. Morphological neuroplasticity includes changes in fiber density, branching, and terminal morphology of neurons, all of which have been demonstrated in vagal afferent nerves under different disease conditions (Phillips & Powley, 2001; Phillips *et al.*, 2010; Brierley & Linden, 2014; Sen *et al.*, 2017; de Lartigue & Xu, 2018). These morphological neuroplastic changes can ultimately affect neuronal signaling and the ability of the neuron to properly transmit sensory stimuli from the gut to the brain, providing an additional route by which a dysregulation of gut-brain signaling can occur. Although it is known that molecular neuroplastic changes occur in vagal afferent neurons in obesity (de Lartigue, 2016), it is not known if the aberrant gut-brain signaling in obesity is also associated with morphological

neuroplastic changes. Thus, I set out to test whether morphological neuroplastic changes occur in obesity, and to investigate the mechanisms associated with these putative morphological neuroplastic changes. Investigation of these changes and their underlying mechanisms may lead to the development of treatments that reverse neuroplastic changes driving aberrant gut-brain signaling in obesity.

1.5 Motor innervation of the small intestine

The autonomic nervous system

Motor innervation of the gut-brain axis is a part of the autonomic nervous system (ANS). The ANS is the division of the peripheral nervous system that controls unconscious functions of the internal organs. The ANS can react quickly to changes in the environment or body state, altering the functions of peripheral organs. The ANS is divided into two branches, the sympathetic nervous system (SNS) and the parasympathetic nervous system (PNS). The SNS controls the 'fight or flight' response, meaning that when the SNS is activated, it prepares the body to confront or escape a predator or other threat. In the small intestine, SNS activation inhibits digestive function, as digestion is not a critical function to promote during a threat (McCorry, 2007). In contrast, the PNS functions to conserve and restore energy to the body while directing necessary 'housekeeping' processes such as waste elimination. Therefore, the PNS is colloquially referred to as the 'rest and digest' branch of the ANS. In the small intestine, PNS activation stimulates digestive functions (McCorry, 2007). The activity of the SNS and PNS are in constant balance, working together to determine the appropriate responses of organs under different circumstances. These 'fight or flight' and 'rest and digest' scenarios are classic examples of SNS and PNS dominance, respectively. However, both systems are constantly active at a basal level to maintain homeostasis (Wehrwein *et al.*, 2016).

SNS and PNS nerve pathways share a common organizational structure. Distinct SNS and PNS pathways project from the CNS to their respective target organs in a two-neuron pathway. The cell bodies of the preganglionic neurons, the first neuron in this pathway, originate in the CNS (autonomic nuclei in the brainstem or spinal cord) and project to a peripheral ganglion. In the ganglion, these preganglionic

neurons synapse onto the postganglionic neuron. The postganglionic neurons, the second neuron in this pathway, then synapse onto the cells within the target organs (Wehrwein *et al.*, 2016). Higher-order control of this SNS and PNS outflow is enacted by preautonomic nuclei that make direct synaptic connections with preganglionic autonomic neurons in the brainstem or spinal cord (Browning & Travagli, 2014). Through these pathways, the CNS can appropriately influence the function of the small intestine under a variety of environmental conditions.

General organization of the sympathetic nervous system

The sympathetic nerve tracts are thoracolumbar, meaning that they originate from the thoracic region of the spinal column, spanning the first thoracic nerve root (T1) through the third lumbar nerve root (L3). Within the spinal cord, the majority of the cell bodies for the sympathetic preganglionic neurons are located in the intermediolateral cell column, or the IML. From the spinal cord, preganglionic SNS neurons project to either paravertebral ganglia within the sympathetic chain, or prevertebral ganglia that are located outside the sympathetic chain closer to the target organ. Within their respective ganglia, the preganglionic SNS neurons synapse onto postganglionic SNS neurons using acetylcholine (ACh) as a neurotransmitter. Finally, these postganglionic SNS neurons project to their respective target organs and make synaptic connections with target cells using norepinephrine (NE) as the main neurotransmitter. This neural pathway supplies the anatomy for the SNS to influence organ physiology and function.

Sympathetic innervation of the small intestine

The sympathetic efferent pathways directly innervate target tissues within the small intestine (Fig. 3), including cells within the circular muscle, the myenteric plexus, the submucosal plexus, the intestinal blood vessels, and the mucosa. Nearly all of the preganglionic SNS neurons that send signals to the small intestine pass through the sympathetic chain, traveling via the splanchnic nerves to synapse onto postganglionic SNS neurons within the in the prevertebral ganglia, specifically the celiac and mesenteric ganglia. The only exception is sympathetic innervation to blood vessels, which is supplied by neurons that synapse within the paravertebral ganglia of the sympathetic chain and then travel via spinal nerves to

innervate intestinal blood vessels. For all other targets, postganglionic PNS neurons project from the celiac or mesenteric ganglia project to both neuronal and non-neuronal targets within the small intestine. Neuronal targets include neurons of the enteric nervous system. Postganglionic SNS neurons make synaptic connections with enteric nervous system neurons located in the myenteric plexus or the submucosal plexus. The myenteric plexus is found in between the circular and longitudinal muscle layers, and sympathetic fibers innervating enteric neurons the myenteric plexus facilitate the inhibition of intestinal muscle movement. The submucosal plexus is located in the submucosal layer, and sympathetic fibers innervating enteric neurons in this plexus inhibit secretory function (Lomax *et al.,* 2010). Non-neuronal targets of sympathetic postganglionic neurons include the circular muscle layer at sphincter regions, which control muscle contractions (Lomax *et al.*, 2010). Sympathetic fibers also come into close contact with epithelial cells in the mucosal layer. In particular, a thick net of nerve fibers are located at the base of the crypts where the stem cells reside (Gabella & Costa, 1968). Sympathetic nerve fibers in close approximation of the intestinal epithelium control electrolyte transport (Greenwood *et al.*, 1987). Together, these nerves participate in controlling the diverse functions of the small intestine.

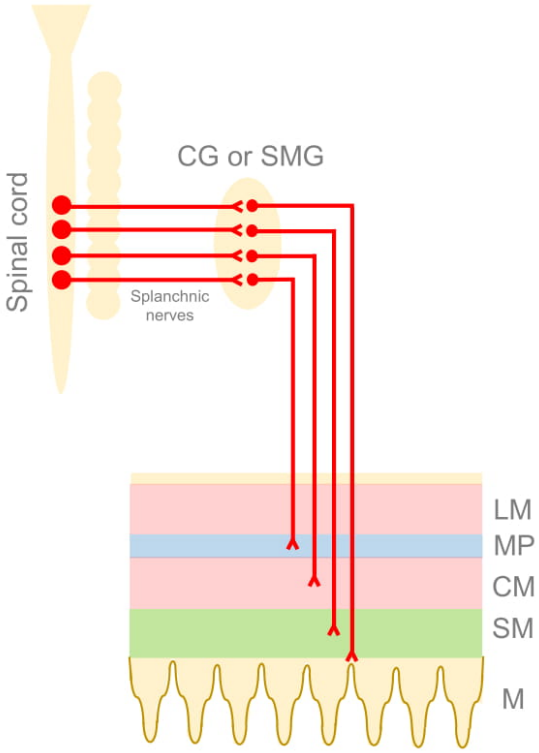

Figure 3. **Sympathetic innervation of the small intestine.** Preganglionic sympathetic (SNS) neurons originate in the spinal cord. These neurons pass through the sympathetic chain and project via splanchnic nerves to the paravertebral ganglia, either the celiac ganglion or superior mesenteric ganglion. Within the ganglia, preganglionic SNS neurons make synaptic connections with postganglionic SNS neurons which project to target cells in the small intestine. These targets include cells in the myenteric plexus, the circular muscle, the submucosal plexus, and the mucosa, with particularly dense innervation of intestinal epithelial crypts in the mucosa. Innervation of intestinal blood vessels is supplied by neurons that synapse in the sympathetic chain (not shown). (Abbreviations in figure: CG = celiac ganglion; SMG: superior mesenteric ganglion; LM = longitudinal muscle; MP = myenteric plexus; CM = circular muscle; SM = submucosa; M = mucosa.)

General organization of the parasympathetic nervous system

The preganglionic neurons of the PNS originate in the cranial and sacral regions of the CNS. The projections that originate in the brain travel to their respective target organs in the head, neck, thorax, and abdomen via cranial nerves. In contrast, the projections that originate in the sacral region of the spinal cord travel in spinal nerves to their target organs within the pelvis. Once reaching their target organs, the preganglionic PNS neurons make synaptic contact with postganglionic PNS neurons within parasympathetic ganglia, which are located in or near the target organs, using ACh as the main neurotransmitter. From the ganglia, the postganglionic neurons project a short distance to target cells, where they use ACh as the main neurotransmitter to effect target cells. Together, the cranial and sacral pathways allow control of peripheral function by the PNS.

Parasympathetic innervation of the small intestine

Parasympathetic innervation of the small intestine (Fig. 4) is provided through the cranial pathway, specifically through the vagus nerve (cranial nerve X). Once reaching the small intestine, the vagal efferent fibers enter the parasympathetic ganglia, which are found in two ganglionated enteric plexuses: the myenteric plexus, between the circular and longitudinal muscle layers, and the submucosal plexus, located in the submucosa as the

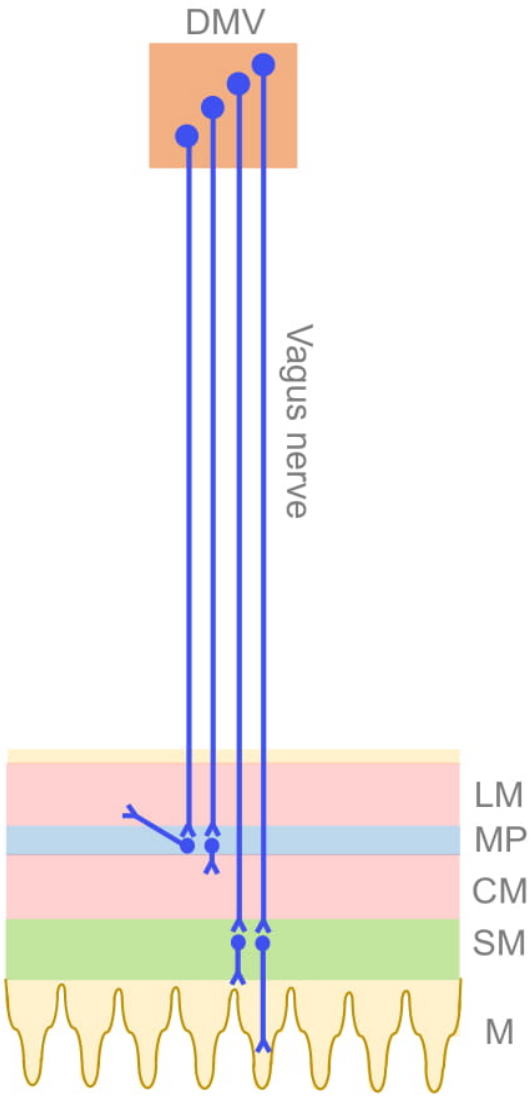

Figure 4. **Parasympathetic innervation of the small intestine.** Preganglionic parasympathetic (PNS) neurons that project to the small intestine originate in the dorsal motor nucleus of the vagus in the brainstem. These neurons project to the small intestine via the vagus nerve. These preganglionic neurons synapse onto postganglionic PNS neurons within the myenteric plexus or the submucosal plexus. From the myenteric plexus, postganglionic neurons synapse onto cells within the longitudinal or circular muscle layers. From the submucosal plexus, postganglionic neurons synapse onto neurons within the mucosa, including both the crypts and villi. (Abbreviations in figure: DMV = dorsal motor nucleus of the vagus; LM = longitudinal muscle; MP = myenteric plexus; CM = circular muscle; SM = submucosa; M = mucosa.)

name implies (Holst *et al.*, 1997; Chang *et al.*, 2003). Within these plexuses, the preganglionic parasympathetic neurons make synaptic connections with postganglionic parasympathetic neurons. At this synapse, ACh is released from the presynaptic terminal of the postganglionic neuron and then binds to nAChRs on the postsynaptic terminal of the postganglionic neurons to effect downstream changes in postganglionic neurons (Albuquerque *et al.*, 2009) (Fig 3). Unmyelinated postganglionic parasympathetic neurons then project from the myenteric plexus or submucosal plexus to target cells within the small intestine (Holst *et al.*, 1997; Chang *et al.*, 2003). It is important to note that postganglionic parasympathetic neurons are intermingled with enteric neurons that do not receive direct parasympathetic input (Powley, 2000). Postganglionic PNS neurons with cell bodies in the myenteric plexus project to longitudinal and circular muscle fibers to control smooth muscle movements of the GI tract (Nezami & Srinivasan, 2010). Postganglionic PNS neurons originating in the submucosal plexus project to the mucosa, terminating directly below intestinal epithelial crypts (Furness *et al.*, 2014), and also have been shown to project to the villi (Chang *et al.*, 2003). These neurons participate in regulating secretory function and hormone release from epithelial cells (Rocca & Brubaker, 1999; Chang *et al.*, 2003; Nezami & Srinivasan, 2010; Bohorquez *et al.*, 2015). Ultimately, these PNS nerves coordinate small intestinal function under conditions of high PNS tone.

1.6 Functional roles of the motor branch of the gut-brain axis

Traditionally-defined roles of the motor gut-brain axis

Like the sensory fibers, several topics have dominated investigation of the motor gut-brain axis functions. These have included control of motility, blood vessel regulation, secretion of hormones and electrolytes, and inflammation under homeostatic and disease conditions (Christensen, 1971; Taylor & Keely, 2007; Lomax *et al.*, 2010; Cheng *et al.*, 2013; Browning & Travagli, 2014; Bonaz *et al.*, 2016). These studies have uncovered many capabilities of the motor gut-brain axis; however, there are additional functions of these efferent nerves to the gut that are becoming evident.

Non-traditional role of the motor gut-brain axis: Control of tissue regeneration

Although the motor fibers of the gut-brain axis are known to modulate specific functions within the layers of the GI tract, they are also thought to play a role in the homeostatic regeneration of the tissue. Denervation (surgical or chemical) of either SNS or PNS nerves to the intestine alters intestinal epithelial crypt cell proliferation (Tutton & Helme, 1974; Musso *et al.*, 1975a; Tsibulevskii & Orlova, 1976; Lachat & Goncalves, 1978; Kennedy *et al.*, 1983; Callaghan, 1991). However, previous studies have not determined whether this effect is direct or indirect. Previous studies may have detected indirect effects on proliferation due to post denervation-induced changes in food intake, inflammation, or other factors that can alter intestinal epithelial cell proliferation (Dailey, 2014; Slater *et al.*, 2017). In contrast, a direct effect could potentially be driven by autonomic neurotransmitters binding to receptors localized on proliferating cells of the intestinal epithelium. Furthermore, previous studies did not determine if these effects of denervation of PNS or SNS nerves on tissue regeneration persist long-term, which may lead to dysregulation of tissue size or function. Thus, I investigated if and how PNS or SNS motor nerves of the gut-brain axis could directly alter intestinal stem cell proliferation and evaluated the effect of loss of the motor nerves of the gut-brain axis in intestinal tissue regeneration *in vivo*. Together, these experiments begin to describe the molecular components and physiology through which a direct ANS control of stem cell proliferation and tissue regeneration may occur. This improved knowledge may lead to innovative treatments for tissue damage or dysfunction in the future.

1.7 Summary

The sensory and motor connections between the small intestine and brain have the ability to sense a wide range of stimuli and subsequently coordinate appropriate responses. However, the full potential of this system has yet to be characterized. The following studies describe several lines of research pursuing improved understanding of non-traditional roles of the gut-brain axis innervation of the small intestine, which may uncover strategies to treat conditions that affect the gut-brain axis or its associated organs. Overall, I hypothesized that vagal afferent nerves undergo morphological neuroplastic changes in obesity,

and that the autonomic motor nerves of the gut-brain axis directly control intestinal epithelial stem cell proliferation. Chapters two through five describe experiments in pursuit of these hypotheses. In chapter two, I developed methods to investigate vagal afferent nerve morphology and function in rats to allow improved techniques to study the effect of obesity on vagal afferent nerves. In chapter three, I used swine to evaluate the effect of obesity on neuron density, glial cell density, and neuroplasticity-associated proteins in the nodose ganglion. In chapter four, I isolated intestinal epithelial stem cells in mice to characterize their expression of autonomic neurotransmitter receptors, and determined the effect of the corresponding autonomic neurotransmitters on a proliferation-related gene in mouse-derived intestinal epithelial organoids. In chapter five, I evaluated the effect of autonomic neurotransmitters on proliferation in mouse-derived intestinal epithelial organoids. In chapter six, I used rats to determine the long-term effect of SNS or PNS nerve ablation on intestinal epithelial proliferation and apoptosis. In chapter seven, I summarize the significance of these results from these experiments and highlight further considerations for future research on these topics. Overall, this work adds to the knowledge base on the diverse roles of the neural gut-brain axis.

1.8 References

Agarwal SK & Calaresu FR (1990). Reciprocal connections between nucleus tractus solitarii and rostral ventrolateral medulla. *Brain Res* **523,** 305-308.

Albuquerque EX, Pereira EFR, Alkondon M & Rogers SW (2009). Mammalian Nicotinic Acetylcholine Receptors: From Structure to Function. *Physiol Rev* **89,** 73-120.

Altschuler SM, Bao XM, Bieger D, Hopkins DA & Miselis RR (1989). Viscerotopic representation of the upper alimentary tract in the rat: sensory ganglia and nuclei of the solitary and spinal trigeminal tracts. *J Comp Neurol* **283,** 248-268.

Altschuler SM, Ferenci DA, Lynn RB & Miselis RR (1991). Representation of the cecum in the lateral dorsal motor nucleus of the vagus nerve and commissural subnucleus of the nucleus tractus solitarii in rat. *J Comp Neurol* **304,** 261-274.

Andresen MC & Kunze DL (1994). Nucleus tractus solitarius--gateway to neural circulatory control. *Annu Rev Physiol* **56,** 93-116.

Barker N, van Es JH, Kuipers J, Kujala P, van den Born M, Cozijnsen M, Haegebarth A, Korving J, Begthel H, Peters PJ & Clevers H (2007). Identification of stem cells in small intestine and colon by marker gene Lgr5. *Nature* **449,** 1003-1007.

Berthoud HR (2008). Vagal and hormonal gut-brain communication: from satiation to satisfaction. *Neurogastroenterol Motil* **20 Suppl 1,** 64-72.

Berthoud HR, Carlson NR & Powley TL (1991). Topography of efferent vagal innervation of the rat gastrointestinal tract. *Am J Physiol* **260,** R200-207.

Berthoud HR, Kressel M, Raybould HE & Neuhuber WL (1995). Vagal sensors in the rat duodenal mucosa: distribution and structure as revealed by in vivo DiI-tracing. *Anat Embryol (Berl)* **191,** 203-212.

Berthoud HR & Neuhuber WL (2000). Functional and chemical anatomy of the afferent vagal system. *Auton Neurosci* **85,** 1-17.

Berthoud HR, Patterson LM, Neumann F & Neuhuber WL (1997). Distribution and structure of vagal afferent intraganglionic laminar endings (IGLEs) in the rat gastrointestinal tract. *Anat Embryol (Berl)* **195,** 183-191.

Bohorquez DV, Shahid RA, Erdmann A, Kreger AM, Wang Y, Calakos N, Wang F & Liddle RA (2015). Neuroepithelial circuit formed by innervation of sensory enteroendocrine cells. *J Clin Invest* **125,** 782-786.

Bonaz B, Sinniger V & Pellissier S (2016). Vagal tone: effects on sensitivity, motility, and inflammation. *Neurogastroenterol Motil* **28,** 455-462.

Bonham A & Chen C (2005). Synaptic Transmission in the Nucleus Tractus Solitarius: Advances in Vagal Afferent Neurobiology.

Brierley SM & Linden DR (2014). Neuroplasticity and dysfunction after gastrointestinal inflammation. *Nat Rev Gastroenterol Hepatol* **11,** 611-627.

Brookes SJ, Spencer NJ, Costa M & Zagorodnyuk VP (2013). Extrinsic primary afferent signalling in the gut. *Nat Rev Gastroenterol Hepatol* **10,** 286-296.

Browning KN & Travagli RA (2014). Central nervous system control of gastrointestinal motility and secretion and modulation of gastrointestinal functions. *Compr Physiol* **4,** 1339-1368.

Callaghan BD (1991). The effect of pinealectomy and autonomic denervation on crypt cell proliferation in the rat small intestine. *J Pineal Res* **10,** 180-185.

Cannon W (1932). The Wisdom of the Body.

Cannon WB (1929). Bodily changes in pain, hunger, fear and rage.

Cano G, Card JP, Rinaman L & Sved AF (2000). Connections of Barrington's nucleus to the sympathetic nervous system in rats. *J Auton Nerv Syst* **79,** 117-128.

Chang HY, Mashimo H & Goyal RK (2003). Musings on the wanderer: what's new in our understanding of vago-vagal reflex? IV. Current concepts of vagal efferent projections to the gut. *Am J Physiol Gastrointest Liver Physiol* **284,** G357-366.

Cheng P, Shih W, Alberto M, Presson AP, Licudine A, Mayer EA, Naliboff BD & Chang L (2013). Autonomic response to a visceral stressor is dysregulated in irritable bowel syndrome and correlates with duration of disease. *Neurogastroenterol Motil* **25,** e650-659.

Christensen J (1971). The controls of gastrointestinal movements: some old and new views. *N Engl J Med* **285,** 85-98.

Christianson JA & Davis BM (2010). Frontiers in Neuroscience. The Role of Visceral Afferents in Disease. In *Translational Pain Research: From Mouse to Man*. ed. Kruger L & Light AR. CRC Press/Taylor & Francis. Llc., Boca Raton, FL.

Clarke GD & Davison JS (1978). Mucosal receptors in the gastric antrum and small intestine of the rat with afferent fibres in the cervical vagus. *J Physiol* **284,** 55-67.

Clevers HC & Bevins CL (2013). Paneth cells: maestros of the small intestinal crypts. *Annu Rev Physiol* **75,** 289-311.

Dailey MJ (2014). Nutrient-induced intestinal adaption and its effect in obesity. *Physiol Behav* **136,** 74-78.

Darling RA, Zhao H, Kinch D, Li AJ, Simasko SM & Ritter S (2014). Mercaptoacetate and fatty acids exert direct and antagonistic effects on nodose neurons via GPR40 fatty acid receptors. *Am J Physiol Regul Integr Comp Physiol* **307,** R35-43.

de Lartigue G (2016). Role of the vagus nerve in the development and treatment of diet-induced obesity. *J Physiol*.

de Lartigue G & Diepenbroek C (2016). Novel developments in vagal afferent nutrient sensing and its role in energy homeostasis. *Curr Opin Pharmacol* **31,** 38-43.

de Lartigue G & Xu C (2018). Mechanisms of vagal plasticity influencing feeding behavior. *Brain Res* **1693,** 146-150.

Deuchars SA & Lall VK (2015). Sympathetic preganglionic neurons: properties and inputs. *Compr Physiol* **5,** 829-869.

Dockray GJ (2014). Gastrointestinal hormones and the dialogue between gut and brain. *J Physiol* **592,** 2927-2941.

Fox EA, Phillips RJ, Martinson FA, Baronowsky EA & Powley TL (2000). Vagal afferent innervation of smooth muscle in the stomach and duodenum of the mouse: morphology and topography. *J Comp Neurol* **428,** 558-576.

Furness JB, Callaghan BP, Rivera LR & Cho HJ (2014). The enteric nervous system and gastrointestinal innervation: integrated local and central control. *Adv Exp Med Biol* **817,** 39-71.

Gabella G & Costa M (1968). Adrenergic fibres in the mucous membrane of guinea pig alimentary tract. *Experientia* **24,** 706-707.

Greenwood B, Tremblay L & Davison JS (1987). Sympathetic control of motility, fluid transport, and transmural potential difference in the rabbit ileum. *Am J Physiol* **253,** G726-729.

Grundy D (2002). Neuroanatomy of visceral nociception: vagal and splanchnic afferent. *Gut* **51 Suppl 1,** i2-5.

Heblich F, England S & Docherty RJ (2001). Indirect actions of bradykinin on neonatal rat dorsal root ganglion neurones: a role for non-neuronal cells as nociceptors. *J Physiol* **536,** 111-121.

Holst MC, Kelly JB & Powley TL (1997). Vagal preganglionic projections to the enteric nervous system characterized with Phaseolus vulgaris-leucoagglutinin. *J Comp Neurol* **381,** 81-100.

Iriki M & Simon E (2012). Differential control of efferent sympathetic activity revisited. *The Journal of Physiological Sciences* **62,** 275-298.

Kalia M & Sullivan JM (1982). Brainstem projections of sensory and motor components of the vagus nerve in the rat. *J Comp Neurol* **211,** 248-265.

Kennedy MF, Tutton PJ & Barkla DH (1983). Adrenergic factors involved in the control of crypt cell proliferation in jejunum and descending colon of mouse. *Clin Exp Pharmacol Physiol* **10,** 577-586.

Lachat JJ & Goncalves RP (1978). Influence of autonomic denervation upon the kinetics of the ileal epithelium of the rat. *Cell Tissue Res* **192,** 285-297.

Leblond CP & Stevens CE (1948). The constant renewal of the intestinal epithelium in the albino rat. *Anat Rec* **100,** 357-377.

Liu C, Bookout Angie L, Lee S, Sun K, Jia L, Lee C, Udit S, Deng Y, Scherer Philipp E, Mangelsdorf David J, Gautron L & Elmquist Joel K (2014). PPARγ in Vagal Neurons Regulates High-Fat Diet Induced Thermogenesis. *Cell Metabolism* **19,** 722-730.

Lomax AE, Sharkey KA & Furness JB (2010). The participation of the sympathetic innervation of the gastrointestinal tract in disease states. *Neurogastroenterol Motil* **22,** 7-18.

McCorry LK (2007). Physiology of the autonomic nervous system. *Am J Pharm Educ* **71,** 78.

Morrison SF (1999). RVLM and raphe differentially regulate sympathetic outflows to splanchnic and brown adipose tissue. *Am J Physiol* **276,** R962-973.

Musso F, Lachat J-J, Cruz AR & Gonçalves RP (1975). Effect of denervation on the mitotic index of the intestinal epithelium of the rat. *Cell and Tissue Research* **163,** 395-402.

Nezami BG & Srinivasan S (2010). Enteric Nervous System in the Small Intestine: Pathophysiology and Clinical Implications. *Curr Gastroenterol Rep* **12,** 358-365.

Norgren R (1983). The gustatory system in mammals. *Am J Otolaryngol* **4,** 234-237.

Oh EJ & Weinreich D (2002). Chemical communication between vagal afferent somata in nodose Ganglia of the rat and the Guinea pig in vitro. *J Neurophysiol* **87,** 2801-2807.

Orts-Del'immagine A, Wanaverbecq N, Tardivel C, Tillement V, Dallaporta M & Trouslard J (2012). Properties of subependymal cerebrospinal fluid contacting neurones in the dorsal vagal complex of the mouse brainstem. *J Physiol* **590,** 3719-3741.

Petras JM & Cummings JF (1972). Autonomic neurons in the spinal cord of the Rhesus monkey: a correlation of the findings of cytoarchitectonics and sympathectomy with fiber degeneration following dorsal rhizotomy. *J Comp Neurol* **146,** 189-218.

Phillips RJ, Baronowsky EA & Powley TL (1997). Afferent innervation of gastrointestinal tract smooth muscle by the hepatic branch of the vagus. *J Comp Neurol* **384,** 248-270.

Phillips RJ & Powley TL (2000). Tension and stretch receptors in gastrointestinal smooth muscle: re-evaluating vagal mechanoreceptor electrophysiology. *Brain Research Reviews* **34,** 1-26.

Phillips RJ & Powley TL (2001). As the gut ages: timetables for aging of innervation vary by organ in the Fischer 344 rat. *J Comp Neurol* **434,** 358-377.

Phillips RJ, Walter GC & Powley TL (2010). Age-related changes in vagal afferents innervating the gastrointestinal tract. *Autonomic Neuroscience* **153,** 90-98.

Powley TL (2000). Vagal input to the enteric nervous system. *Gut* **47 Suppl 4,** iv30-32; discussion iv36.

Powley TL, Hudson CN, McAdams JL, Baronowsky EA, Martin FN, Mason JK & Phillips RJ (2014). Organization of vagal afferents in pylorus: mechanoreceptors arrayed for high sensitivity and fine spatial resolution? *Auton Neurosci* **183,** 36-48.

Powley TL & Phillips RJ (2002). Musings on the wanderer: what's new in our understanding of vago-vagal reflexes? I. Morphology and topography of vagal afferents innervating the GI tract. *Am J Physiol Gastrointest Liver Physiol* **283,** G1217-1225.

Powley TL & Phillips RJ (2004). Gastric satiation is volumetric, intestinal satiation is nutritive. *Physiology & behavior* **82,** 69-74.

Powley TL, Spaulding RA & Haglof SA (2011). Vagal afferent innervation of the proximal gastrointestinal tract mucosa: chemoreceptor and mechanoreceptor architecture. *J Comp Neurol* **519,** 644-660.

Prechtl JC & Powley TL (1990). The fiber composition of the abdominal vagus of the rat. *Anat Embryol (Berl)* **181,** 101-115.

Price CJ, Hoyda TD & Ferguson AV (2007). The Area Postrema: A Brain Monitor and Integrator of Systemic Autonomic State. *The Neuroscientist* **14,** 182-194.

Raybould HE (2010). Gut chemosensing: Interactions between gut endocrine cells and visceral afferents. *Autonomic Neuroscience* **153,** 41-46.

Rinaman L (2010). Ascending projections from the caudal visceral nucleus of the solitary tract to brain regions involved in food intake and energy expenditure. *Brain Res* **1350,** 18-34.

Rinaman L (2011). Hindbrain noradrenergic A2 neurons: diverse roles in autonomic, endocrine, cognitive, and behavioral functions. *Am J Physiol Regul Integr Comp Physiol* **300,** R222-235.

Rinaman L, Card JP, Schwaber JS & Miselis RR (1989). Ultrastructural demonstration of a gastric monosynaptic vagal circuit in the nucleus of the solitary tract in rat. *J Neurosci* **9,** 1985-1996.

Rocca AS & Brubaker PL (1999). Role of the vagus nerve in mediating proximal nutrient-induced glucagon-like peptide-1 secretion. *Endocrinology* **140,** 1687-1694.

Sen T, Cawthon CR, Ihde BT, Hajnal A, DiLorenzo PM, de La Serre CB & Czaja K (2017). Diet-driven microbiota dysbiosis is associated with vagal remodeling and obesity. *Physiol Behav* **173,** 305-317.

Slater TW, Finkielsztein A, Mascarenhas LA, Mehl LC, Butin-Israeli V & Sumagin R (2017). Neutrophil Microparticles Deliver Active Myeloperoxidase to Injured Mucosa To Inhibit Epithelial Wound Healing. *J Immunol* **198,** 2886-2897.

Stjarne L (1989). Basic mechanisms and local modulation of nerve impulse-induced secretion of neurotransmitters from individual sympathetic nerve varicosities. *Rev Physiol Biochem Pharmacol* **112,** 1-137.

Sved AF, Cano G & Card JP (2001). Neuroanatomical specificity of the circuits controlling sympathetic outflow to different targets. *Clin Exp Pharmacol Physiol* **28,** 115-119.

Tank AW & Lee Wong D (2015). Peripheral and central effects of circulating catecholamines. *Compr Physiol* **5,** 1-15.

Taylor CT & Keely SJ (2007). The autonomic nervous system and inflammatory bowel disease. *Auton Neurosci* **133,** 104-114.

Travagli RA, Hermann GE, Browning KN & Rogers RC (2006). Brainstem circuits regulating gastric function. *Annu Rev Physiol* **68,** 279-305.

Tsibulevskii A & Orlova EN (1976). [Physiologic regeneration of jejunal epithelium following bilateral subdiaphragmatic vagotomy in rats]. *Biull Eksp Biol Med* **81,** 236-237.

Tutton PJ & Helme RD (1974). The influence of adrenoreceptor activity on crypt cell proliferation in the rat jejunum. *Cell Tissue Kinet* **7,** 125-136.

Wang FB & Powley TL (2000). Topographic inventories of vagal afferents in gastrointestinal muscle. *J Comp Neurol* **421,** 302-324.

Wehrwein EA, Orer HS & Barman SM (2016). Overview of the Anatomy, Physiology, and Pharmacology of the Autonomic Nervous System. *Compr Physiol* **6,** 1239-1278.

Weinreich D (2005). Advances in Vagal Afferent Neurobiology: Electrophysiological Studies of Target-Identified. Vagal Afferent Cell Bodies *CRC Press*.

Zagorodnyuk VP, Chen BN & Brookes SJ (2001). Intraganglionic laminar endings are mechano-transduction sites of vagal tension receptors in the guinea-pig stomach. *J Physiol* **534,** 255-268.

Zhang X, Fogel R & Renehan WE (1992). Physiology and morphology of neurons in the dorsal motor nucleus of the vagus and the nucleus of the solitary tract that are sensitive to distension of the small intestine. *J Comp Neurol* **323,** 432-448.

Zhang X, Renehan WE & Fogel R (2000). Vagal innervation of the rat duodenum. *J Auton Nerv Syst* **79,** 8-18.

CHAPTER 2: PRACTICAL CONSIDERATIONS FOR EVALUATING VAGAL AFFERENT NEURONS

(Modified from a publication submitted to Journal of Visualized Experiments)

2.1 Introduction

The vagal afferent neurons are critical for the transmission of sensory afferent information from the periphery to the brain. The vagal afferents innervating the gastrointestinal (GI) tract have been widely studied in the control of food intake (Ritter *et al.*, 2017), and are considered an important part of the gut brain axis. More recently, this field has expanded to include GI vagal afferent modulation of higher order cognitive processes, such as motivated approach and avoidance behaviors (Maniscalco & Rinaman, 2018) and declarative memory (Suarez *et al.*, 2018). Thus, experimental methods to study vagal afferent neurons are of great interest to scientists in a diverse range of fields.

Vagal afferent cell bodies are located in the nodose ganglia, which are located bilaterally at the major bifurcation of the carotid artery. Experimental manipulation of this ganglion is a useful technique, but the surgical approach is deceptively difficult primarily due to the location of the nodose ganglion. Many delicate structures that require careful handling are encountered during the surgical approach. If damage to these structures is incurred during surgery, the animal's post-surgical viability may be reduced. Thus, we describe in detail the approach to the nodose ganglia in rats, aiming to make this protocol more accessible to those who would like to embark on this technique for the first time. Standardization and improvement of this difficult technique throughout the scientific community can increase the post-surgical viability of the animals and reduce post-surgical pain, improving overall experimental outcomes.

Once the surgical procedure is mastered, there are a variety of opportunities for further investigation of the vagal afferents nerves through the manipulation of this ganglion. These include intraganglionic nodose injections, tissue harvest for subsequent evaluation of gene and/or protein

expression, and cell culture protocols to grow nodose ganglion neurons *in vitro*. As a supplement to the surgical protocol, we describe the various techniques that may be used following the surgical approach to this ganglion. Ultimately, successful surgeries and effective use of the subsequent protocols described here can support research efforts to increase the overall understanding of the vagal afferent nerves.

2.2 Protocol

Ethics Statement

Procedures involving animal subjects have been approved by the Institutional Animal Care and Use Committee at the University of Illinois at Urbana-Champaign.

1) Pre-surgical procedures

1.1) Initiate food deprivation (~12 h) at the end of the dark cycle prior to the surgery, even though rats do not normally eat at this time. The rats will undergo both surgical procedures near the end of the light cycle. This step is done to reduce anesthesia-induced nausea.

1.2) Induce anesthesia in chamber with 5% isoflurane at 1.5L/min.

CAUTION: Isoflurane is a potentially toxic anesthetic agent. Please refer to the SDS (Safety Data Sheet) for isoflurane to ensure proper administration of anesthesia for this procedure.

1.2) Continue administration of 1.5-2% isoflurane through a nose cone at rate of 1.5L/min.

1.3) Place the rat in a supine position, or dorsal recumbency, with the neck extended. Using surgical tape, tape down the arms, legs, and tail of the rat, taking care to minimize tension placed upon the limbs due to the tape restraints. Place a small amount of folded surgical gauze under the head of the rat in order to reduce pressure on the trachea.

1.4) Clip the area from the rostral intermandibular space to the point of the shoulders with electric clippers to remove hair bilaterally to the base of the ear.

1.5) Aseptically prepare the clipped area and surgical site by alternately wiping with povidone-iodine scrub and 70% isopropyl alcohol.

1.6) Provide physiologic monitoring of rats during anesthesia with an electrocardiogram and pulse oximetry. Place rats on a warming pad to maintain temperature. Monitor rectal temperature every 5 minutes. Perform assessment of pain by toe pinch every 5 minutes.

2) Dissection to the salivary gland and the linguofacial vein

2.1) Using a #15 blade, incise the full thickness of the skin along the ventral midline from just rostral to the angle of the mandible to just cranial to the manubrium.

2.2) Dissect the subcutaneous tissue along the same incision line with iris scissors. During this dissection, avoid causing damage to the mandibular salivary glands, which are lying on either side just deep to the incision.

2.3) Carefully undermine the skin for approximately 1.5 cm bilaterally. Avoid causing damage to the blood vessels of the subdermal plexus in the skin.

2.4) Identify the linguofacial vein running laterally to either mandibular salivary gland. The surgeon may operate the right or left side to identify the nodose ganglion, as the approach is the same.

2.5) Carefully install blunt-tipped self-retaining retractors, retracting the skin bilaterally in order to improve visualization of the surgical field.

3) Dissection to the intermuscular septum

3.1) Lightly dissect the adipose and connective tissue lateral to the salivary gland and linguofacial vein using angled jeweler's or other fine forceps and microvascular scissors.

3.2) Carefully retract the mandibular salivary gland medially and cranially to allow identification of the intermuscular septum between the sternohyoideus and sternocephalicus muscles, lying deep to thin fascia.

3.3) Dissect the thin fascia to allow access to the intermuscular septum.

4) Dissection to the carotid artery

4.1) Separate the muscles along the intermuscular septum for their length using a combination of blunt dissection with angled jeweler's forceps and sharp dissection with microvascular scissors.

4.2) Retract the sternocephalicus muscle laterally, permitting identification of the omohyoideus muscle located deep to the sternohyoid and sternocephalicus muscles and slightly medial and cranial.

4.3) Lightly dissect the axial line of the omohyoideus muscle to permit visualization of the carotid artery.

5) Dissection to the nodose ganglion

5.1) Lightly dissect the fascia surrounding the common carotid artery, extending in a cranial direction in order to locate its major bifurcation.

5.2) Identify the vagus nerve and sympathetic nerve adjacent to the common carotid artery.

5.3) Identify the nodose ganglion at the level of the major bifurcation in the carotid artery. The nodose ganglion can be identified as an ovoid structure ~3mm in diameter and light tan-grey in color, lying deep and axial to the branches of the common carotid artery. The branches of the common carotid artery include the internal carotid artery, occipital artery, and the cranial thyroid artery.

5.4) Dissect the thin connective tissue overlying the nodose ganglion and around the carotid branches with an angled jeweler's forceps to improve access to the nodose ganglion.

6) Tracer injection (optional)

Inject 2 uL of the tracer into the ganglion in the vicinity of the afferent cell bodies using a Hamilton syringe. Since the nodose is heavily encapsulated, it is practical to inject the appropriate tracer into the ganglion without significant leakage. Fast Green (F7252-5G, Sigma Aldrich) may be added to the tracer to visualize the tracer solution during injection.

7) Wound closure

7.1) Release retractors from the sternocephalicus muscle.

7.2) Close the sternohyoid and sternocephalicus muscles using continuous suture pattern of 5-0 polydioxanone or poliglecaprone 25.

7.3) Release retractors from the skin.

7.4) Close the subcutaneous tissues using a continuous pattern of 6-0 polydioxanone or poliglecaprone 25. Apply ethyl-cyanoacrylate skin glue topically to the skin edges while approximating the skin edges gently with forceps.

7.5) Gently cleanse the incision of blood using sterile saline and gauze.

8) Post-operative care

8.1) Post-operatively after the tracer injection surgery, administer 0.02 mg/kg buprenorphine subcutaneously. (This dose will be repeated 12 hours following surgery.)

8.2) Recover the animals in a clean, dry, single cage with warming pad with frequent observation by trained personnel.

8.2.1) Give particular attention to thermoregulation, monitoring of heart rate, respiratory rate and respiratory effort, and management of postoperative pain or discomfort.

8.2.2) Assess pain and level of consciousness by toe-pinch every 5 minutes.

8.3) Once the animal is freely moving after recovery from anesthesia, place the animal back in their home cage with free access to food and water or return the animal to group housing.

8.4) Monitoring can be less intense but should include attention to basic biologic functions of food intake and urine and feces elimination and to behavioral signs of post-operative pain including haunching, immobility anorexia, and lethargy.

8.5) Twelve hours post-operatively after the tracer injection surgery, administer 0.02 mg/kg buprenorphine subcutaneously.

8.6) Monitor the surgical site twice daily for postsurgical infections and signs of dehiscence.

9) Critical steps within the protocol

9.1) Surgeons must avoid damage to the salivary glands of the rat due to improper handling. Damage to the salivary glands may cause an inability to produce saliva post-operatively, which will severely compromise ingestive function. Damage to the salivary glands can be avoided by gently and completely removing connective tissue around the perimeter of the gland, eventually allowing the gland to ‘flip up’

without tearing the gland. Then, blunt retractors must be used to lightly retract the gland away from the surgical field of view. Retraction using sharp retractors or applied with too much force will damage the salivary glands.

9.2) The carotid artery is another structure that should be handled with extra caution. The nodose ganglion's close proximity to the carotid artery necessitates the thorough dissection of the connective tissue surrounding carotid to expose the ganglion, especially since the ganglion lies deep to the carotid. It is recommended that after the clearing away of these connective tissues, the carotid is gently moved in the attempt to better visualize the ganglion. However, a common mistake is grabbing the artery by the full thickness. In order to prevent damage to the artery and possible thrombotic events, the artery must be gently moved by carefully by grasping onto the adventitia as opposed to grasping the full thickness of the artery.

9.3) Another critical point of the protocol is the use of a proper dissection microscope, as it is crucial to the success of the surgery. It is not advisable to attempt this surgery using only the unaided eye, as this greatly increases the risk of damage to delicate structures as discussed above or incorrect execution of the injection of the neuroanatomical tracer.

2.3 Discussion

The surgical approach to the nodose ganglion described above is a valuable experimental technique. This surgical method can be combined with other techniques to investigate the morphology and/or function of vagal afferent neurons. Scientists who have become proficient at this surgical approach have the option of performing neuroanatomical tracing of vagal afferents, regulating vagal afferent gene expression, selectively denervating vagal afferents originating in specific target tissues, or harvesting the nodose ganglion for evaluation of genes and proteins or culturing nodose ganglion neurons *in vitro*. Here, we briefly describe the available protocols to study vagal afferent neurons after successful surgical approach to the nodose ganglion.

Monosynaptic neuronal tracers such as biotinylated dextran amines injected into the nodose ganglion are a useful option to label the vagal afferent nerves *in vivo*, including the ascending projections to the NTS (Shin *et al.*, 2009) and descending projections to all innervated target organs, including the gut (Powley *et al.*, 2011). Within the gut in particular, monosynaptic neuronal tracers are helpful to discern the vagal afferents from sensory neurons of the enteric nervous system or the spinal afferent neurons, and identify the structures with which they make synaptic connections (Powley *et al.*, 2008). Morphological investigation of vagal afferent terminals can also provide insight into regeneration after injury (Phillips *et al.*, 2000, 2003; Phillips & Powley, 2005; Powley *et al.*, 2005), maladaptive neuroplasticity during aging (Phillips & Powley, 2001) or other neuroplastic changes within these nerves.

In addition to morphological evaluation, genetic manipulation of vagal afferent neurons can be achieved by intraganglionic injection protocols. Viral vectors injected into the nodose ganglion can conditionally knockdown or upregulate genes in vagal afferent neurons (Lai *et al.*, 2003; Zhang *et al.*, 2014). This technique provides an opportunity for researchers to elucidate the function of different genes within the vagal afferent nerves *in vivo*.

Selective ablation of vagal afferent fibers can be achieved by injections of neurotoxins into the nodose ganglion. Specifically, the neurotoxin saporin conjugated to the GI peptide cholecystokinin (CCK) has been used to denervate GI vagal afferents only, while leaving vagal fibers that innervate other organs intact (Diepenbroek *et al.*, 2017). When investigating GI vagal sensory function, this method is preferable compared with traditional techniques that are less selective in their denervation profile. Subdiaphragmatic vagotomy surgically eliminates all vagal sensory and motor fibers, which makes it impossible to discriminate the contributions of the sensory versus motor fibers in the effect being investigated (Davis *et al.*, 2017). Selective deafferentation surgically eliminates just the vagal afferents, but encompasses vagal sensory projections to all innervated organs, not exclusively the GI tract (Sclafani *et al.*, 2003). The neurotoxin capsaicin has been used in the past to selectively denervate vagal afferent C-fibers, but there is evidence that this method destroys both motor and sensory C-fibers, and therefore is

not as selective as intended (Browning *et al.*, 2013). Thus, the innovative CCK-SAP method to selectively ablate GI vagal afferents is a useful application of the surgical approach to the nodose ganglion, and can contribute greatly to the understanding of vagal afferent neurobiology.

The nodose ganglion can also be harvested during animal euthanization for electrophysiological analysis, analysis of genes or proteins, or cell culture. Specifically, whole cell patch clamp protocols have been developed to evaluate electrophysiological properties of nodose ganglia after they have been harvested (Li & Schild, 2002). Techniques can be applied to harvested nodose ganglia to investigate proteins and genes within the nodose. Nodose ganglion mmunohistochemistry has been used for localization of proteins, whereas Western blotting is used for quantification of protein levels (de La Serre *et al.*, 2015). In addition, quantitative polymerase chain reaction (qPCR) and fluorescent in-situ hybridization can be used in the nodose ganglion to investigate gene expression or localization, respectively (Czyzyk-Krzeska *et al.*, 1991; Zhuo & Helke, 1996; Page *et al.*, 2007; Kentish *et al.*, 2013). Although rat nodose ganglia contain a sufficient amount of tissue for these protocols, the ganglion is just 3 mm in diameter. Therefore, nodose ganglia harvested from larger animals yield more tissue, affording the opportunity to evaluate more genes and proteins from the same animal. Finally, nodose ganglia can be harvested to perform primary cell culture *in vitro*. Traditional cell culture methods entail dissociation of the cells for subsequent growth (de Lartigue *et al.*, 2007). Protocols have also been developed to grow the intact nodose ganglion in a 3D culture matrix, which are useful for evaluating axonal regeneration of ganglia *in vitro* (Lindsay & Rohrer, 1985; Wiklund & Ekstrom, 2000). Thus, the harvest of the nodose ganglion provides a variety of techniques to expand upon.

In summary, the surgical approach to the nodose ganglion can be a formidable task for those attempting the technique without guidance. However, proficiency can be achieved with the appropriate resources, after which there is a great deal opportunity for expansion upon this protocol. Proper application of this collection of methods can lead to further understanding of vagal morphology and function.

2.4 References

Browning KN, Babic T, Holmes GM, Swartz E & Travagli RA (2013). A critical re-evaluation of the specificity of action of perivagal capsaicin. *J Physiol* **591,** 1563-1580.

Czyzyk-Krzeska MF, Bayliss DA, Seroogy KB & Millhorn DE (1991). Gene expression for peptides in neurons of the petrosal and nodose ganglia in rat. *Exp Brain Res* **83,** 411-418.

Davis EA, Washington MC, Yaniz ER, Phillips H, Sayegh AI & Dailey MJ (2017). Long-term effect of parasympathetic or sympathetic denervation on intestinal epithelial cell proliferation and apoptosis. *Exp Biol Med (Maywood)* **242,** 1499-1507.

de La Serre CB, de Lartigue G & Raybould HE (2015). Chronic exposure to low dose bacterial lipopolysaccharide inhibits leptin signaling in vagal afferent neurons. *Physiol Behav* **139,** 188-194.

de Lartigue G, Dimaline R, Varro A & Dockray GJ (2007). Cocaine- and amphetamine-regulated transcript: stimulation of expression in rat vagal afferent neurons by cholecystokinin and suppression by ghrelin. *J Neurosci* **27,** 2876-2882.

Diepenbroek C, Quinn D, Stephens R, Zollinger B, Anderson S, Pan A & de Lartigue G (2017). Validation and characterization of a novel method for selective vagal deafferentation of the gut. *Am J Physiol Gastrointest Liver Physiol* **313,** G342-g352.

Kentish SJ, Frisby CL, Kennaway DJ, Wittert GA & Page AJ (2013). Circadian variation in gastric vagal afferent mechanosensitivity. *J Neurosci* **33,** 19238-19242.

Lai YL, Yu SC & Chen MJ (2003). RNA interference prevents lipopolysaccharide-induced preprotachykinin gene expression. *Toxicol Appl Pharmacol* **193,** 47-54.

Li BY & Schild JH (2002). Patch clamp electrophysiology in nodose ganglia of adult rat. *J Neurosci Methods* **115,** 157-167.

Lindsay RM & Rohrer H (1985). Placodal sensory neurons in culture: Nodose ganglion neurons are unresponsive to NGF, lack NGF receptors but are supported by a liver-derived neurotrophic factor. *Dev Biol* **112,** 30-48.

Maniscalco JW & Rinaman L (2018). Vagal Interoceptive Modulation of Motivated Behavior. *Physiology (Bethesda)* **33,** 151-167.

Page AJ, Slattery JA, Milte C, Laker R, O'Donnell T, Dorian C, Brierley SM & Blackshaw LA (2007). Ghrelin selectively reduces mechanosensitivity of upper gastrointestinal vagal afferents. *Am J Physiol Gastrointest Liver Physiol* **292,** G1376-1384.

Phillips RJ, Baronowsky EA & Powley TL (2000). Regenerating vagal afferents reinnervate gastrointestinal tract smooth muscle of the rat. *J Comp Neurol* **421,** 325-346.

Phillips RJ, Baronowsky EA & Powley TL (2003). Long-term regeneration of abdominal vagus: efferents fail while afferents succeed. *J Comp Neurol* **455,** 222-237.

Phillips RJ & Powley TL (2001). As the gut ages: timetables for aging of innervation vary by organ in the Fischer 344 rat. *J Comp Neurol* **434,** 358-377.

Phillips RJ & Powley TL (2005). Plasticity of vagal afferents at the site of an incision in the wall of the stomach. *Auton Neurosci* **123,** 44-53.

Popesko P, Rajtova V & Horák J (2002). *A colour atlas of anatomy of small laboratory animals. Vol. II, Rat, mouse, golden hamster*. Saunders, [Philadelphia] :.

Powley TL, Chi MM, Baronowsky EA & Phillips RJ (2005). Gastrointestinal tract innervation of the mouse: afferent regeneration and meal patterning after vagotomy. *Am J Physiol Regul Integr Comp Physiol* **289,** R563-r574.

Powley TL, Spaulding RA & Haglof SA (2011). Vagal afferent innervation of the proximal gastrointestinal tract mucosa: chemoreceptor and mechanoreceptor architecture. *J Comp Neurol* **519,** 644-660.

Powley TL, Wang XY, Fox EA, Phillips RJ, Liu LW & Huizinga JD (2008). Ultrastructural evidence for communication between intramuscular vagal mechanoreceptors and interstitial cells of Cajal in the rat fundus. *Neurogastroenterol Motil* **20,** 69-79.

Ritter RC, Campos CA, Nasse J & Peters JH (2017). Vagal Afferent Signaling and the Integration of Direct and Indirect Controls of Food Intake. In *Appetite and Food Intake: Central Control*. ed. Nd & Harris RBS, pp. 229-258. CRC Press/Taylor & Francis(c). 2017 by Taylor & Francis Group, LLC., Boca Raton (FL).

Sclafani A, Ackroff K & Schwartz GJ (2003). Selective effects of vagal deafferentation and celiac-superior mesenteric ganglionectomy on the reinforcing and satiating action of intestinal nutrients. *Physiol Behav* **78,** 285-294.

Shin J-W, Geerling JC & Loewy AD (2009). Vagal innervation of the aldosterone-sensitive HSD2 neurons in the NTS. *Brain Res* **1249,** 135-147.

Suarez AN, Hsu TM, Liu CM, Noble EE, Cortella AM, Nakamoto EM, Hahn JD, de Lartigue G & Kanoski SE (2018). Gut vagal sensory signaling regulates hippocampus function through multi-order pathways. *Nat Commun* **9,** 2181.

Wiklund P & Ekstrom PA (2000). Axonal outgrowth from adult mouse nodose ganglia in vitro is stimulated by neurotrophin-4 in a Trk receptor and mitogen-activated protein kinase-dependent way. *J Neurobiol* **45,** 142-151.

Zhang D, Liu J, Tu H, Muelleman RL, Cornish KG & Li YL (2014). In vivo transfection of manganese superoxide dismutase gene or nuclear factor kappaB shRNA in nodose ganglia improves aortic baroreceptor function in heart failure rats. *Hypertension* **63,** 88-95.

Zhuo H & Helke CJ (1996). Presence and localization of neurotrophin receptor tyrosine kinase (TrkA, TrkB, TrkC) mRNAs in visceral afferent neurons of the nodose and petrosal ganglia. *Brain Res Mol Brain Res* **38,** 63-70.

CHAPTER 3: EFFECT OF OBESITY ON THE NODOSE GANGLION IN SWINE

3.1 Rationale

Due to the lack of data generated from methods developed in chapter 2, an alternative approach was used to study the effect obesity of the vagal afferent pathway in swine. We initiated a collaboration with a research group that routinely uses groups of obese and lean Ossabaw minipigs. A surgical approach to collect nodose ganglion tissue was developed, and tissues were collected from lean and obese animals. To determine the effect of obesity on cell number in the nodose ganglion, we measured neuron and glial cell density. We also investigated furin, a protein implicated in neuroplasticity, by measuring relative optical intensity of the furin protein after immunohistochemistry in the nodose ganglion. This pilot study will serve to inform our future research directions on the effect of obesity in the vagal afferent system.

3.2 Materials and methods

Animals

This protocol was approved by the Indiana University School of Medicine Animal Care and Use Committee and conducted in accordance with the "Guide for the Care and Use of Laboratory Animals". For a total of 8 months, male Ossabaw miniature swine were fed either an excess-calorie, atherogenic diet (KT-324, Purina Test Diet; Purina, Richmond, IN) (n = 3) and consequently became obese, or a standard chow diet (n = 3) and remained lean. All pigs were individually housed with a 12-hour light/dark cycle and free access to drinking water.

Tissue harvest

After conduction of the primary research project procedures under anesthesia, animals were euthanized by administration of sodium pentobarbital and subsequent removal of the heart. After collection of the carotid artery below the major bifurcation in the neck, the major bifurcation of the carotid artery was located and the right and left nodose ganglia were collected.

Tissue processing

Ganglia were were postfixed in 10% formalin for 24h at RT, then transferred to a 30% sucrose solution and stored at 4°C until sectioning. Ganglia were cut on a cryostat at 20 μm and mounted on Superfrost™ Plus Microscope Slides (Fisher Scientific, Pittsburgh, PA), with every fourth section mounted onto the same slide.

Nissl staining and immunohistochemistry

Nissl staining on one set of slides was performed using a standard cresyl violet staining protocol to visualize neurons and glia. To visualize the furin protein in the nodose ganglia, immunohistochemistry with an anti-furin antibody was performed on another set of slides. Briefly, antigen retrieval was performed by immersing the slides in sodium citrate buffer (Sodium Citrate Hydrochloride, Fisher Scientific and Tween 20, Sigma- Aldrich, Germany, pH 6.0) for 20 min in a water bath at 95°C, then allowed to cool while still immersed in the sodium citrate buffer solution for 30 min at RT. Slides were rinsed between each step in 1X PBS. Slides were incubated in blocking solution containing 0.3% Triton-X (Sigma-Aldrich, St. Louis, MO) and 3% Normal Donkey Serum (JacksonImmunoResearch, West Grove, PA) diluted in 1X PBS at RT for 1h. Sections were then incubated overnight in an anti-furin primary antibody (1:50, ab1831495, Abcam, San Francisco, CA) diluted in the blocking solution. Sections were incubated in a donkey anti-rabbit IgG H&L secondary antibody (1:500, ab6899, Abcam, San Francisco, CA) diluted in 1X PBS for 1h at RT. Sections were then incubated in an avidin–biotin complex (Vectastain Elite reagents, Vector Labs, Burlingame, CA) for 1h at RT. A diaminobenzidine-hydrogen peroxidase reaction was performed using a substrate kit (SK-4100, Vector Laboratories, Burlingame, CA). Sections were left at an angle to dry overnight and then dehydrated in a series of graded ethanols followed by xylenes. Slides were coverslipped with Permount mounting media (Fisher Scientific, Fair Lawn, NJ) and stored at RT.

Immunohistochemical testing in swine nodose ganglia

The nodose ganglion tissue was unable to be perfused due to the requirements of the primary research project, and thus, was lower quality than would be acceptable for a full investigation using this tissue. The following antibodies were tested in the tissue, with all antibody tests including sets with and without antigen retrieval: 1.) Anti-furin monoclonal antibody, ab1831495, Abcam, San Francisco, CA 2.) Anti-furin polyclonal antibody, ab28547, Abcam, San Francisco, CA 3.) Anti-furin polyclonal antibody, ab3467, Abcam, San Francisco and 4.) Anti-SirT1 polyclonal antibody, 13161-AP; ProteinTech, Rosemont, IL. The results of this antibody testing showed that only the ab28547 monoclonal antibody with antigen retrieval was suitable for ROI investigation, and thus this antibody and procedure was used for the above experiments. These findings may suggest that monoclonal antibodies with antigen retrieval are preferable for immunohistochemical procedures in swine nodose ganglion tissue.

Quantification

Intestinal tissue sections were visualized using a NanoZoomer Digital Pathology System (Hamamatsu, Hamamatsu City, Japan) using a 40x objective and NDP Scan software. Quantification was performed by visual inspection of the images on a desktop computer using NDP View 2 software by one individual that was blinded to the treatments. Neuron number and glial cell number per mm^2 were determined in slides that underwent a Nissl stain. Relative optical density was determined in slides that underwent immunohistochemical staining with an anti-furin primary antibody by using the measure function in ImageJ.

Statistical analysis

All variables were analyzed using Number Crunching Statistical Software (NCSS LLC, Kaysville, UT). Results were expressed as Mean ± SEM (n = 2-3). Measures of differences between lean and obese groups in neuron density, glial cell density, or furin ROI were performed for each ganglion (left or right) using Student's t tests. Assumptions of normality, homogeneity of variance, and independence were met. Differences between groups were considered statistically significant if $p < 0.05$.

3.3 Results

Effect of obesity on neuron density in the nodose ganglion

Obesity increased neuron density in the left nodose ganglion compared with lean animals (Fig. 5A). However, there was no effect of obesity on neuron density in the right nodose ganglion (Fig. 5B).

Effect of obesity on glial cell density in the nodose ganglion

There was no effect of obesity on glia cell density in the left (Fig. 6A) or right (Fig. 6B) nodose ganglion.

Effect of obesity on furin protein relative optical density in the nodose ganglion

There was no effect of obesity on furin protein relative optical density (ROI) in the left (Fig. 7A) or right (Fig. 7B) nodose ganglion.

3.4 Conclusions

These findings suggest that obesity increases neuron number in the left nodose ganglion. This increase in neuron number may be a result of neural proliferation. Neural proliferation in the adult nodose ganglion has been demonstrated after injury (Gallaher, Ryu, Larios, Sprunger, & Czaja, 2011), and our findings may add obesity as the second phenomenon capable of inducing this effect. Interestingly, the effect was seen in the left nodose ganglion, but not the right. As the left nodose ganglion innervates a disproportionately high level of the GI tract compared with the right nodose ganglion (Berthoud, Patterson, Neumann, & Neuhuber, 1997; Wang & Powley, 2000), the lateralization of this effect may be linked to greater amounts of GI sensory stimuli sent to the left nodose ganglion. Despite these interesting results, further experiments must be pursued to increase power and confirm findings from this pilot experiment.

3.5 Figures and captions

Figure 5

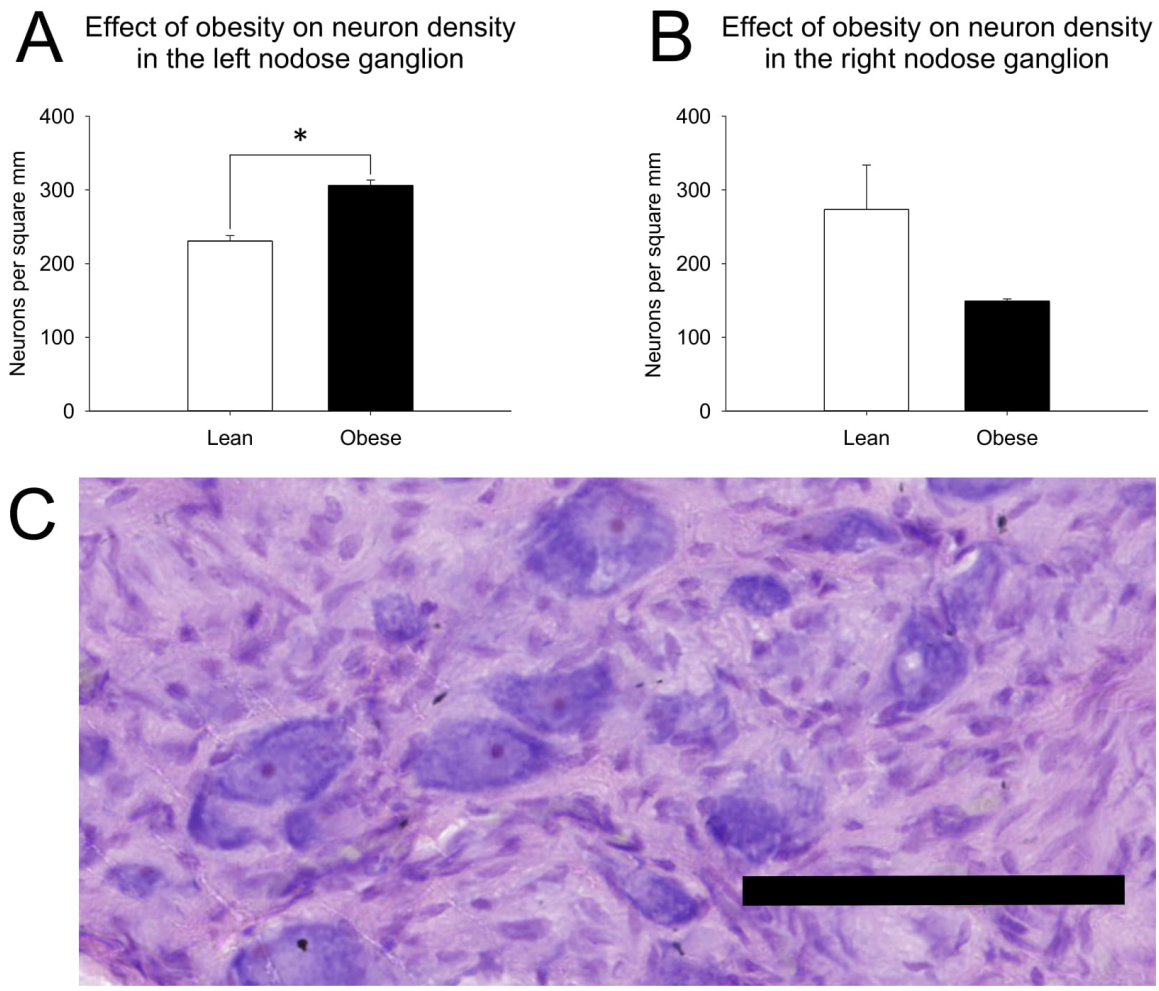

Figure 5. **Effect of obesity on neuron density in the nodose ganglion.** Obesity increases neuron density in increased in the left nodose ganglion (A), but there is no effect of obesity on neuron density in the right nodose ganglion (B). Representative image of Nissl stained tissue used to quantify neuron and glial cell density (C), scale bar, 100 µm.

Figure 6

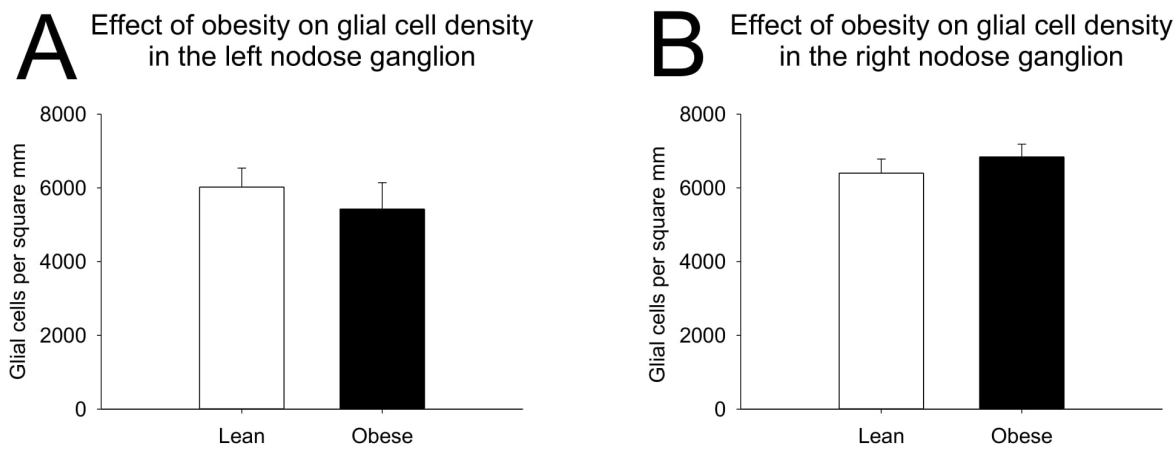

Figure 6. **Effect of obesity on glial cell density in the nodose ganglion.** There is no effect of obesity on glial cell density in the left (A) or right (B) nodose ganglion.

Figure 7

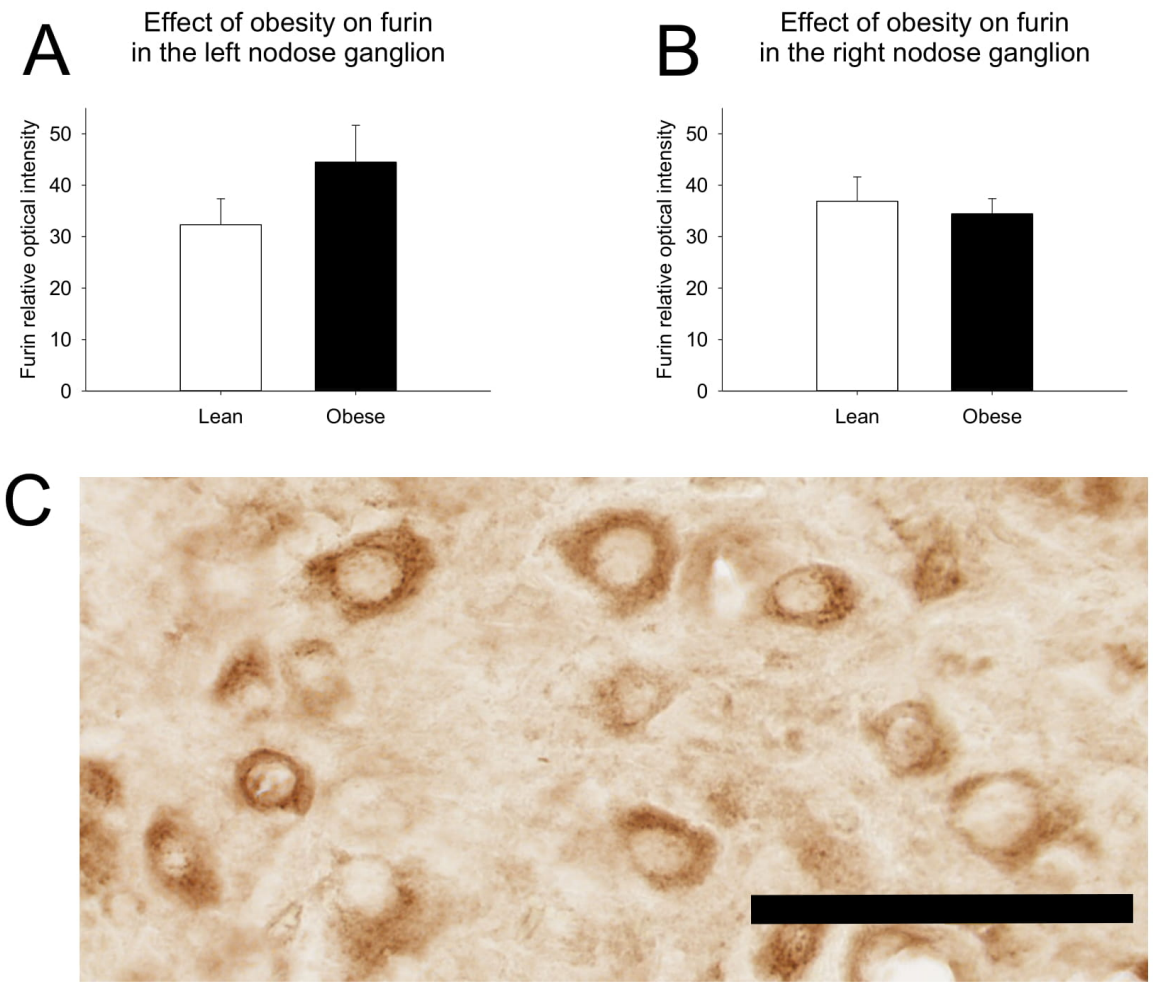

Figure 7. **Effect of obesity on furin relative optical intensity in the nodose ganglion.** There is no effect of obesity on furin relative optical density (ROI) in the left (A) or right (B) nodose ganglion. Representative image of tissue with furin immunohistochemistry used to quantify furin ROI (C), scale bar, 100 µm.

3.6 References

Berthoud, H. R., Patterson, L. M., Neumann, F., & Neuhuber, W. L. (1997). Distribution and structure of vagal afferent intraganglionic laminar endings (IGLEs) in the rat gastrointestinal tract. *Anat Embryol (Berl), 195*(2), 183-191.

Gallaher, Z. R., Ryu, V., Larios, R. M., Sprunger, L. K., & Czaja, K. (2011). Neural proliferation and restoration of neurochemical phenotypes and compromised functions following capsaicin-induced neuronal damage in the nodose ganglion of the adult rat. *Front Neurosci, 5*, 12. doi:10.3389/fnins.2011.00012

Wang, F. B., & Powley, T. L. (2000). Topographic inventories of vagal afferents in gastrointestinal muscle. *J Comp Neurol, 421*(3), 302-324.

CHAPTER 4: EVIDENCE FOR A DIRECT EFFECT OF THE AUTONOMIC NERVOUS SYSTEM ON INTESTINAL EPITHELIAL STEM CELL PROLIFERATION

(Published in Physiological Reports; Citation: Davis EA, Zhou W & Dailey MJ (2018). Evidence for a direct effect of the autonomic nervous system on intestinal epithelial stem cell proliferation. *Physiol Rep* **6,** e13745.)

4.1 Abstract

The sympathetic (SNS) and parasympathetic (PNS) branches of the autonomic nervous system have been implicated in the modulation of the renewal of many tissues, including the intestinal epithelium. However, it is not known whether these mechanisms are direct, requiring an interaction between autonomic neurotransmitters and receptors on proliferating epithelial cells. To evaluate the existence of a molecular framework for a direct effect of the SNS or PNS on intestinal epithelial renewal, we measured gene expression for the main autonomic neurotransmitter receptors in this tissue. We separately evaluated intestinal epithelial regions comprised of the stem, progenitor, and mature cells, which allowed us to investigate the distinct contributions of each cell population to this proposed autonomic effect. Notably, we found that the stem cells expressed the receptors for the SNS-associated alpha2A adrenoreceptor and the PNS-associated muscarinic acetylcholine receptors (M1 and M3). In a separate experiment, we found that the application of norepinephrine or acetylcholine decreases the expression of cyclin D1, a gene necessary for cell cycle progression, in intestinal epithelial organoids compared with controls ($p < 0.05$). Together, these results provide evidence of a direct mechanism for the autonomic nervous system influence on intestinal epithelial stem cell proliferation.

4.2 Introduction

The intestinal epithelium is critical for nutrient absorption, hormone release, and immune barrier function. In order to maintain proper tissue function, intestinal epithelial cells undergo rapid turnover, a

process that is driven by proliferating intestinal epithelial stem cells in the crypt (Barker *et al.*, 2007). The stem cells divide to produce transit amplifying (TA) progenitor cells, which proliferate and differentiate as they migrate up the crypt. Once they reach the base of the villus, these cells are fully differentiated, and will serve their mature functions until eventually undergoing apoptosis at the villus tip (Fig. 8). Both branches of the autonomic nervous system (ANS) have been implicated in the control of this turnover process, as denervation (surgical or chemical) of either sympathetic (SNS) or parasympathetic (PNS) nerves to the intestine alters intestinal epithelial cell proliferation (Tutton & Helme, 1974; Musso *et al.*, 1975a; Tsibulevskii & Orlova, 1976; Lachat & Goncalves, 1978; Kennedy *et al.*, 1983; Callaghan, 1991). However, it is not known if these changes occur via direct or indirect mechanisms. Previous studies may have detected indirect effects on proliferation due to post denervation-induced changes in food intake, inflammation, or other factors that can alter intestinal epithelial cell proliferation (Dailey, 2014; Slater *et al.*, 2017). In contrast, a direct effect could potentially be driven by autonomic neurotransmitters binding to receptors localized on proliferating cells of the intestinal epithelium. SNS and PNS neurotransmitter receptors are expressed by cells of the intestinal epithelium (Valet *et al.*, 1993; Greig & Cowles, 2017b) and mediate various epithelial functions (e.g., fluid transport and hormone release) (Greenwood *et al.*, 1987; Rocca & Brubaker, 1999), but whether the stem cells or TA cells express these receptors and mediate changes in the cell cycle has not been investigated. Because a direct effect of the SNS and PNS has been shown to alter the regeneration of other tissues [e.g., liver (Cruise *et al.*, 1985; Oben *et al.*, 2003a)], we postulate that the SNS and PNS could modulate intestinal epithelial regeneration through direct control of the cell cycle downstream of neurotransmitter receptors.

To determine if the main neurotransmitters for the SNS and PNS, norepinephrine (NE) and acetylcholine (ACh), can mediate a direct action on the proliferating cells of the intestinal epithelium, we evaluated gene expression for the alpha2A adrenoreceptor (*Adra2a*) and the muscarinic acetylcholine receptors M1-M5 (*Chrm1-5,* also known as cholinergic receptor muscarinic 1-5), which were selected due to previous studies localizing them within the intestine and implicating them in control of proliferation

(Valet *et al.*, 1993; Schaak *et al.*, 2000; Greig & Cowles, 2017b). We analyzed the expression of these receptors in the two major regions of the intestinal epithelium, the crypts (where the proliferating cells reside) and the villi (where the mature cells reside) in mice. Then, we further analyzed whether crypt cell receptor expression occurred in the stem cells or the other non-stem crypt cells (the vast majority of which are the TA cells). In addition, to investigate the presence of the molecular framework for the autonomic nervous system to influence intestinal epithelial turnover, we also investigated whether NE or ACh could induce changes in the cell cycle. We used intestinal epithelial organoids grown *in vitro* to measure the response of NE or ACh on the expression of cyclin D1 (*Ccnd1*), which is critical for the progression of the cell cycle from G1 to the S phase and remains at high levels until the end of mitosis. Both alpha2A adrenoreceptor and muscarinic acetylcholine receptor signaling have been linked to changes in cyclin D1 in other tissues, resulting in changes in the cell cycle and/or proliferation (Arredondo *et al.*, 2003; Karkoulias & Flordellis, 2007; Braga *et al.*, 2013; Peng *et al.*, 2013). Thus, these experiments begin to describe the molecular components and physiology through which a direct ANS control of stem cell proliferation and tissue regeneration may occur.

4.3 Materials and methods

Ethical Approval

All procedures were approved by the Institutional Animal Care and Use Committee at the University of Illinois at Urbana-Champaign, which operates under the Association for Assessment and Accreditation of Laboratory Animal Care International guidelines.

Animals

Adult male Lgr5-GFP (B6.129P2-Lgr5tm1(cre/ERT2)Cle/J; n = 3 for receptor expression experiment) and wild type (C57BL/6J; n = 3 for the receptor expression experiment and n = 3 for the proliferation-related gene expression experiment) mice were used (Jackson Laboratory, Bar Harbor, ME). These transgenic animals were selected for their global and constitutive expression of a green fluorescent protein tag on the intestinal epithelial stem cell marker Lgr5 (Barker *et al.*, 2007). An n = 3 mice per

group was chosen based on previously published data investigating mRNA expression differences between IESCs and other crypt cells (Mustata *et al.*, 2011; Akcora *et al.*, 2013; Tsai *et al.*, 2014; Kechele *et al.*, 2017; Zhou *et al.*, 2018). Animals were single housed in shoebox cages and maintained with *ad libitum* access to tap water and laboratory chow (Teklad 22/5, Envigo, Madison, WI) on a 12:12 light:dark cycle (lights on 0700) in a climate-controlled room (temperature = 21±2°C and humidity = 50±10%).

Isolation of small intestinal crypts and villi

Small intestinal crypts were isolated as previously described (Sato & Clevers, 2013; Zhou *et al.*, 2018). Briefly, the animals were anesthetized under 3% isoflurane at 1.5L/min in an anesthesia induction chamber and then decapitated. The entire small intestine was harvested, opened longitudinally and washed with cold 1x PBS to remove luminal contents. The villi were scraped off with a coverslip. Villi from the wild type mice (biological replicates, n = 3) were collected into a falcon tube, and centrifuged at 300 g at 4°C for 5 min. The supernatant was removed and the pellet containing the villus cells was immediately stored at -80°C to await processing. The remaining intestinal tissue was cut into 2-4 mm pieces with scissors and washed 5-10 times with cold 1x PBS until the supernatant was almost clear. Tissue fragments were incubated with 2 mM EDTA (Fisher Scientific, Pittsburgh, PA) and gently rocked at 4°C for 30 min. After removal of EDTA, tissue fragments were washed with 1x PBS 3 times. The supernatant was then collected and passed through a 70-um cell strainer (Corning, Corning, NY) and centrifuged at 300 g at 4°C for 5 min. The cell pellet was resuspended with basal culture medium [Advanced DMEM/F-12 Medium (Gibco, Grand Island, NY) containing 2 mM GlutaMax (Gibco, Grand Island, NY), 10 mM HEPES (Gibco, Grand Island, NY) and 100 U/mL Penicillin-Streptomycin (Gibco, Grand Island, NY)] and centrifuged at 300 g 4°C for 5 min. The supernatant was removed. The isolated crypts from the wild type mice (biological replicates, n = 3) were immediately stored at -80°C to await processing. The isolated crypts from the Lgr5-GFP mice (biological replicates, n = 3) were used for intestinal epithelial stem cell isolation (see *Isolation of IESCs*). Both sets of samples were then processed

to evaluate gene expression (see *Quantitative real time polymerase chain reaction*). Isolated crypts from the second set of wild type mice were grown into organoids (see *Organoid growth*).

Isolation of IESCs

Isolated crypts from Lgr5-GFP mice were resuspended with single cell dissociation medium [basal culture medium containing 1x N2 (Gibco, Grand Island, NY), 1x B27 (Gibco, Grand Island, NY) and 10 uM Y-27632 (Sigma-Aldrich, St. Louis, MO)] at 37 °C for 40 min. During incubation, the cell suspension was resuspended every 10 min. Dissociated cells were passed through a 40-um cell strainer (pluriSelect, Leipzig, Germany), followed by a 20-um cell strainer (pluriSelect, Leipzig, Germany) and centrifuged at 300 g at 4 °C for 5 min. Single, live IESCs were sorted as GFP^{high} (stem cells) or GFP^{low} (other crypt cells) by fluorescence-activated cell sorting (FACS) with a BD FACS ARIA II sorter into single cell dissociation medium as previously defined cell populations (Sato & Clevers, 2013). Dead cells were excluded from the FACS with the viability dye propidium iodide (Invitrogen, Carlsbad, CA). Sorted cells were centrifuged at 300 g 4°C for 5 min, supernatants were removed, and the pellet was immediately stored at -80°C to await processing for qPCR (see *Quantitative real-time polymerase chain reaction)*.

Organoid growth

After the final centrifugation in the crypt isolation process, the supernatant was removed and crypts were re-suspended in Matrigel (Corning Inc., Corning, NY) and plated in triplicate (three technical replicates (i.e., wells) per treatment from each biological replicate) onto a pre-warmed 24-well plate. Matrigel-crypt mix was applied to the center of each well and then allowed to solidify for 10 minutes in a 37°C incubator. Once the Matrigel solidified, 500 µL of IntestiCult Organoid Growth Medium (StemCell Technologies, Cambridge, MA) was added per well. Media were changed after 4 days of growth. After 5 days of growth, organoids received one of 3 treatments: 1 µM norepinephrine (A0937, Sigma Aldrich, St. Louis, MO), 1 µM acetylcholine (A2261, Sigma Aldrich, St. Louis, MO), or a vehicle control. The physiological neurotransmitters of the ANS were used instead of pharmacological agents targeting specific autonomic neurotransmitter receptors in order to most closely mimic the *in vivo* physiology of

this system. Doses were chosen based on other studies demonstrating NE- or ACh-induced proliferation in other cell types *in vitro* (Cruise *et al.*, 1985; Oben *et al.*, 2003a; Oben *et al.*, 2003b; Liu *et al.*, 2014b; Liu *et al.*, 2017). 24 hours after treatment administration, Matrigel was dissolved using 1 mL QIAzol (QIAGEN; Germantown, MD), the cells vortexed, and stored at -80°C to await processing (see *Quantitative real-time polymerase chain reaction).*

Quantitative real-time polymerase chain reaction (qPCR)

Total RNA was extracted from samples using RNeasy Plus Universal Mini Kit (Qiagen, Hilden, Germany). RNA was reverse transcribed to cDNA using QuantiTect Reverse Transcription Kit (Qiagen, Hilden, Germany). qPCR was performed with TaqMan Universal PCR Master Mix (Applied Biosystems, Foster City, CA) and TaqMan probes (Applied Biosystems, Foster City, CA) using Applied Biosystems QuantStudio™ 7 Flex Real-Time PCR System. Negative reverse-transcribed samples were generated and all reactions were carried out in triplicate. Technical triplicates were generated from each biological sample in the autonomic neurotransmitter gene expression experiment, and from each cell culture well in the experiment using organoids. The following TaqMan probes were used: *Adra2a*: Mm00845383_s1, *Chrm1*: Mm00432509_s1, *Chrm2*: Mm01701855_s1, *Chrm3*: Mm00446300_s1, *Chrm4:* Mm00432514_s1*, Chrm5:* Mm01701883_s1, *Ccnd1:* Mm00432359_m1, *Gapdh*: Mm99999915_g1. To determine relative expression values, the 2-ΔΔCt method was used, where triplicate Ct values for each sample were averaged and subtracted from those derived from GAPDH.

Confirmation of compliance

The investigators understand the ethical principles under which *Experimental Physiology* operates. This work complies with the animal ethics checklist outlined in 'Principles and Standards for Reporting Animal Experiments in *Experimental Physiology*.

Data analysis

All variables were analyzed using Number Crunching Statistical Software (NCSS LLC, Kaysville, UT). Data were expressed as fold change compared to control, and are expressed as mean fold

change ± SD. Two-tailed independent two-sample student's t-tests were used to determine differences between: 1) *Adra2a* expression in villi versus crypts, 2) *Chrm1* expression in villi versus crypts, 3) *Chrm3* expression in villi versus crypts, 4) *Chrm4* expression in villi versus crypts, 5) *Adra2a* expression in stem cells versus other crypt cells, 6) *Chrm1* expression in stem cells versus other crypt cells 7) *Chrm3* expression in stem cells versus other crypt cells, 8) *Ccnd1* expression between NE treatment and control, and 9) *Ccnd1* expression between ACh treatment and control. Assumptions of normality, homogeneity of variance, and independence were met. No inclusion or exclusion criteria were applied to the datasets. Differences were considered to be statistically significant at $p < 0.05$.

4.4 Results

Autonomic neurotransmitter receptor expression in the intestinal epithelial crypts and villi

We found that the crypts expressed *Adra2a* (122.3-fold $\pm$ 45.8), *Chrm1* (26.4-fold $\pm$ 0.8), *Chrm3* (17.2-fold $\pm$ 8.4), and *Chrm4* (2.4-fold $\pm$ 0.7), but there was no detectable expression of *Chrm2* nor *Chrm5* (Fig. 9). We found that the villi expressed *Adra2a* (2.4-fold $\pm$ 0.7), *Chrm1* (6.2-fold $\pm$ 0.2), *Chrm2* (1.0-fold $\pm$ 0.7), *Chrm3* (5.1-fold $\pm$ 0.4), and *Chrm4* (3.6-fold $\pm$ 0.7), but there was no detectable expression of *Chrm5* (Fig. 9). *Adra2a* was expressed at higher levels in the crypt compared with the villi ($p = 0.015$; crypt: 122.3-fold $\pm$ 45.8 versus villi: 2.4-fold $\pm$ 0.7, estimated difference: 119.9-fold, 95% confidence limits of difference: $78.4 \leq d \leq 161.5$; Fig. 9). Similarly, *Chrm1* was also expressed at higher levels in the crypt compared with the villi ($p = 2.0 \times 10^{-6}$; crypt: 26.4-fold $\pm$ 0.8-fold versus villi: 6.2-fold $\pm$ 0.2 estimated difference: 20.2-fold, 95% confidence limits of the difference: $18.9 \leq d \leq 21.6$, Fig. 9).

Autonomic neurotransmitter receptor expression in intestinal epithelial stem cells and other crypt cells

We found that the stem cells expressed *Adra2a* (13.5-fold $\pm$ 2.8), *Chrm1* (5.9-fold $\pm$ 0.9), and *Chrm3* (3.0-fold $\pm$ 2.0) (Fig. 10). We found that the other crypt cells also expressed *Adra2a* (6.4-fold $\pm$ 2.0), *Chrm1* (4.9-fold $\pm$ 0.6), and *Chrm3* (1.0-fold $\pm$ 0.03) (Fig. 10). *Adra2a* was expressed in the stem cells to a higher level than the other crypt cells ($p = 0.022$; stem cells: 13.5-fold $\pm$ 2.8 versus other

crypt cells: 6.4-fold ± 2.0, estimated difference: 7.1-fold, 95 % confidence limits of the difference: 1.6 ≤ d ≤12.5, Fig. 10).

Effect of autonomic neurotransmitters on expression of a proliferation-related gene in intestinal epithelial organoids

NE decreased relative mRNA expression of *Ccnd1* in intestinal epithelial organoids compared with control (p = 0.037; NE: 0.78-fold ± 0.06 versus control: 1.0-fold ± 0.10, estimated difference: 0.21-fold, 95% confidence limits of the difference: 0.02 ≤ d ≤0.41, Fig. 11A). ACh decreased expression of *Ccnd1* intestinal epithelial organoids compared with control (p = 0.047; ACh: 0.77-fold ± 0.10 versus control: 1.0-fold ± 0.10, estimated difference: 0.23-fold, 95% confidence limits of the difference: 0.003 ≤ d ≤ 0.36, Fig. 11B).

4.5 Discussion

The present study determined that the SNS and PNS autonomic neurotransmitter receptors are expressed in the villus, crypt and stem cells of the intestinal epithelium. Notably, *Adra2a*, *Chrm1*, and *Chrm3* were expressed in both populations of proliferating cells, the stem cells and the TA cells. In addition, we found that application of NE or ACh decreased the expression of cyclin D1 in intestinal epithelial organoids. Together, these findings suggest that both the SNS and PNS may be capable of directly influencing intestinal epithelial cell proliferation by a direct modulation of the stem cells.

SNS and PNS nerves come in close contact with the intestinal epithelium, which supports the idea of a direct autonomic effect on intestinal epithelial cell proliferation and tissue renewal (Gabella & Costa, 1968; Bohorquez *et al.*, 2015). NE and ACh released from these terminals may bind to receptors on the stem cells and/or the TA cells to affect proliferation. Both NE and ACh have been shown to directly alter proliferation in other cell types, mediated through a variety of adrenoreceptor and muscarinic receptor subtypes (Cruise *et al.*, 1985; Geloen *et al.*, 1988; Bronnikov *et al.*, 1992; Oben *et al.*, 2003a; Oben *et al.*, 2003b; Liu *et al.*, 2014b; Sloniecka *et al.*, 2015; Morgan *et al.*, 2016; Liu *et al.*, 2017). However, in contrast to other organ systems, the gastrointestinal (GI) tract is innervated by the enteric nervous system

(ENS). The ENS makes synaptic contacts with both the SNS and PNS, but also provides intrinsic neural control of gastrointestinal functions independent of extrinsic innervation. Due to input from multiple neural systems, the source of neurotransmitters effecting changes in intestinal epithelial cells must be considered. All noradrenergic innervation of the GI tract is sympathetic, as the ENS does not utilize NE as a neurotransmitter (McConalogue & Furness, 1994). Thus, our results demonstrating that NE alters expression of cyclin D1 can be attributed exclusively to the SNS, without participation of enteric neurotransmission. In contrast, since ACh is both a PNS and ENS neurotransmitter, it is not possible to elucidate the effect of PNS versus ENS sources of ACh in the present experiment alone. However, considering PNS denervation alters intestinal epithelial cell proliferation despite enteric circuitry remaining intact (Musso *et al.*, 1975a; Tsibulevskii & Orlova, 1976; Lachat & Goncalves, 1978; Callaghan, 1991), it is plausible that the PNS participates in mediating intestinal epithelial cell proliferation via ACh signaling. Thus, our results support the narrative that the intestinal epithelium is among the tissues in which regeneration is under direct SNS and PNS control.

We found that both NE and ACh both decrease expression of cyclin D1 in intestinal epithelial cells *in vitro*. As the effects of the SNS and PNS are usually thought of as antagonistic, opposing effects of NE and ACh on cyclin D1 might be expected. However, a more nuanced description of the ANS includes cooperative function of the SNS and PNS on certain organs (e.g., sexual organs (Wehrwein *et al.*, 2016)). This SNS and PNS cooperation is also seen in regard to control of cell proliferation, as NE and ACh both increase proliferation of hepatic myofibroblastic stellate cells, reflecting the dual participation of the SNS and PNS in liver regeneration after injury (Oben *et al.*, 2003a; Oben *et al.*, 2003b). Similarly, the SNS and PNS may differentially coordinate suppression of intestinal epithelial cell proliferation *in vivo.* This may be a strategy for the ANS to inhibit proliferation during specific body states. When sympathetic tone is high, the SNS coordinates an overall decrease in energy and resources to the intestine (Browning & Travagli, 2014; Wehrwein *et al.*, 2016), which may subsequently limit the energy available for cell proliferation. In contrast, PNS tone is increased during digestion, which is

accompanied by increased cellular metabolism and subsequent reactive oxygen species (ROS) byproducts (Granger *et al.*, 2015). Because ROS induces DNA damage that can cause DNA synthesis errors, this may not be an ideal environment for cell proliferation (Oberreuther-Moschner *et al.*, 2005; Cadet & Wagner, 2013). Thus, by decreasing cyclin D1 expression under conditions of exceptionally high SNS or PNS tone, the ANS may be restricting progression of the cell cycle during physiological states that are unfavorable for proliferation. The present study also revealed which autonomic neurotransmitter receptors are expressed in proliferating cell populations of the intestinal epithelium, thus identifying candidates for mediation of this proposed direct effect of the ANS on proliferation. Previous research has shown that the disruption of these receptors can modulate proliferation. Intestinal epithelial cell proliferation is increased in transgenic mice with global knockouts of M1 (*Chrm1*) or M3 (*Chrm3*) compared with wild type controls (Greig & Cowles, 2017b). In addition, proliferation is altered in a CaCo2 cell line model of intestinal epithelial cells transfected to express the alpha2A adrenoreceptor (*Adra2a*) (Schaak *et al.*, 2000). The alpha2A adrenoreceptor receptor is traditionally thought of as a presynaptic receptor that modulates neurotransmission (Docherty, 1998). However, alpha2A adrenoreceptor localization on intestinal epithelial cells is, by definition, post-synaptic. Thus, these cells are poised to alter target cell function, as is seen with localization of alpha2A adrenoreceptor on pancreatic beta cells, which function to decrease insulin release (Fagerholm *et al.*, 2004; Rosengren *et al.*, 2010). Therefore, under homeostatic conditions, it is likely that the specific receptors we have identified on the stem cells and the TA cells are directly modulating proliferation via autonomic neurotransmitter signaling.

We can now use the results from this study as a framework to definitively demonstrate which specific proliferating cell subpopulation is driving these changes in proliferation-related events: the stem cells, the TA cells, or a combination of both cell types. Stem cell isolation techniques used in this paper can be further employed to answer these research questions, which will add to the understanding of the interactions between somatic stem cells and the autonomic nervous system. In addition, we can also reveal the exact intracellular signaling mechanisms that are causing changes in cyclin D1 downstream of

the autonomic neurotransmitter receptors. Our current results provide a foundation for in-depth exploration of neural control of stem cells in the intestinal epithelium, and can be expanded to investigate stem cells from other tissues throughout the body. Further research on this topic is necessary to elucidate the mechanistic details and physiological function of this phenomenon.

4.6 Figures and captions

Figure 8

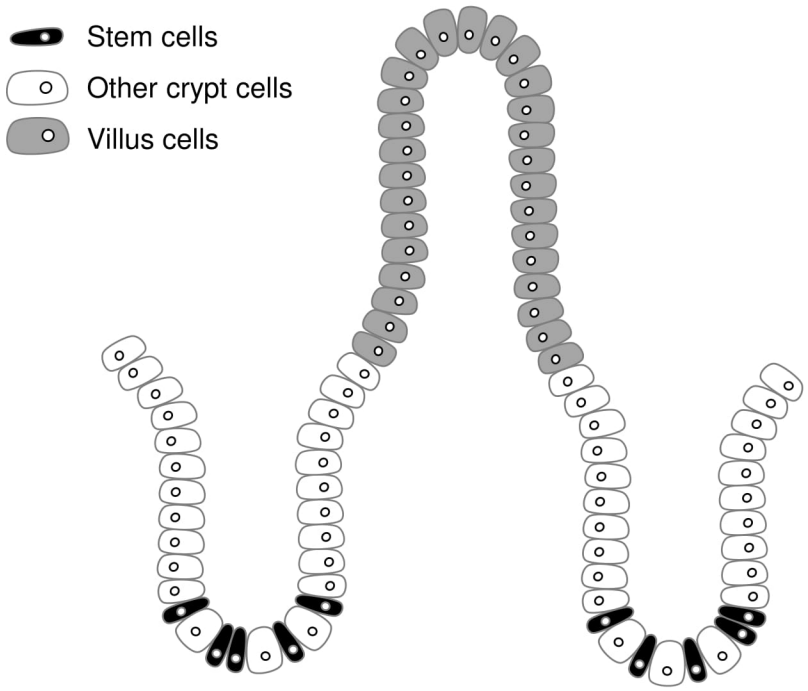

Figure 8. **Intestinal epithelial morphology.** Stem cells (black) reside at the base of the crypt. Other crypt cells (white) are primarily comprised of transit amplifying (TA) progenitor cells. The stem cells and TA cells proliferate to produce mature intestinal epithelial cells (gray), which reside in the villus and serve the major functions of the intestinal epithelium.

Figure 9

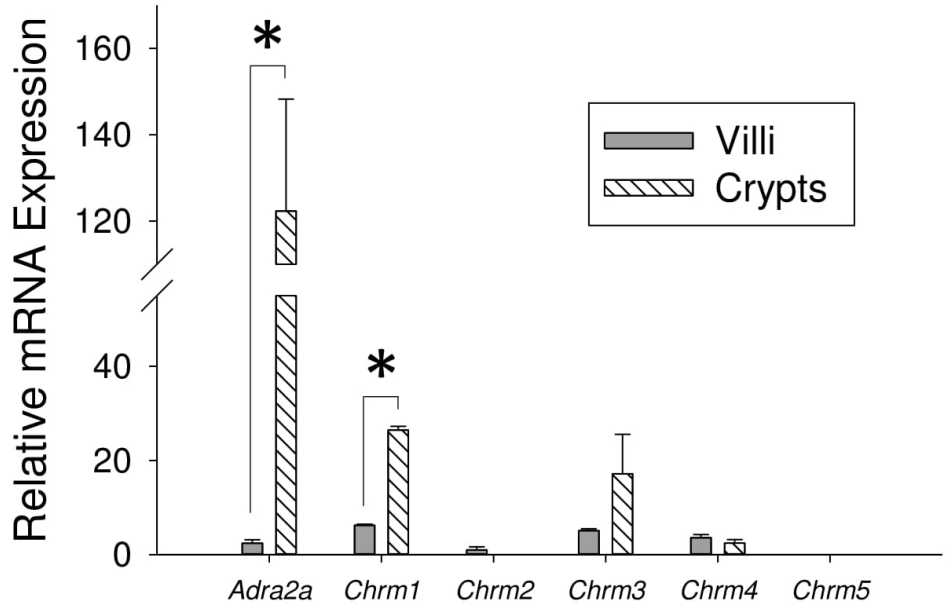

Figure 9. **Expression of autonomic neurotransmitter receptor genes in villus and crypt cells.** Relative mRNA expression of *Adra2a*, *Chrm1*, *Chrm2*, *Chrm3*, *Chrm4*, and *Chrm5* in the intestinal epithelial villi and crypts (n = 3, * $p < 0.05$).

Figure 10

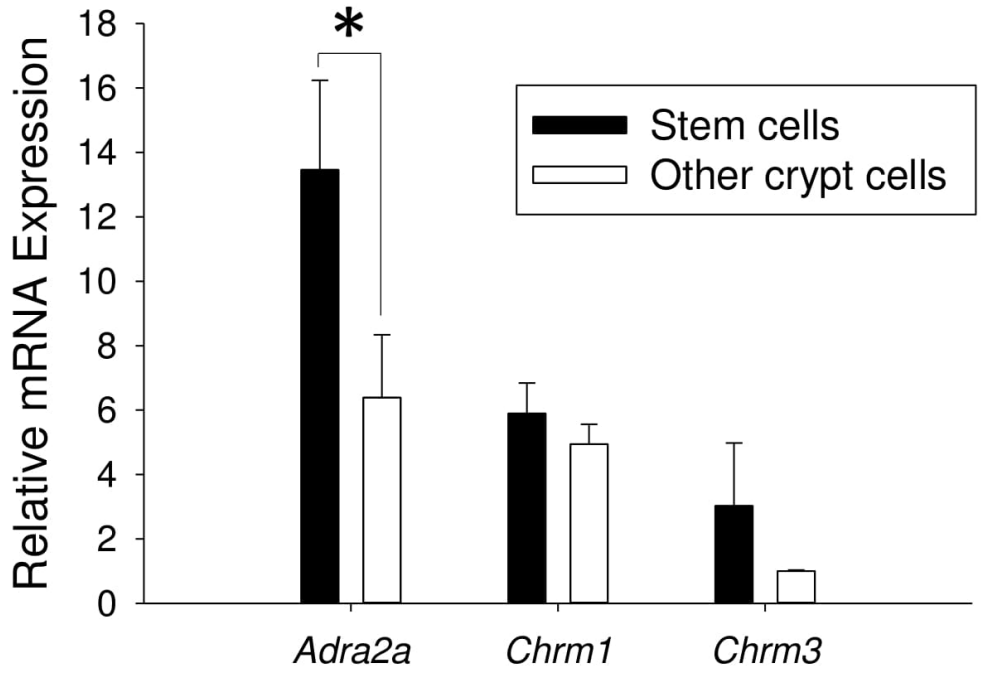

Figure 10. **Expression of autonomic neurotransmitter receptor genes in stem cells and other crypt cells.** Relative mRNA expression of *Adra2a*, *Chrm1*, and *Chrm3* in the intestinal epithelial stem cells and other crypt cells (n = 3, * $p < 0.05$).

Figure 11

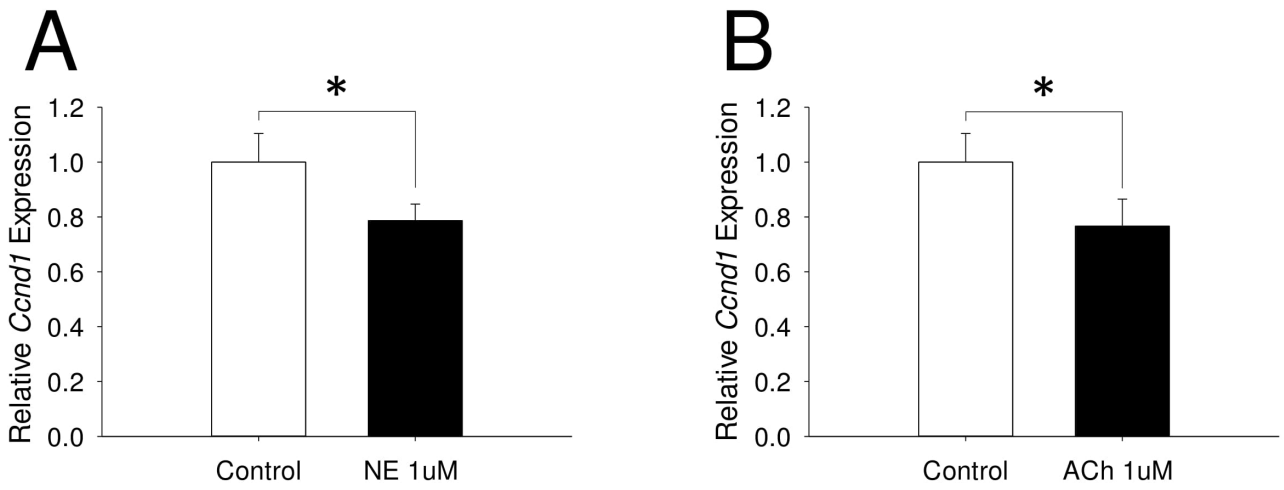

Figure 11. **Effect of autonomic neurotransmitters on expression of a proliferation-related gene in intestinal epithelial organoids.** (A) Effect of NE on relative *Ccnd1* mRNA expression in intestinal epithelial organoids compared with control (n = 3; * $p < 0.05$). (B) Effect of ACh on relative *Ccnd1* mRNA expression in intestinal epithelial organoids compared with control (n = 3; * $p < 0.05$).

4.7 References

Akcora D, Huynh D, Lightowler S, Germann M, Robine S, de May JR, Pollard JW, Stanley ER, Malaterre J & Ramsay RG (2013). The CSF-1 receptor fashions the intestinal stem cell niche. *Stem Cell Res* **10,** 203-212.

Arredondo J, Hall LL, Ndoye A, Chernyavsky AI, Jolkovsky DL & Grando SA (2003). Muscarinic acetylcholine receptors regulating cell cycle progression are expressed in human gingival keratinocytes. *J Periodontal Res* **38,** 79-89.

Barker N, van Es JH, Kuipers J, Kujala P, van den Born M, Cozijnsen M, Haegebarth A, Korving J, Begthel H, Peters PJ & Clevers H (2007). Identification of stem cells in small intestine and colon by marker gene Lgr5. *Nature* **449,** 1003-1007.

Bohorquez DV, Shahid RA, Erdmann A, Kreger AM, Wang Y, Calakos N, Wang F & Liddle RA (2015). Neuroepithelial circuit formed by innervation of sensory enteroendocrine cells. *J Clin Invest* **125,** 782-786.

Braga LE, Granja MG, da Silva GM, Giestal-de-Araujo E & dos Santos AA (2013). PMA increases M3 muscarinic receptor levels and decreases retinal cells proliferation through a change in the levels of cell-cycle regulatory proteins. *Neurosci Lett* **550,** 29-34.

Bronnikov G, Houstěk J & Nedergaard J (1992). Beta-adrenergic, cAMP-mediated stimulation of proliferation of brown fat cells in primary culture. Mediation via beta 1 but not via beta 3 adrenoceptors. *Journal of Biological Chemistry* **267,** 2006-2013.

Browning KN & Travagli RA (2014). Central nervous system control of gastrointestinal motility and secretion and modulation of gastrointestinal functions. *Compr Physiol* **4,** 1339-1368.

Cadet J & Wagner JR (2013). DNA base damage by reactive oxygen species, oxidizing agents, and UV radiation. *Cold Spring Harb Perspect Biol* **5**.

Callaghan BD (1991). The effect of pinealectomy and autonomic denervation on crypt cell proliferation in the rat small intestine. *J Pineal Res* **10,** 180-185.

Cruise JL, Houck KA & Michalopoulos GK (1985). Induction of DNA synthesis in cultured rat hepatocytes through stimulation of alpha 1 adrenoreceptor by norepinephrine. *Science* **227,** 749-751.

Dailey MJ (2014). Nutrient-induced intestinal adaption and its effect in obesity. *Physiol Behav* **136,** 74-78.

Gabella G & Costa M (1968). Adrenergic fibres in the mucous membrane of guinea pig alimentary tract. *Experientia* **24,** 706-707.

Geloen A, Collet AJ, Guay G & Bukowiecki LJ (1988). Beta-adrenergic stimulation of brown adipocyte proliferation. *Am J Physiol* **254,** C175-182.

Granger DN, Holm L & Kvietys P (2015). The Gastrointestinal Circulation: Physiology and Pathophysiology. *Compr Physiol* **5,** 1541-1583.

Greenwood B, Tremblay L & Davison JS (1987). Sympathetic control of motility, fluid transport, and transmural potential difference in the rabbit ileum. *Am J Physiol* **253,** G726-729.

Greig CJ & Cowles RA (2017). Muscarinic acetylcholine receptors participate in small intestinal mucosal homeostasis. *J Pediatr Surg*.

Karkoulias G & Flordellis C (2007). Delayed transactivation of the receptor for nerve growth factor is required for sustained signaling and differentiation by alpha2-adrenergic receptors in transfected PC12 cells. *Cell Signal* **19,** 945-957.

Kechele DO, Blue RE, Zwarycz B, Espenschied ST, Mah AT, Siegel MB, Perou CM, Ding S, Magness ST, Lund PK & Caron KM (2017). Orphan Gpr182 suppresses ERK-mediated intestinal proliferation during regeneration and adenoma formation. *J Clin Invest* **127,** 593-607.

Kennedy MF, Tutton PJ & Barkla DH (1983). Adrenergic factors involved in the control of crypt cell proliferation in jejunum and descending colon of mouse. *Clin Exp Pharmacol Physiol* **10,** 577-586.

Lachat JJ & Goncalves RP (1978). Influence of autonomic denervation upon the kinetics of the ileal epithelium of the rat. *Cell Tissue Res* **192,** 285-297.

Liu R, Zhang Q, Luo Q, Qiao H, Wang P, Yu J, Cao Y, Lu B & Qu L (2017). Norepinephrine stimulation of alpha1D-adrenoceptor promotes proliferation of pulmonary artery smooth muscle cells via ERK-1/2 signaling. *Int J Biochem Cell Biol* **88,** 100-112.

Liu TT, Ding TL, Ma Y & Wei W (2014). Selective alpha1B- and alpha1D-adrenoceptor antagonists suppress noradrenaline-induced activation, proliferation and ECM secretion of rat hepatic stellate cells in vitro. *Acta Pharmacol Sin* **35,** 1385-1392.

McConalogue K & Furness JB (1994). Gastrointestinal neurotransmitters. *Baillieres Clin Endocrinol Metab* **8,** 51-76.

Morgan ML, Sigala B, Soeda J, Cordero P, Nguyen V, McKee C, Mouraliderane A, Vinciguerra M & Oben JA (2016). Acetylcholine induces fibrogenic effects via M2/M3 acetylcholine receptors in non-alcoholic steatohepatitis and in primary human hepatic stellate cells. *J Gastroenterol Hepatol* **31,** 475-483.

Musso F, Lachat J-J, Cruz AR & Gonçalves RP (1975). Effect of denervation on the mitotic index of the intestinal epithelium of the rat. *Cell and Tissue Research* **163,** 395-402.

Mustata RC, Van Loy T, Lefort A, Libert F, Strollo S, Vassart G & Garcia MI (2011). Lgr4 is required for Paneth cell differentiation and maintenance of intestinal stem cells ex vivo. *EMBO Rep* **12,** 558-564.

Oben JA, Yang S, Lin H, Ono M & Diehl AM (2003a). Acetylcholine promotes the proliferation and collagen gene expression of myofibroblastic hepatic stellate cells. *Biochem Biophys Res Commun* **300,** 172-177.

Oben JA, Yang S, Lin H, Ono M & Diehl AM (2003b). Norepinephrine and neuropeptide Y promote proliferation and collagen gene expression of hepatic myofibroblastic stellate cells. *Biochem Biophys Res Commun* **302,** 685-690.

Oberreuther-Moschner DL, Rechkemmer G & Pool-Zobel BL (2005). Basal colon crypt cells are more sensitive than surface cells toward hydrogen peroxide, a factor of oxidative stress. *Toxicol Lett* **159,** 212-218.

Peng Z, Heath J, Drachenberg C, Raufman JP & Xie G (2013). Cholinergic muscarinic receptor activation augments murine intestinal epithelial cell proliferation and tumorigenesis. *BMC Cancer* **13,** 204.

Rocca AS & Brubaker PL (1999). Role of the vagus nerve in mediating proximal nutrient-induced glucagon-like peptide-1 secretion. *Endocrinology* **140,** 1687-1694.

Sato T & Clevers H (2013). Primary mouse small intestinal epithelial cell cultures. *Methods Mol Biol* **945,** 319-328.

Schaak S, Cussac D, Cayla C, Devedjian JC, Guyot R, Paris H & Denis C (2000). Alpha(2) adrenoceptors regulate proliferation of human intestinal epithelial cells. *Gut* **47,** 242-250.

Slater TW, Finkielsztein A, Mascarenhas LA, Mehl LC, Butin-Israeli V & Sumagin R (2017). Neutrophil Microparticles Deliver Active Myeloperoxidase to Injured Mucosa To Inhibit Epithelial Wound Healing. *J Immunol* **198,** 2886-2897.

Sloniecka M, Backman LJ & Danielson P (2015). Acetylcholine enhances keratocyte proliferation through muscarinic receptor activation. *Int Immunopharmacol* **29,** 57-62.

Tsai YH, VanDussen KL, Sawey ET, Wade AW, Kasper C, Rakshit S, Bhatt RG, Stoeck A, Maillard I, Crawford HC, Samuelson LC & Dempsey PJ (2014). ADAM10 regulates Notch function in intestinal stem cells of mice. *Gastroenterology* **147,** 822-834.e813.

Tsibulevskii A & Orlova EN (1976). [Physiologic regeneration of jejunal epithelium following bilateral subdiaphragmatic vagotomy in rats]. *Biull Eksp Biol Med* **81,** 236-237.

Tutton PJ & Helme RD (1974). The influence of adrenoreceptor activity on crypt cell proliferation in the rat jejunum. *Cell Tissue Kinet* **7,** 125-136.

Valet P, Senard JM, Devedjian JC, Planat V, Salomon R, Voisin T, Drean G, Couvineau A, Daviaud D, Denis C & et al. (1993). Characterization and distribution of alpha 2-adrenergic receptors in the human intestinal mucosa. *J Clin Invest* **91,** 2049-2057.

Wehrwein EA, Orer HS & Barman SM (2016). Overview of the Anatomy, Physiology, and Pharmacology of the Autonomic Nervous System. *Compr Physiol* **6,** 1239-1278.

Zhou W, Ramachandran D, Mansouri A & Dailey MJ (2018). Glucose stimulates intestinal epithelial crypt proliferation by modulating cellular energy metabolism. *Journal of cellular physiology* **233,** 3465-3475.

CHAPTER 5: EFFECT OF NOREPINEPHRINE ON INTESTINAL EPITHELIAL STEM CELL PROLIFERATION

PART I: Alpha$_{2A}$ adrenoreceptor influence on intestinal epithelial stem cell proliferation

PART II: Effect of norepinephrine on intestinal epithelial crypt cell proliferation

Chapter Introduction

The development of intestinal epithelial organoids has allowed primary cell culture of intestinal epithelial cells for the first time (Sato & Clevers, 2013). These organoids include all of the cell types of the intestinal epithelium found *in vivo*, including stem cells, progenitor cells, and mature cell types (e.g., enterocytes, enteroendocrine cells, goblet cells, paneth cells) (Sato & Clevers, 2013). Organoids are also able to recapitulate the crypt-villus morphology found *in vivo* when culturing using a 3-dimensional (3-D) matrix, which provides a scaffolding for this morphology to develop (Sato & Clevers, 2013). Despite being an innovative and physiologically relevant model, the use of organoids presents several issues when measuring proliferation compared with traditional cell culture methods. Below, we provide a description of each of these limitations and how they interfere with the most common methods to measure proliferation *in vitro*. We also describe the strategies we used to minimize variability in the subsequently presented experiments (Part I and Part II), which aimed to accurately measure the effect of norepinephrine on intestinal epithelial organoid proliferation.

A persistent problem with measuring proliferation in organoids is the inability to control for starting cell number between wells and rate of proliferation of these cells. To generate organoids *in vitro*, intestinal epithelial crypts are harvested, and these crypts remain in their aggregate cell clusters when plated. Although equal crypt numbers are plated in each well, these crypts vary in cell number and therefore it is impossible to control for equal cell number per well at the start of the experiment. This is in contrast to traditional cell culture protocols that use dissociated single cells, which can be plated using an accurate and equal number of cells per well. It is possible to isolate and plate equal numbers of stem cells,

which can ameliorate the cell number issue that is a limitation to working with crypts. However, after plating, both crypts and stem cells continually proliferate and grow into organoids, but these cells do not proliferate at equal rates. This also contributes to variability in experiments using organoids. Overall, these sources of variability may reduce the ability to detect differences in proliferation between experimental groups when performing experiments using organoids.

The 3-D matrix that is required to grow organoids can also interfere with proliferation measurements. These 3-D matrices mimic basement membranes in order to provide an extracellular matrix for the organoids to adhere to and use it as a scaffold to grow (Kleinman & Martin, 2005). As these matrices are biologics that contain proteins, they will produce background staining with the use of antibody-based methods of measuring proliferation. In addition, these proteins will cause the matrix to autofluoresce when using methods with fluorophores. Subsequently, unwanted staining may interfere with accurate quantification of cell proliferation in 3-D matrices. In addition, methods for measuring proliferation that require imaging of these 3-D matrix structures must rely on confocal microscopy to image the entire x, y and z-planes (Blackmore *et al.*, 2017). This adds an additional burden of time and specialized equipment in comparison to imaging of traditional 2-D cell cultures. Furthermore, due to the expansion and growth of these organoids in all directions within a 3-D space, it is impossible to track the growth of the same organoids over time. To address the issues surrounding quantification of proliferation of cells embedded in matrices, matrix dissociation and cell recovery is possible. However, this protocol requires time to release the organoids from the matrix (Nozaki *et al.*, 2016), and then requires the use of harsh dissociation buffers to dissociate the cells that may cause cell death (Miyoshi & Stappenbeck, 2013). Given this variety of limitations, it is clear that 3-D matrices require special consideration when selecting methods to measure proliferation.

There are a variety of methods to measure proliferation *in vitro*, with both direct and indirect methods available. Direct measurements of proliferation require the quantification of proliferative events in a cell population. A common method is the use of thymidine analogs, such as 5-bromo-2′-deoxyuridine

(BrdU) or 5-ethynyl-2′-deoxyuridine (EdU). These molecules replace thymidine nucleotides in DNA during synthesis. Following integration of the thymidine analog, the cells are labeled using antibody-based immunocytochemistry for BrdU, or click chemistry that affixes a fluorescent tag to EdU. Through this process, all cells that have undergone proliferation since the addition of the thymidine analog are identified and can be subsequently quantified (Cavanagh *et al.*, 2011). Other direct methods include antibody-based immunocytochemical labeling of proliferation markers, such as the protein Ki67 (Brown & Gatter, 1990). In context of the issues regarding measurement of proliferation in organoids described above, all of these direct methods would require either 1) time consuming 3-D confocal imaging and counting while navigating undesired background staining/autofluorescence from the matrix, or 2) matrix dissociation and subsequent evaluation with a live/dead assay followed by cell counting by flow cytometry or a coulter counter. For these reasons, indirect measures of proliferation are generally preferable when using organoids.

Metabolic proliferation assays are a popular method indirect measure of proliferation. These assays use tetrazolium salts, including MTT (3-(4,5-Dimethylthiazol-2-yl)-2,5-Diphenyltetrazolium Bromide), WST-1 (water soluble tetrazolium salt), or XTT (2,3-Bis-(2-Methoxy-4-Nitro-5-Sulfophenyl)-2H-Tetrazolium-5-Carboxanilide). These assays measure markers of cell metabolism as an indirect indicator of proliferation. The reagents produce a dye that directly correlates to the number of metabolically active cells in the culture, which can then be measured as an indirect measure of proliferation using a plate reader (Präbst *et al.*, 2017). Metabolic proliferation assays offer advantages when it comes to their use with 3-D matrices, as there is no need to image the cultures nor dissociate the cells. However, there is evidence that there are discrepancies between metabolic activity and cell proliferation (Maghni *et al.*, 1999; Quent *et al.*, 2010), which ultimately makes metabolic assays an unreliable choice for measuring proliferation.

Another indirect option for measuring proliferation is the use of a DNA-binding fluorescent dye. The amount of dye bound to DNA directly correlates to the total cell number, and therefore the dye

content in the sample can be measured by a plate reader to quantify total cell number as an indirect measure of proliferation (Jones *et al.*, 2001). This method is advantageous due to the ability to quantify proliferation in a high-throughput manner without imaging or dissociating the cells for further analysis. However, the autofluorescence of the matrigel when measuring DNA content with a fluorescent dye can artificially increase the measurement of total cell number. As in all of the proliferation techniques, the inability to control for initial cell number when using organoids adds to variability to the results of this assay. Despite these limitations, the DNA-binding fluorescent dye is the most suitable option for determining proliferation in organoids.

To determine the effect of norepinephrine on intestinal epithelial cell proliferation, we conducted two experiments using the CyQUANT proliferation assay, which uses a DNA-binding fluorescent dye to indirectly measure proliferation as described above (Jones *et al.*, 2001). These experiments are outlined in Chapter 5a and 5b. In both of the experiments, we controlled for the autofluorescence of the matrigel by plating a subset of matrigel blanks without any cells in them and then subtracting the average blank value from all of the experimental values. Furthermore, we reported our results in fold changes to standardize the variability within groups due to the inability to control for initial cell numbers. For the experiment in Chapter 5a, we used n = 3 mice to determine the effect of norepinephrine on organoid proliferation. Due to the high variability in the raw data of this experiment, we repeated a similar experiment in Chapter 5b and employed several techniques to reduce variability. In this second experiment, we doubled our animal numbers to n = 6, used crypts instead of organoids in order to reduce the variability in cell number that may result during growth of isolated crypts into organoids, and eliminated the contribution of dead cells to the total DNA content measurement by using a background suppression agent. We found different results in these two experiments, which we believe demonstrates the inaccuracy of measuring proliferation in intestinal epithelial organoids. Due to these discrepancies, we cannot make confident interpretations of these datasets at this time. We conclude that it is important to critically evaluate methods for measuring proliferation in organoids, as it is an often overlooked technical issue that can alter

results and interpretations of scientific research. Future technical advancements in this field will hopefully allow accurate data collection on proliferation from not only intestinal epithelial organoids, but organoids derived from all tissues.

PART I: ALPHA$_{2A}$ ADRENORECEPTOR INFLUENCE ON INTESTINAL EPITHELIAL STEM CELL PROLIFERATION

5.1 Abstract

The intestinal epithelium is critical for nutrient absorption, immune function, and hormone release. The mature cell types that are responsible for these functions are produced by crypt base columnar (CBC) stem cells located within the intestinal crypts. These stem cells constitutively divide to produce complete turnover of the entire intestinal epithelial layer every few days. The division of the CBC stem cells can be influenced by a variety of factors, including nutrient availability. There is research that suggests the sympathetic nervous system can contribute to changes in stem cell proliferation. However, it is not known whether this effect is direct via the CBC stem cells, or instead through an indirect mechanism. Thus, we tested whether CBC stem cells express alpha2A adrenoreceptors (α2A-ARs), a receptor subtype utilized by norepinephrine (NE; the primary neurotransmitter of the SNS) and whether NE induces proliferation of intestinal epithelial organoids in vitro. Results showed that α2A-ARs mRNA is expressed in CBC stem cells and that there is a trend towards higher expression of α2A-AR mRNA in CBC stem cells compared with other cells of the crypt. We also found a significant decrease in proliferation after application of NE to organoids in vitro ($p<.05$). These data support a role for the SNS in regulation of CBC stem cells proliferation, which may influence intestinal epithelial size and function as a whole.

5.2 Introduction

The intestinal epithelium is a single layer of cells that form the inner lining of the small intestine. The mature cells of the intestinal epithelium absorb nutrients (enterocytes), secrete hormones (enteroendocrine cells), and secrete mucus to create an immune barrier (goblet cells) (Schaak *et al.*, 2000). To replace these mature cells as they die off, crypt base columnar (CBC) intestinal epithelial stem cells located in the base of the crypt divide constitutively to produce daughter cells of each cell type. The

newly produced daughter cells, which are progenitor cells that are referred to as transit amplifying (TA) cells, differentiate and continue to divide as they migrate up the crypt. As these cells reach maturity, they move into the villi. When the cells reach the apex of the villus, they undergo apoptosis and are sloughed off into the lumen of the intestine. Via this process, complete turnover of the entire intestinal epithelial layer occurs every three to five days (van der Flier & Clevers, 2009). Consequently, proper CBC stem cell proliferation is critical to maintain the morphology and function of the entire intestinal epithelium.

The sympathetic nervous system (SNS), one of two branches of the autonomic nervous system (ANS), innervates the intestinal epithelium. Data has shown that the SNS may play a role in CBC stem cell proliferation. Specifically, our laboratory has found that surgical sympathectomy increases intestinal epithelial crypt cell proliferation in rats (Davis *et al.*, 2016). Others have also documented changes in crypt cell proliferation after partial ablation of the SNS nerves innervating the small intestine (Tutton & Helme, 1974). Despite these data demonstrating that the SNS is involved in regulating proliferation of crypt cells, it is not known if the SNS directly influences proliferation of the CBC stem cells themselves. The alpha2A adrenoreceptor (α2A-AR), a receptor subtype that binds the primary SNS neurotransmitter norepinephrine (NE) (Jacobowitz, 1965), has been localized within the intestinal epithelium, including in the crypt cells (Paris *et al.*, 1990). It is not known, though, whether this receptor is expressed by the CBC stem cells, providing a molecular mechanism for direct SNS influence. Thus, we hypothesized that: 1) α2A-AR mRNA is expressed in CBC stem cells and 2) application of NE to intestinal epithelial organoids will alter proliferation rate of intestinal epithelial cells compared to untreated controls. In order to test these hypotheses, we isolated CBC intestinal epithelial stem cells from mice and measured the gene expression of α2A-AR. We compared these mRNA levels of other crypt cells from the same mice in order to evaluate expression of the α2A-AR between intestinal epithelial cell populations. In a separate experiment, crypts were isolated from mice and grown into functioning intestinal epithelial organoids in order to test the proliferation of intestinal epithelial crypt cells in response to NE application. Together,

these experiments evaluated SNS influence on intestinal epithelial stem cell proliferation, which contributes to current knowledge of neural control of stem cells.

5.3 Materials and methods

Animal housing

Lgr5-GFP (B6.129P2-Lgr5tm1(cre/ERT2)Cle/J; The Jackson Laboratory) and C57BL/6J mice were single-housed in shoeboxcages. Animals were maintained on a 12:12 light:dark cycle with ad libitum access to food (Teklad 22/5 Rodent Diet 8640 (Envigo, Madison, WI) and tap water. All procedures were approved by the Institutional Animal Care and Use Committee of the University of Illinois Urbana-Champaign.

Crypt isolation

Small intestinal crypts were isolated from adult Lgr5-GFP and wild-type mice using a previously published protocol (Sato & Clevers, 2013). Briefly, mice were euthanized using decapitation under isoflurane (Phoenix, St. Joseph, MO). An incision was made at the base of the abdomen and extended up the sides to open the body cavity. The small intestine was located and removed, cutting at the level of the pyloric sphincter and the ileocecal sphincter. The small intestine was then cut into 10cm-long segments. An 18-gauge needle and syringe were used to flush the intestinal segments with ice-cold 1X phosphate-buffered saline (PBS) (Lonza, Walkersville, MD). The segments were then cut open longitudinally and scraped with glass coverslips to remove the villi. Sections were further cut into 2-4 mm fragments. The fragments were placed in a 1X PBS-filled 50 mL Falcon tube and washed by inverting the tube at least 10 times. The PBS was then removed and 30 mL Crypt Isolation Buffer (Promega, Madison, WI) was added to each tube and rocked for 30 minutes at 4°C. Samples were washed again with 1X PBS and then passed through a 70-µm cell strainer (Corning, Tewksbury, MA) and collected into 1% BSA-coated (Sigma-Aldrich, St. Louis, MO) 50 mL Falcon tube. Samples were centrifuged at 300 x g for 10 minutes at 4°C.

Single cell dissociation

After centrifugation, samples were re-suspended with single cell dissociation medium prepared as described in a previously published protocol (Sato & Clevers, 2013). The samples were passed through a 40-µm-cell strainer followed by a 20-µm cell strainer (PluriSelect, Leipzig, Germany). The cells were re-suspended in basal culture medium as described in a previously published primary cell culture protocol (Sato & Clevers, 2013). The samples were centrifuged twice at 300 x g for 5 minutes, and then re-suspended with single cell dissociation medium.

Flow cytometry

The isolated crypt cells were prepared for flow cytometry and FACS as described in a previously published protocol (Sato & Clevers, 2013). Briefly, dead cells were excluded using propidium iodide and intestinal crypt cell populations were sorted using a BD FACS ARIA II. Results were analyzed using a BD LSR II. The analyzed cells had a green fluorescent protein (GFP) tag on the Lgr5 receptor, which are highly expressed in CBC stem cells. Samples were sorted into two populations: high GFP expression (CBC stem cells) and low GFP expression (crypt cells other than CBC stem cells, including the Paneth and transit amplifying cells).

RNA isolation

RNA was extracted from each isolated cell population using the commercially available RNeasy Mini Kit (Qiagen, Valencia, CA). The RNA concentration was measured using a Nanodrop ND-1000 Spectrophotometer.

cDNA synthesis

The isolated RNA was amplified using a commercially available iScript cDNA Synthesis Kit following manufacturer's instructions (Bio-Rad, Hercules, CA). Samples were incubated in the PTC-100 Programmable Thermal Controller for 5 minutes at 25°C, 30 minutes at 42°C, then 5 minutes at 85°C.

Quantitative real-time PCR (qRT-PCR)

Alpha2A-AR mRNA expression was quantified by quantitative real time-PCR per manufacturer's instructions of the commercially available Taqman kit (Applied Systems, Foster City, CA). PCR Reaction Mix was made using Taqman Universal PCR Master Mix, Taqman Gene Expression Assay, and cDNA template + H2O. Expression of the α2A-AR was determined by the TaqMan probe and measured in the Applied Biosystems 7900HT Fast Real-Time PCR System. The expression of GAPDH was utilized a control. Each cell population was plated in triplicate. The following Taqman probes were used: α2A-AR: Mm00845383_S1 and GAPDH: Mm99999915_g1.

Organoid growth

A wild-type mouse was euthanized and intestinal epithelial crypts were isolated using the procedures previously described. After crypts were centrifuged for the final time, the supernatant was removed and crypts were re-suspended in Matrigel (Corning Inc., Corning, NY) and plated onto a pre-warmed 24-well plate. Matrigel-crypt mix was applied to the center of each well and then allowed to solidify for 10 minutes in a 37°C incubator. Once the Matrigel solidified, 500 µL of IntestiCult Organoid Growth Medium (StemCell Technologies, Cambridge, MA) was added per well. Media were changed every 3 days and cells were split after 7 days.

Organoid treatment with norepinephrine

After ten days of growth, organoids received one of three treatments: 1 µM norepinephrine, 10 µM norepinephrine, or a sterile deionized water vehicle control. The drugs were made from norepinephrine bitartrate salt (Sigma Aldrich, St. Louis, MO) dissolved in deionized water. At 0h, 2h, 4h and 6h after administration of the respective drug treatment; proliferation was assayed using the CyQUANT NF Cell Proliferation Assay Kit (Thermo-Fischer, Austin, TX). One hour before the desired time point, a dye binding solution was added in order to bind the cellular DNA. The fluorescence intensity of each of the samples was measured using a Monochromator based absorbance 96 and 384-well

plate reader with excitation at ~485 nm and emission detection at ~530 nm. The higher the intensity of the fluorescence, the more DNA is bound indicating higher numbers of cells.

Data analysis

Results were expressed as mean ± SEM. Gene expression for α2A-AR was analyzed using Student's t-test using Number Crunching Statistical Software (NCSS). Proliferation was analyzed using one-way analyses of variance (ANOVA) using NCSS. Each time point of the experiment was analyzed independently and not compared across time points because different cells are used at each time point. Assumptions of normality, homogeneity of variance, and independence were met. Tukey-Kramer post hoc analysis was utilized where appropriate. Differences between treatments were considered statistically significant if $p<0.05$.

5.4 Results

Alpha2A adrenoreceptor mRNA expression

Alpha2A adrenoreceptor mRNA is expressed in CBC stem cells (Fig. 12). Although there was no significant difference in α2A-AR mRNA between the CBC stem cells and the other crypt cells (not including CBC stem cells), there is a trend toward increased α2A-AR mRNA expression in the CBC stem cells compared to the other crypt cells (Fig. 12; $p = 0.06$). Further, we also confirmed the expression of alpha2A adrenoreceptor mRNA in a separate population of crypt cells that were not divided into different cell types (Fig. 13).

Organoid response to the addition of norepinephrine

Application of NE significantly decreased the proliferation rate of intestinal epithelial organoids at the 2-hour time point (Fig. 14; $p<.05$). No other time points showed a significant change in the proliferation rate.

5.5 Discussion

Our data revealed that CBC stem cells express α2A-AR mRNA and that intestinal epithelial organoids in vitro decrease proliferation in response to NE. Together, these experiments demonstrate a

mechanism through which the SNS may be directly influencing intestinal epithelial stem cell proliferation.

When we investigated the expression of α2A-AR mRNA in all crypt cells, we found greater expression of α2A-AR in the stem cells compared with other crypt cells. This finding suggests that the SNS may have a greater influence on the stem cells through this receptor when compared with other crypt cells. Further, a low (1μM) dose of NE decreased proliferation of organoids 2h after application. These data suggest that an increase in SNS influence may lead to a decrease in proliferation rate in the intestinal epithelial cells, perhaps through α2A-AR signaling. Since α2A-ARs are typically defined as inhibitory receptors, activating this receptor with NE would likely suppress proliferation. This idea is consistent with our results showing that intestinal epithelial organoids decrease proliferation in response to NE.

In a separate study, our laboratory has also demonstrated that the in vivo denervation of the SNS in rats leads to an increase in intestinal epithelial cell proliferation rate (Davis *et al.,* 2016). This finding complements the present in vitro data from the current study because it suggests that decrease in SNS influence leads to an increase in proliferation of intestinal epithelial crypt cells.

Our data reveal interesting trends with respect to the time points and concentration of NE application. After addition of NE to intestinal epithelial organoids, we see a significant decrease in proliferation at the 2h time point. However, there was no significant difference in proliferation at the 4h or 6h time points. It can be inferred that a significant decrease in proliferation was seen at the 2h time point and not the 4h or 6h time points because neurotransmitters have a short reaction time (Straub *et al.*, 2006). Although normally this reaction time is within seconds of NE application, it takes time for an effect to take place. Signal transduction and activation of cellular pathways involved in decreasing cell proliferation take time to act. Additionally, the time for cell number to significantly decrease requires time. Normally, the intestinal epithelial tissue compensates for cell loss by proliferating, thus the number of cells should remain the same. This trend is displayed in Figure 14, with each of the control populations remaining around a similar value. At the 4h and 6h time points, the organoids have had enough time to

recover population size after the decrease in proliferation. This is demonstrated by the lack of significant differences in organoid cell number at these time points. In order to further explore the duration of NE's effect on organoid proliferation, shorter time points can be investigated in future experiments.

Another interesting finding showed that only the application of the 1 μM concentration of NE lead to a significant decrease in proliferation, whereas the 10 μM concentration of NE did not. This may be explained by the fact that there are only a limited number of receptors available for the NE to bind, meaning that a higher concentration of NE does not necessarily yield a larger suppression of proliferation. This trend can be further explored with more trials that utilize multiple different concentrations of NE.

We would like to continue to pursue research on SNS influence of CBC stem cell proliferation by studying intracellular signaling downstream of alpha2A adrenoreceptor activation. The α2A-AR is a G-protein receptor that has been linked to the inhibition of cAMP production (Schaak *et al.*, 2000). Inhibition of cAMP production can in turn alter the MAPK pathway, which is linked to regulation of proliferation (Schaak *et al.*, 2000). By understanding the molecular mechanism underlying our data showing changes in proliferation rate, it may be possible to manipulate the pathway in order to alter CBC stem cell proliferation for therapeutic purposes.

5.6 Conclusions

Our data support a role for direct neural control of intestinal epithelial stem cells, a topic which has not yet been extensively explored in existing scientific literature. By continuing to evaluate the effects of the SNS on CBC stem cell proliferation, we can better understand how changes in neural function can alter our intestine, further establishing the gut-brain axis.

5.7 Figures and captions

Figure 12

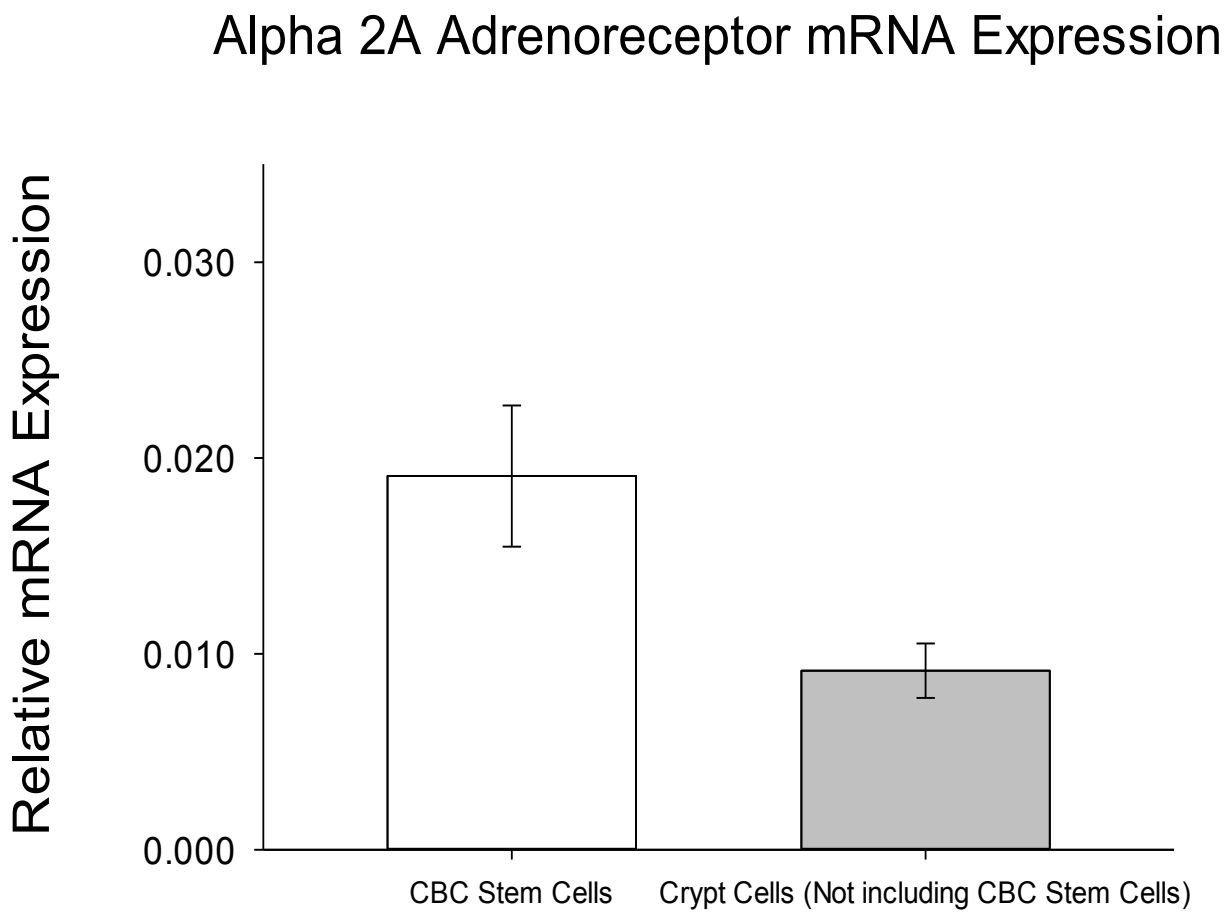

Figure 12. **Comparison of α2A-AR relative mRNA expression between CBC stem cells and other crypt cells.**

Figure 13

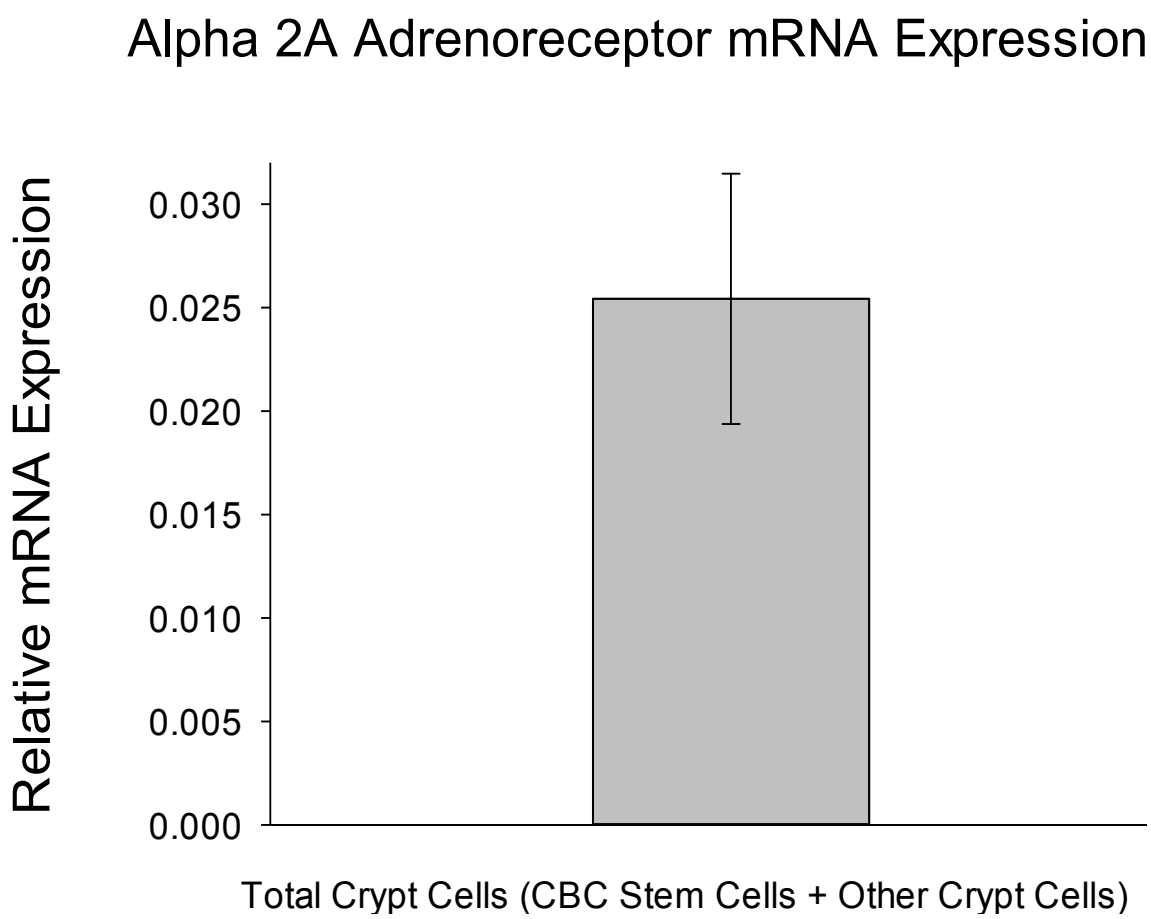

Figure 13. **α2A-AR relative mRNA expression in crypt cells.**

Figure 14

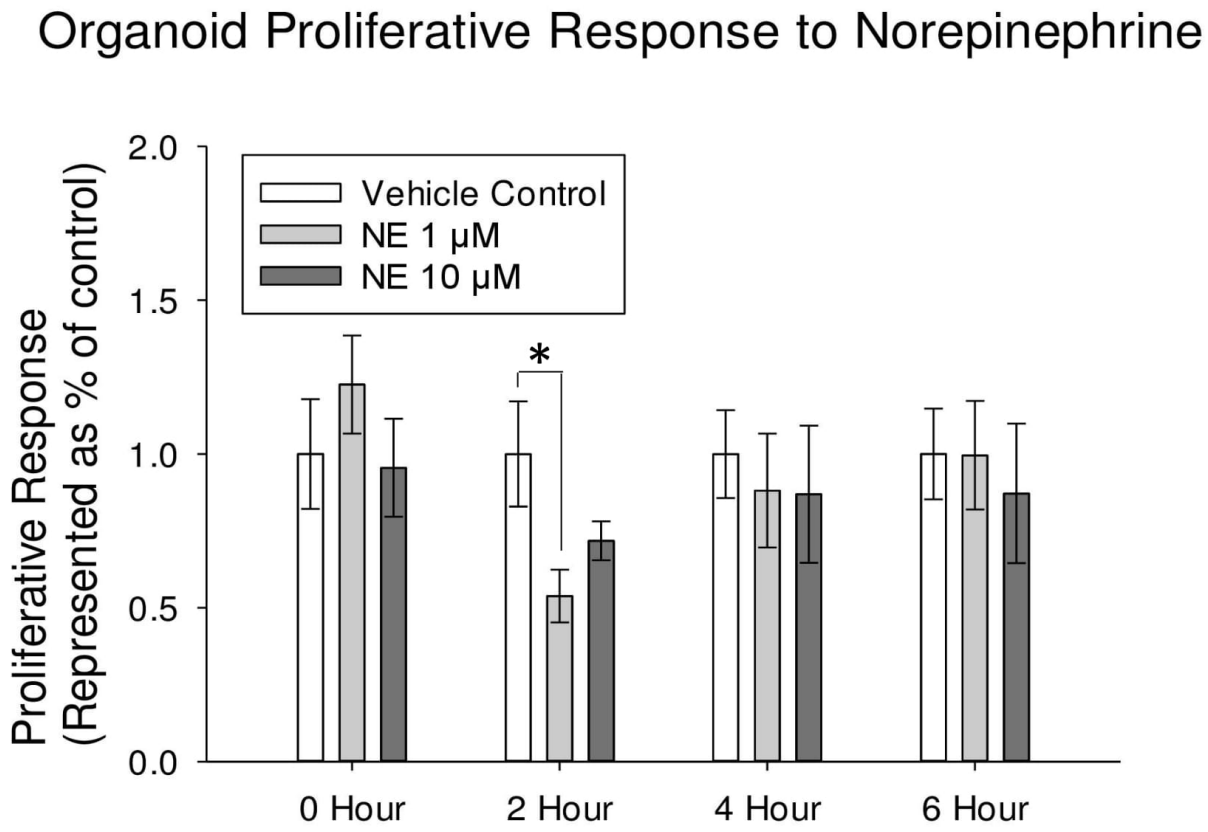

Figure 14. **Proliferative response to the addition of either a low or high dose of norepinephrine to organoids represented as percent of control.**

PART II: EFFECT OF NOREPINEPHRINE ON INTESTINAL EPITHELIAL CRYPT CELL PROLIFERATION

5.8 Abstract

The sympathetic nervous system (SNS) has been implicated in modulating the intestinal epithelial cell proliferation, as interruption of the SNS nerves to the intestine alters proliferation. Recent data has suggested that this phenomenon is mediated by a direct effect, as 1.) SNS neurotransmitter receptors are localized on intestinal epithelial stem and progenitor cells and 2.) intestinal epithelial organoids show decreased expression of cyclin D1, a gene necessary for cell cycle progression, in response to norepinephrine (NE) *in vitro*. Thus, we hypothesized that application of NE would decrease intestinal epithelial crypt proliferation *in vitro*. To test this, small intestinal crypts were isolated from adult male wild-type mice (n = 6) and cultured overnight. Crypts were treated with NE (0.1 μM or 1 μM) or a vehicle control. Proliferation was quantified using the CyQUANT Direct Cell Proliferation Assay Kit at 0h, 2h, 4h, 12h, and 24h. Results demonstrated no significant differences of NE on crypt proliferation compared to controls. Although these results do not support a direct effect of the SNS on intestinal epithelial cell proliferation, further investigation is necessary to determine the nuances of what may be a subtle modulation of tissue turnover by the SNS.

5.9 Introduction

The sympathetic nervous system (SNS) participates in control of peripheral organs and tissues, including the intestinal epithelium. SNS nerves innervate the intestinal epithelium (Jacobowitz, 1965) and control aspects of intestinal epithelial function, such as fluid transport (Greenwood *et al.*, 1987). In addition, the SNS has been implicated in direct control of intestinal epithelial tissue turnover, as it is well-established that surgical or chemical denervation of the SNS nerves to the intestine alters intestinal epithelial crypt cell proliferation (Tutton & Helme, 1974; Lachat & Goncalves, 1978; Kennedy *et al.*, 1983; Callaghan, 1991). More recently, there is emerging evidence from our laboratory that this effect

may be direct, involving sympathetic neurotransmitters binding to receptors directly localized on intestinal epithelial cells to affect proliferation downstream (Davis *et al.*, 2018). Specifically, we have shown that the SNS-associated α_{2A}-adrenoreceptor is expressed in proliferating cells of the intestinal epithelium, including the stem cells and the transit amplifying progenitor cells (Davis *et al.*, 2018). We have also demonstrated that norepinephrine decreases Cyclin D1 in intestinal epithelial organoids *in vitro* (Davis *et al.*, 2018). Cyclin D1 is a key cell cycle gene that is critical for the progression from G1 to S phase, and is rate limiting in proliferation (Ohtsubo & Roberts, 1993; Quelle *et al.*, 1993; Albanese *et al.*, 1995; Watanabe *et al.*, 1996; Resnitzky, 1997; Joyce *et al.*, 1999). Therefore, it is likely that NE-induced changes in Cyclin D1 causes downstream changes in intestinal epithelial cell proliferation, further supported by evidence of NE-induced changes in proliferation in other cell types (Cruise *et al.*, 1985; Geloen *et al.*, 1988; Bronnikov *et al.*, 1992; Oben *et al.*, 2003b; Liu *et al.*, 2014b; Liu *et al.*, 2017). Thus, we hypothesized that NE would decrease intestinal epithelial organoid proliferation *in vitro* compared with controls.

5.10 Materials and methods

Animals

Male wild type (C57BL/6J; n = 6) mice at 2 months of age (Jackson Laboratory, Bar Harbor, ME) were used. Animals were group housed in shoebox cages and maintained with *ad libitum* access to tap water and laboratory chow (Teklad 22/5, Envigo, Madison, WI) on a 12:12 light:dark cycle (lights on 0700) in a climate-controlled room (temperature = 21±2°C and humidity = 50±10%).

Crypt isolation and culture

Small intestinal crypts were isolated as previously described (Sato & Clevers, 2013; Zhou *et al.*, 2018). Briefly, the animals were anesthetized under 3% isoflurane at 1.5L/min in an anesthesia induction chamber and then decapitated. The entire small intestine was harvested, opened longitudinally and washed with cold 1x PBS to remove luminal contents. The villi were scraped off with a coverslip. Villi from the wild type mice were collected into a falcon tube, and centrifuged at 300 g at 4°C for 5 min. The

supernatant was removed and the pellet containing the villus cells was immediately stored at -80°C to await processing. The remaining intestinal tissue was cut into 2-4 mm pieces with scissors and washed 5-10 times with cold 1x PBS until the supernatant was almost clear. Tissue fragments were incubated with 2 mM EDTA (Fisher Scientific, Pittsburgh, PA) and gently rocked at 4°C for 30 min. After removal of EDTA, tissue fragments were washed with 1x PBS 3 times. The supernatant was then collected and passed through a 70-um cell strainer (Corning, Corning, NY) and centrifuged at 300 g at 4°C for 5 min. The cell pellet was resuspended with basal culture medium [Advanced DMEM/F-12 Medium (Gibco, Grand Island, NY) containing 2 mM GlutaMax (Gibco, Grand Island, NY), 10 mM HEPES (Gibco, Grand Island, NY) and 100 U/mL Penicillin-Streptomycin (Gibco, Grand Island, NY)] and centrifuged at 300 g 4°C for 5 min. After centrifugation, the supernatant was removed and isolated crypts were embedded in Matrigel at 170 crypts/8.5 µL and seeded in six replicates a on a pre-warmed 96-well costar clear bottom black plate (Corning, Tewkstar, MA). The matrigel was allowed to solidify for 10 minutes without media in a 37°C incubator and was then incubated in IntestiCult Organoid Growth Medium (StemCell Technologies, Cambridge, MA) at 100 per well. Crypts were grown overnight before cell proliferation experiments were begun.

Cell proliferation measurements

For determination of cell proliferation in response to norepinephrine, crypts received one of 3 treatments: 1 µM or 0.1 µM norepinephrine (A0937, Sigma Aldrich, St. Louis, MO) or a vehicle control. Differences between treatments were evaluated in different sets of cells at one of five time points: 0h, 2h, 4h, 6h, or 24h. Proliferation was assayed using the CyQUANT Direct Cell Proliferation Assay Kit (Thermo-Fischer, Austin, TX) according to the manufacturer's instructions. Fluorescence intensity at 485 nm excitation and 528 nm emission was recorded using a Synergy HT BioTek microplate reader.

Data analysis

All variables were analyzed using Number Crunching Statistical Software (NCSS LLC, Kaysville, UT). Data were expressed as fold change compared to control, and are expressed as mean fold

change ± SEM. One-way ANOVAs were used to detect differences between treatments at individual time points. Assumptions of normality, homogeneity of variance, and independence were met. Differences were considered to be statistically significant at $p < 0.05$.

5.11 Results

There was no effect of NE on intestinal epithelial crypt proliferation *in vitro* compared to controls at 0h, 2h, 4h, 12h, or 24h. (Fig. 15A-E).

5.12 Discussion

This study investigated the effect of the major sympathetic neurotransmitter, NE, on intestinal epithelial crypt cell proliferation *in vitro*. We hypothesized that NE would decrease proliferation compared with controls. However, we found no effect of NE on proliferation compared with controls at 0h, 2h, 4h, 12h, or 24h.

In contrast to the present results, we have previously shown that NE decreases cyclin D1 in intestinal epithelial organoids *in vitro* (Davis *et al.*, 2018). This decrease in cyclin D1 would typically accompany a corresponding decrease in proliferation. Cyclin D1 is required for the G1/S transition in the cell cycle, and subsequently participates in determining a cell's proliferative fate (Fu *et al.*, 2004). In other cell types, adrenergic signaling alters cyclin D1 and proliferation (Karkoulias & Flordellis, 2007). In addition, a suppression of cyclin D1 in intestinal epithelial organoids by another autonomic neurotransmitter, acetylcholine, is accompanied by suppression of growth by cholinergic signaling (Takahashi *et al.*, 2014; Davis *et al.*, 2018). Although there is evidence in support of NE-driven modulation of intestinal epithelial cell proliferation, our results showed no effect.

A possible explanation for the discrepancy in our results is the increased variability in measuring proliferation compared with measuring gene expression. Accuracy of measuring crypt cell proliferation is limited compared with traditional cell culture systems because we are unable to plate exactly the same number of cells in each well at the start of the experiment. Although an equal number of crypts are plated per well, the total number of cells in each crypt varies. This inability to control starting number of cells

introduces deviations that will persist to the endpoint proliferation measurements. Therefore, the modest effect of NE on cyclin D1/proliferation may be masked by variability when measuring proliferation, but revealed when cyclin D1 gene expression per cell is tightly controlled in qPCR by the use of a housekeeping gene. Thus, careful attention to details regarding use of proliferation assays and further exploration of this possible effect using improved techniques and expanded conditions is merited.

If there is indeed a direct effect of the SNS on intestinal epithelial cell proliferation under homeostatic conditions, it is unlikely to be a robust modulator of proliferation, but instead a system that fine tunes proliferation according to subtle fluctuations in sympathetic tone. This proves to be a challenging phenomenon to study, but persistence will allow us to unravel the complex interactions between the SNS and somatic stem cells.

5.13 Figure and caption

Figure 1

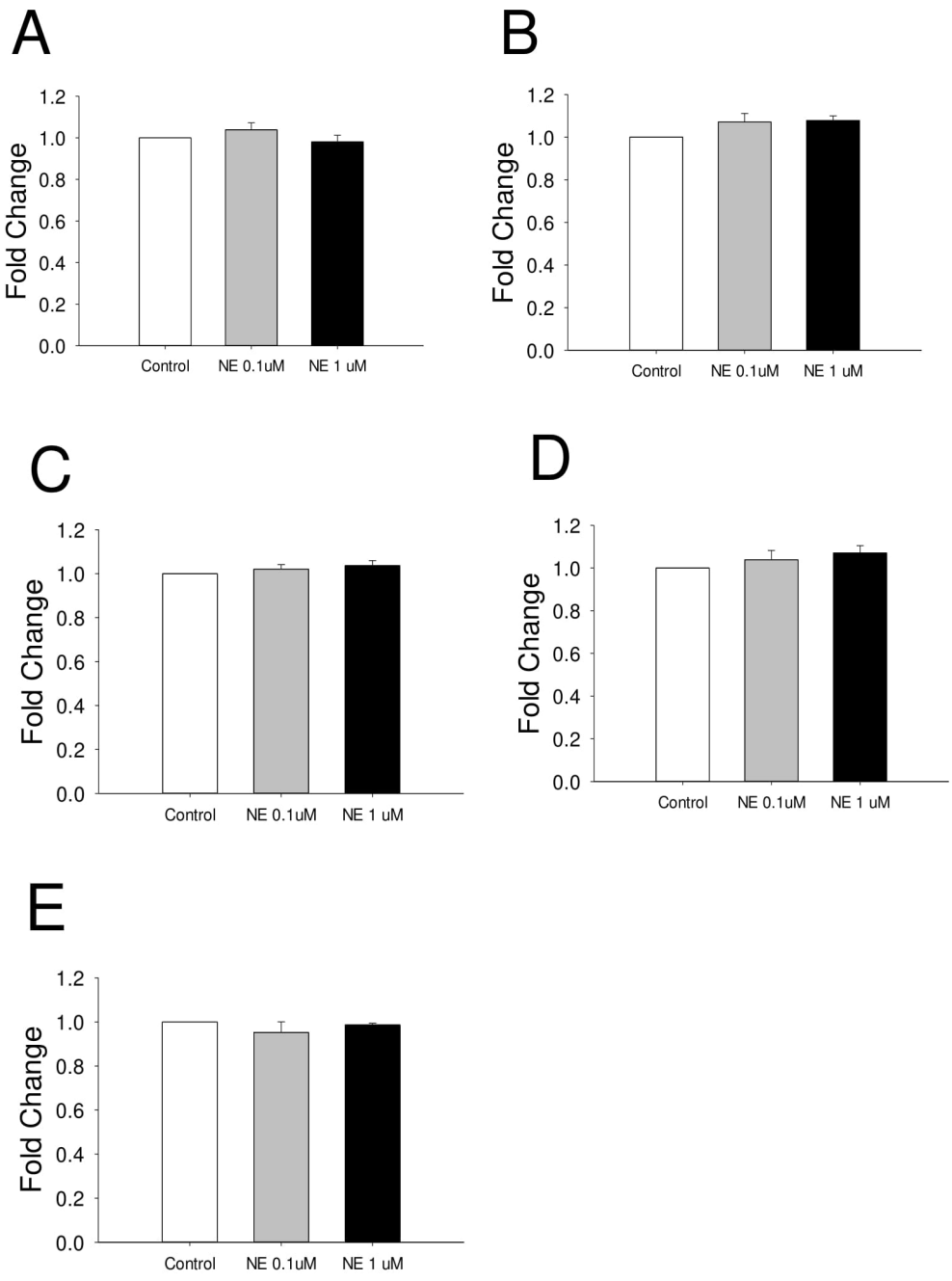

Figure 1. **Effect of norepinephrine on proliferation in intestinal epithelial crypts.** NE has no effect on intestinal epithelial crypt proliferation at (A) 0h, (B) 2h, (C) 4h, (D) 12h, or (E) 24h. Results expressed as Mean Fold Change +/- SEM.

5.14 References

Albanese C, Johnson J, Watanabe G, Eklund N, Vu D, Arnold A & Pestell RG (1995). Transforming p21ras mutants and c-Ets-2 activate the cyclin D1 promoter through distinguishable regions. *J Biol Chem* **270,** 23589-23597.

Blackmore K, Zhou W & Dailey MJ (2017). LKB1-AMPK modulates nutrient-induced changes in the mode of division of intestinal epithelial crypt cells in mice. *Exp Biol Med (Maywood)* **242,** 1490-1498.

Bronnikov G, Houstěk J & Nedergaard J (1992). Beta-adrenergic, cAMP-mediated stimulation of proliferation of brown fat cells in primary culture. Mediation via beta 1 but not via beta 3 adrenoceptors. *Journal of Biological Chemistry* **267,** 2006-2013.

Brown DC & Gatter KC (1990). Monoclonal antibody Ki-67: its use in histopathology. *Histopathology* **17,** 489-503.

Callaghan BD (1991). The effect of pinealectomy and autonomic denervation on crypt cell proliferation in the rat small intestine. *J Pineal Res* **10,** 180-185.

Cavanagh BL, Walker T, Norazit A & Meedeniya AC (2011). Thymidine analogues for tracking DNA synthesis. *Molecules* **16,** 7980-7993.

Cruise JL, Houck KA & Michalopoulos GK (1985). Induction of DNA synthesis in cultured rat hepatocytes through stimulation of alpha 1 adrenoreceptor by norepinephrine. *Science* **227,** 749-751.

Davis EA Washington MC, Phillips H, Sayegh AI, and Dailey MJ (2016). Effect of Sympathetic or Parasympathetic Denervation on Intestinal Epithelial Stem Cell Proliferation. In *Society for Neuroscience*, San Diego, CA.

Davis EA, Zhou W & Dailey MJ (2018). Evidence for a direct effect of the autonomic nervous system on intestinal epithelial stem cell proliferation. *Physiol Rep* **6,** e13745.

Fu M, Wang C, Li Z, Sakamaki T & Pestell RG (2004). Minireview: Cyclin D1: normal and abnormal functions. *Endocrinology* **145,** 5439-5447.

Geloen A, Collet AJ, Guay G & Bukowiecki LJ (1988). Beta-adrenergic stimulation of brown adipocyte proliferation. *Am J Physiol* **254,** C175-182.

Greenwood B, Tremblay L & Davison JS (1987). Sympathetic control of motility, fluid transport, and transmural potential difference in the rabbit ileum. *Am J Physiol* **253,** G726-729.

Jacobowitz D (1965). Histochemical studies of the autonomic innervation of the gut. *J Pharmacol Exp Ther* **149,** 358-364.

Jones LJ, Gray M, Yue ST, Haugland RP & Singer VL (2001). Sensitive determination of cell number using the CyQUANT cell proliferation assay. *J Immunol Methods* **254,** 85-98.

Joyce D, Bouzahzah B, Fu M, Albanese C, D'Amico M, Steer J, Klein JU, Lee RJ, Segall JE, Westwick JK, Der CJ & Pestell RG (1999). Integration of Rac-dependent regulation of cyclin D1 transcription through a nuclear factor-kappaB-dependent pathway. *J Biol Chem* **274,** 25245-25249.

Karkoulias G & Flordellis C (2007). Delayed transactivation of the receptor for nerve growth factor is required for sustained signaling and differentiation by alpha2-adrenergic receptors in transfected PC12 cells. *Cell Signal* **19,** 945-957.

Kennedy MF, Tutton PJ & Barkla DH (1983). Adrenergic factors involved in the control of crypt cell proliferation in jejunum and descending colon of mouse. *Clin Exp Pharmacol Physiol* **10,** 577-586.

Kleinman HK & Martin GR (2005). Matrigel: basement membrane matrix with biological activity. *Semin Cancer Biol* **15,** 378-386.

Lachat JJ & Goncalves RP (1978). Influence of autonomic denervation upon the kinetics of the ileal epithelium of the rat. *Cell Tissue Res* **192,** 285-297.

Liu R, Zhang Q, Luo Q, Qiao H, Wang P, Yu J, Cao Y, Lu B & Qu L (2017). Norepinephrine stimulation of alpha1D-adrenoceptor promotes proliferation of pulmonary artery smooth muscle cells via ERK-1/2 signaling. *Int J Biochem Cell Biol* **88,** 100-112.

Liu TT, Ding TL, Ma Y & Wei W (2014). Selective alpha1B- and alpha1D-adrenoceptor antagonists suppress noradrenaline-induced activation, proliferation and ECM secretion of rat hepatic stellate cells in vitro. *Acta Pharmacol Sin* **35,** 1385-1392.

Maghni K, Nicolescu OM & Martin JG (1999). Suitability of cell metabolic colorimetric assays for assessment of CD4+ T cell proliferation: comparison to 5-bromo-2-deoxyuridine (BrdU) ELISA. *J Immunol Methods* **223,** 185-194.

Miyoshi H & Stappenbeck TS (2013). In vitro expansion and genetic modification of gastrointestinal stem cells as organoids. *Nat Protoc* **8,** 2471-2482.

Nozaki K, Mochizuki W, Matsumoto Y, Matsumoto T, Fukuda M, Mizutani T, Watanabe M & Nakamura T (2016). Co-culture with intestinal epithelial organoids allows efficient expansion and motility analysis of intraepithelial lymphocytes. *J Gastroenterol* **51,** 206-213.

Oben JA, Yang S, Lin H, Ono M & Diehl AM (2003). Norepinephrine and neuropeptide Y promote proliferation and collagen gene expression of hepatic myofibroblastic stellate cells. *Biochem Biophys Res Commun* **302,** 685-690.

Ohtsubo M & Roberts JM (1993). Cyclin-dependent regulation of G1 in mammalian fibroblasts. *Science* **259,** 1908-1912.

Paris H, Voisin T, Remaury A, Rouyer-Fessard C, Daviaud D, Langin D & Laburthe M (1990). Alpha-2 adrenoceptor in rat jejunum epithelial cells: characterization with [3H]RX821002 and distribution along the villus-crypt axis. *J Pharmacol Exp Ther* **254,** 888-893.

Präbst K, Engelhardt H, Ringgeler S & Hübner H (2017). Basic Colorimetric Proliferation Assays: MTT, WST, and Resazurin. In *Cell Viability Assays: Methods and Protocols*. ed. Gilbert DF & Friedrich O, pp. 1-17. Springer New York, New York, NY.

Quelle DE, Ashmun RA, Shurtleff SA, Kato JY, Bar-Sagi D, Roussel MF & Sherr CJ (1993). Overexpression of mouse D-type cyclins accelerates G1 phase in rodent fibroblasts. *Genes Dev* **7,** 1559-1571.

Quent VM, Loessner D, Friis T, Reichert JC & Hutmacher DW (2010). Discrepancies between metabolic activity and DNA content as tool to assess cell proliferation in cancer research. *J Cell Mol Med* **14,** 1003-1013.

Resnitzky D (1997). Ectopic expression of cyclin D1 but not cyclin E induces anchorage-independent cell cycle progression. *Mol Cell Biol* **17,** 5640-5647.

Sato T & Clevers H (2013). Primary mouse small intestinal epithelial cell cultures. *Methods Mol Biol* **945,** 319-328.

Schaak S, Cussac D, Cayla C, Devedjian JC, Guyot R, Paris H & Denis C (2000). Alpha(2) adrenoceptors regulate proliferation of human intestinal epithelial cells. *Gut* **47,** 242-250.

Straub RH, Wiest R, Strauch UG, Harle P & Scholmerich J (2006). The role of the sympathetic nervous system in intestinal inflammation. *Gut* **55,** 1640-1649.

Takahashi T, Ohnishi H, Sugiura Y, Honda K, Suematsu M, Kawasaki T, Deguchi T, Fujii T, Orihashi K, Hippo Y, Watanabe T, Yamagaki T & Yuba S (2014). Non-neuronal acetylcholine as an endogenous regulator of proliferation and differentiation of Lgr5-positive stem cells in mice. *Febs j* **281,** 4672-4690.

Tutton PJ & Helme RD (1974). The influence of adrenoreceptor activity on crypt cell proliferation in the rat jejunum. *Cell Tissue Kinet* **7,** 125-136.

van der Flier LG & Clevers H (2009). Stem cells, self-renewal, and differentiation in the intestinal epithelium. *Annu Rev Physiol* **71,** 241-260.

Watanabe G, Lee RJ, Albanese C, Rainey WE, Batlle D & Pestell RG (1996). Angiotensin II activation of cyclin D1-dependent kinase activity. *J Biol Chem* **271,** 22570-22577.

Zhou W, Ramachandran D, Mansouri A & Dailey MJ (2018). Glucose stimulates intestinal epithelial crypt proliferation by modulating cellular energy metabolism. *Journal of cellular physiology* **233,** 3465-3475.

CHAPTER 6: LONG-TERM EFFECT OF PARASYMPATHETIC OR SYMPATHETIC DENERVATION ON INTESTINAL EPITHELIAL CELL PROLIFERATION AND APOPTOSIS

(Published in Experimental Biology and Medicine; Citation: Davis EA, Washington MC, Yaniz ER*, Phillips H, Sayegh AI, & Dailey MJ. (2017). Long-term effect of parasympathetic or sympathetic denervation on intestinal epithelial cell proliferation and apoptosis. *Experimental Biology and Medicine*, *242*(15), 1499-1507.)

*Undergraduate mentee of EAD

6.1 Abstract

Intestinal epithelial tissue is constantly regenerated as a means to maintain proper tissue function. Previous studies have demonstrated that denervation of the parasympathetic (PNS) or sympathetic (SNS) nervous system to the intestine alters this process. However, results are inconsistent between studies, showing both increases and decreases in proliferation after denervation of the PNS or SNS. The effect appears to correlate with 1) the timing post-denervation, 2) denervation-induced changes in food intake, 3) the denervation technique used, and 4) which intestinal segment is investigated. Thus, we proposed that PNS or SNS denervation does not have an effect on intestinal epithelial regeneration when you 1) evaluate denervation after long-term denervation, 2) control for post-surgical changes in food intake, 3) use minimally invasive surgical techniques and 4) include a segmental analysis. To test this, adult male Sprague Dawley rats underwent PNS denervation via subdiaphragmatic vagotomy, SNS denervation via celiacomesenteric ganglionectomy, a PNS denervation sham surgery, or an SNS denervation sham surgery. Sham surgery *ad libitum* fed groups and sham surgery pair fed groups were used to control for surgically-induced changes in food intake. Three weeks post-surgery, animals were euthanized and tissue from the duodenum, jejunum, and ileum was excised and immunohistochemically processed to visualize indicators of proliferation (bromodeoxyuridine-positive cells) and apoptosis (caspase-3-positive cells).

Results showed no differences between groups in proliferation, apoptosis, or total cell number in any intestinal segment. These results suggest that PNS or SNS denervation does not have a significant long-term effect on intestinal epithelial turnover. Thus, intestinal epithelial regeneration is able to recover after ANS injury.

6.2 Introduction

The autonomic nervous system (ANS) is implicated in the control of tissue regeneration. A focus of prior research has been on the ANS control of intestinal epithelial cell turnover, as it is among the most rapidly regenerating tissues of the body (van der Flier & Clevers, 2009). Ablation of either branch of the ANS, the parasympathetic (PNS) or sympathetic (SNS), alters intestinal epithelial cell proliferation as indicated by a change in the mitotic index (Tutton & Helme, 1974; Musso *et al.*, 1975a; Tsibulevskii & Orlova, 1976; Lachat & Goncalves, 1978; Kennedy *et al.*, 1983; Callaghan, 1991) and length of the cell cycle (Tutton & Helme, 1974). These data, though, are inconsistent across studies. After PNS denervation, the direction of fluctuation in proliferation appears to be time dependent. At early time points post-denervation, intestinal epithelial cell proliferation is decreased (Musso *et al.*, 1975a; Lachat & Goncalves, 1978). The early decrease in proliferation may be due to a concomitant decrease in food intake, which is known to decrease intestinal epithelial cell proliferation independent of an ANS influence (Brown *et al.*, 1963). At later time points post-PNS denervation, proliferation has been shown to be increased (Tsibulevskii & Orlova, 1976; Callaghan, 1991) or equal to that of control animals (Bejar *et al.*, 1968; Musso *et al.*, 1975a), perhaps demonstrating a recovery over time (Musso *et al.*, 1975a). Thus, these changes may be indirectly driven by changes in food intake after PNS denervation, rather than a direct influence of the loss of the PNS. Sympathetic denervation also exhibits varied results for regeneration of this tissue. The effect on intestinal epithelial proliferation appears to correlate with the extent of denervation induced by specific SNS denervation techniques and which intestinal segment (duodenum, jejunum or ileum) is investigated. A long-term decrease in proliferation is seen after extreme techniques (e.g., chemical sympathectomy) (Tutton & Helme, 1974; Kennedy *et al.*, 1983). However, a

more focused surgical denervation targeting the celiacomesenteric nerves that innervate the intestine results in no change in proliferation along most of the proximal to distal axis of the intestine (Tutton & Helme, 1974; Musso *et al.*, 1975a; Lachat & Goncalves, 1978; Callaghan, 1991). Thus, we propose that PNS or SNS denervation does not have a long-term effect on intestinal epithelial regeneration when you control for post-surgical changes in food intake and use minimally invasive surgical techniques. A recovery of function after long-term ANS denervation is seen in processes related to intestinal function, including motility (Andrews & Bingham, 1990), food intake (Rezek *et al.*, 1975; Schneider *et al.*, 1976) and blood flow (Mackie & Turner, 1971). Recovery is also seen in aspects of tissue regeneration in other organs, including the liver (Kato & Shimazu, 1983; Tanaka *et al.*, 1987) and the pancreas (Edvell & Lindstrom, 1998). Thus, it is possible that intestinal epithelial turnover exhibits this same pattern of recovery after a long-term loss of ANS input. In order to test this, male Sprague Dawley rats were subjected to PNS denervation or SNS denervation. To control for surgical effects, we included sham surgical control conditions for each surgical procedure. To control for the change in food intake that often occurs post-ANS denervation, we included a pair fed sham surgical group for both the PNS and the SNS denervation. We euthanized the animals 3 wks post-surgery because this is generally regarded to be a minimum time for recovery of other intestinal physiological processes after ANS denervation (Mackie & Turner, 1971; Rezek *et al.*, 1975; Schneider *et al.*, 1976; Andrews & Bingham, 1990). We have defined this 3 wk time point as 'long-term' based on the timeline of these other recovery processes. We collected intestinal tissue from three intestinal segments (duodenum, jejunum and ileum) and immunohistochemically processed the tissue to measure levels of proliferation, apoptosis, and total crypt and villus cell numbers. This study contributes to the basic understanding of autonomic influence on tissue regeneration.

6.3 Materials and methods

Animals

All procedures were approved by the Institutional Animal Care and Use Committee at the University of Illinois at Urbana-Champaign. Male Sprague-Dawley rats (n = 56; Harlan, Hsd:Sprague Dawley® SD®; 225-275g). Upon arrival, the animals were single-housed in tub cages with ad libitum access to chow diet (Harlan 8640, Harlan Sprague Dawley Inc, Indianapolis, IN), tap water, and a ceramic bowl for enrichment. They were maintained on a 12:12 light:dark cycle (lights on 0700h, lights off 1900h). Food intake and body weight were measured daily at 1500h. The animals acclimated to these conditions for 1 wk prior to surgery.

Surgical procedures

Animals underwent an overnight fast prior to undergoing surgery. Animals were given an anesthesia mixture (0.1mL/100g body weight intramuscularly containing the following: 100mg/mL ketamine (Henry Schein Animal Health, Dublin OH), 100mg/mL xylazine (Akorn, Decatur, IL), 10mg/mL Acepromazine Maleate (Boehringer Ingelheim, St. Joseph, MO) in 0.9% sterile saline (Henry Schein Animal Health, Dublin, OH). For PNS denervation (n = 12) the body cavity was opened with a midline incision of the skin. The dorsal and ventral branches of the subdiaphragmatic vagus were located by blunt dissection of the overlying tissues, isolated, and ligated above the hepatic, celiac, and accessory celiac branches. Each nerve trunk was cut distal to the ligature and above the vagal branches, producing total vagal transection. The portion of the nerve distal to the cut was carefully stripped away from the underlying esophagus. For sham vagotomy surgeries (n=15), the esophagus, stomach, dorsal and ventral branches of the subdiaphragmatic vagus were manipulated, but the vagi were left intact. These procedures were performed as previously described (Kalia & Sullivan, 1982; Yox *et al.*, 1991; Sullivan *et al.*, 2007; Brown *et al.*, 2011; Hunt *et al.*, 2012). For sympathetic denervation (n=11), the body cavity was opened with a midline incision of the skin. The left kidney, cranial mesenteric artery and celiac artery were exposed by blunt dissection of the overlying tissues, and the celiac and mesenteric ganglia were located

between the arteries and were removed under 40× magnification using jeweler's scissors and forceps as previously described (Brown *et al.*, 2011; Hunt *et al.*, 2012; Wright *et al.*, 2012). The removal was made to ensure no severing of other nerve branches (e.g., the celiac branch of the vagus nerve) that run in close proximity to the ganglia. Sham celiacomesenteric ganglionectomy surgeries (n=14) were performed by manipulating the tissue without removal of the celiac or mesenteric ganglia. Before closure of the surgical sites, 0.25% bupivacaine (Hospira, Lake Forest, IL) was applied to the incision site at a dose of 2mg/kg as a local anesthetic. The animals received a dose of Rimadyl (Pfizer, New York, NY) at 5mg/kg subcutaneously while still under anesthesia as an analgesic. Two more doses of Rimadyl at 5mg/kg were administered subcutaneously for two days after surgery.

Feeding protocol

After a 1 wk recovery period, animals either had ad libitum access to food or were pair fed during a 2 wk feeding period. All animals that underwent PNS or SNS surgical denervation, had ad libitum access to chow diet throughout the 2 wk feeding period. PNS or SNS sham surgery animals were divided into two groups based on average body weight: ad libitum access to chow or pair fed chow in equal average kcal to that eaten by the denervated rats. These animals underwent a sham surgery, and were then provided the same amount of food consumed by the corresponding denervated group. Thus, the six groups were 1) PNS denervated, 2) PNS pair fed sham, 3) PNS ad lib fed sham, 4) SNS denervated, 5) SNS pair fed sham and 6) SNS ad lib fed sham.

Euthanasia

After the 2 wk feeding period, animals had their food removed at the beginning of the light cycle and continued to be fasted for the remaining 12h prior to euthanization at the beginning of the dark cycle. This fasting period was sufficient minimize the amount of food present in the intestine at the time of euthanization. At 6h prior to euthanization, 5-bromo-2'-deoxyuridine (BrdU; Sigma-Aldrich, St. Louis, MO) injections were administered IP at 50mg/kg body weight in a volume of 1.5mL sterile deionized

water. Animals were then euthanized under isoflurane (Henry Schein Animal Health, Dublin, OH) anesthesia by decapitation. Tissue was collected from the duodenum, jejunum and ileum.

Tissue processing

Intestinal segments were flushed with 1X phosphate buffered saline (PBS) and filled with 4% paraformaldehyde (PFA; Sigma-Aldrich, St. Louis, MO) for 12h at 4°C and then stored in 1X PBS at 4°C prior to paraffin embedding. Paraffin embedding was done in a Leica ASP300 Tissue Processor (Leica, Wetzlar Germany) and embedded using Paraplast tissue embedding media (Fisher Scientific, West Lawn, NJ). For slide preparation, sections were cut on a microtome at 5µm and then mounted on Superfrost™ Plus Microscope Slides (Fisher Scientific, Pittsburgh, PA).

Immunohistochemistry: Proliferation

Tissue sections were deparaffinized in xylenes followed by a series of graded ethanols, then rinsed in deionized water. Antigen retrieval was performed by immersing the slides in sodium citrate buffer (Sodium Citrate Hydrochloride, Fisher Scientific and Tween 20, Sigma- Aldrich, Germany, pH 6.0) for 20 min in a water bath at 95°C, then allowed to cool while still immersed in the sodium citrate buffer solution for 30 min at RT. Slides were rinsed between each step in 1X PBS. Slides were incubated in blocking solution containing 0.3% Triton-X (Sigma-Aldrich, St. Louis, MO) and 3% Normal Donkey Serum (JacksonImmunoResearch, West Grove, PA) diluted in 1X PBS at RT for 1h. Sections were then incubated overnight in an anti-BrdU primary antibody (1:1000, ab1893, Abcam, San Francisco, CA) diluted in the blocking solution. Sections were incubated in a donkey anti-sheep IgG H&L secondary antibody (1:500, ab6899, Abcam, San Francisco, CA) diluted in 1X PBS for 1h at RT. Sections were then incubated in an avidin–biotin complex (Vectastain Elite reagents, Vector Labs, Burlingame, CA) for 1h at RT. A diaminobenzidine-hydrogen peroxidase reaction was performed using a substrate kit (SK-4100, Vector Laboratories, Burlingame, CA). Sections were counterstained in hematoxylin (Fisher HealthCare, Houston, TX) and dehydrated in a series of graded ethanols followed by xylenes. Slides were coverslipped with Permount mounting media (Fisher Scientific, Fair Lawn, NJ) and stored at RT.

Immunohistochemistry: Apoptosis

Slides were processed as described above with the following exceptions: Slides were incubated in the blocking solution for 1.5h at RT. The primary antibody used was an anti-caspase-3 antibody (1:2500, cat. no. 9662, Cell Signaling Technologies, Danvers, MA). After washing in PB, sections were incubated in donkey anti-rabbit IgG (711-065-152, Jackson ImmunoResearch, West Grove, PA) diluted in 1X PB for 1h at RT. Sections were then washed in 1X PB and processing continued as described above except that PB was used instead of PBS.

Quantification

Intestinal tissue sections were visualized using a NanoZoomer Digital Pathology System (Hamamatsu, Hamamatsu City, Japan) using a 40x objective and NDP Scan software. Quantification was performed by visual inspection of the images on a desktop computer using NDP View 2 software by two individuals that were blinded to the treatments. Nine crypts or villi per section were chosen based on intact morphology of the intestine. Total crypt cell number, BrdU-positive crypt cell number, proliferation ratio (defined as BrdU-positive crypt cell number divided by total crypt cell number), and crypt depth were determined from slides immunohistochemically processed for BrdU. Total villus cell number, caspase-3-positive villus cell number, apoptotic ratio (defined as caspase-3-positive villus cell number divided by total villus cell number), and villus height were determined from slides immunohistochemically processed for caspase-3.

Statistical analysis

All variables were analyzed using Number Crunching Statistical Software (NCSS LLC, Kaysville, UT). Food intake and body weight were analyzed using separate two-way repeated measures analyses of variance (ANOVA; 3×13; treatment group × day) for PNS and SNS experiments. Measures of proliferation and apoptosis were analyzed using separate one-way ANOVA (treatment group) for each intestinal segment (duodenum, jejunum or ileum). Assumptions of normality, homogeneity of variance,

and independence were met. Tukey-Kramer post hoc analyses were utilized where appropriate. Differences among groups were considered statistically significant if $p < 0.05$.

6.4 Results

Food intake

Average 24h food intake (kcal) was decreased in PNS denervated and pair fed sham groups compared with *ad lib* fed sham animals on days 8 through 12 post-surgery ($p < 0.05$; Fig. 16A). There were no differences in average 24h food intake (kcal) between SNS denervated, *ad lib* fed sham, or pair fed sham animals at any time point (Fig. 16B).

Body weight

Body weight was significantly different between all three PNS groups across all time points, with the lowest body weight seen in the PNS denervated animals and the highest in the *ad lib* fed sham animals ($p < 0.05$; Fig. 17A). Body weight was increased in the SNS denervated animals compared with the *ad lib* fed sham animals only on day 20 post-surgery ($p < 0.05$; Fig. 17B).

Effect of PNS denervation on proliferation

BrdU-positive cells (representative image, Fig. 18A) in the jejunum were increased in the PNS denervated animals compared with pair fed sham animals ($p < 0.05$, Fig. 18B), but PNS denervated and *ad lib* fed sham were not different from each other. There were no differences in the number of BrdU-positive cells between the groups when the duodenum or ileum were analyzed (Fig. 18B). Proliferation ratio and total number of crypt cells were not different between the groups across all segments of the intestine (Figs. 18C&D).

Effect of SNS denervation on proliferation

There were no differences between the groups in BrdU-positive cell number, proliferation ratio, or total crypt cell number in the duodenum, jejunum, or ileum (Figs. 19A-C).

Effect of PNS denervation on apoptosis

There were no differences between groups in caspase-3-positive (representative image, Fig. 20A) villus cell number, apoptotic ratio, or total number of villus cells (Figs. 20 B-D) in the duodenum, jejunum, or ileum.

Effect of SNS denervation on apoptosis

There were no differences between groups in caspase-3-positive villus cell number or proliferation ratio in the duodenum, jejunum, or ileum (Figs 21A&B). However, total crypt cell number was increased in the SNS denervated animals compared with pair fed sham animals ($p < 0.05$; Fig. 21C).

6.5 Discussion

We found no differences in proliferation, apoptosis, crypt or villus cell number in the intestinal epithelium after long term PNS or SNS denervation (3 wks) compared to the sham control groups. These results coincide with those of others when the denervated groups are compared with sham surgical control animals at later time points post-denervation (Musso *et al.*, 1975a; Lachat & Goncalves, 1978) and has been found in humans post-ANS denervation (Bejar *et al.*, 1968; Hansen *et al.*, 1978). It appears that the mechanisms controlling proliferation and apoptosis are able to recover post-denervation as has been found in other processes related to intestinal function [motility (Andrews & Bingham, 1990), food intake (Rezek *et al.*, 1975; Schneider *et al.*, 1976) and blood flow (Mackie & Turner, 1971)] and in aspects of tissue regeneration in other organs [liver (Kato & Shimazu, 1983; Tanaka *et al.*, 1987) and the pancreas (Edvell & Lindstrom, 1998)]. Because cell turnover is vital in maintaining proper tissue function, these results are important in order to reveal possible implications of the use of ANS denervation in human medicine.

Previous research supports the idea that the direction of fluctuation in proliferation after PNS denervation appears to be time dependent. Within the first few days after PNS denervation, intestinal epithelial proliferation decreases, as measured in the rat ileum at four different post-denervation time points, including 6h, 1 day, 2 days, and 3 days (Musso *et al.*, 1975a; Lachat & Goncalves, 1978). Several

groups demonstrate that proliferation increases 1 wk post-PNS denervation in the jejunum (Tsibulevskii & Orlova, 1976; Callaghan, 1991) and the ileum in rats (Callaghan, 1991). However, others suggest that there is no difference in the ileum compared to sham controls at 6 or 10 days post-denervation (Musso *et al.*, 1975a). Despite these discrepancies in proliferation at early time points, human jejunal biopsies post-PNS denervation have suggested that there is no change in intestinal proliferation 3 and 6 weeks post-surgery (Bejar *et al.*, 1968). Long-term studies in the rat did not measure proliferation specifically, but no histological changes were seen in the jejunum or ileum from 12 to 32 wks post-PNS denervation (Ellis & Pryse-Davies, 1967). Together, these studies suggest changes in proliferation at early time points after PNS denervation followed by eventual stabilization of proliferation. However, these studies did not control for surgically-driven decreases in food intake, a known influence on intestinal epithelial cell proliferation (Brown *et al.*, 1963). The present study accounted for surgically-induced changes in food intake and still demonstrated recovery of intestinal epithelial proliferation after PNS denervation in all three intestinal segments.

The effect of SNS denervation on intestinal epithelial proliferation appears to correlate with the extent of denervation induced by specific denervation techniques. Chemical denervation techniques, which ablate sympathetic nerves globally, produce a long lasting decrease in proliferation (Tutton & Helme, 1974; Kennedy *et al.*, 1983). However, more precise surgical denervations produce a short-term effect in the jejunum (Tutton & Helme, 1974; Callaghan, 1991) or no effect in the ileum (Musso *et al.*, 1975a; Lachat & Goncalves, 1978). As surgical rather than chemical denervation of the SNS is used in human medicine, we were interested in the effect of surgical SNS denervation (i.e., celiacomesenteric ganglionectomy) on intestinal epithelial turnover in each segment of the intestine. The present results revealed no differences in intestinal epithelial proliferation or apoptosis in the duodenum, jejunum or the ileum 3 wks post-SNS denervation. These results are similar to those of others using the same surgical approach (Musso *et al.*, 1975a; Lachat & Goncalves, 1978). Thus, it appears that intestinal epithelial turnover may also recover after minimally-invasive surgical SNS denervation.

Even though there was no difference in the proliferation or apoptosis of the intestinal epithelium in the denervated compared with the sham surgical control groups in any segment of the intestine, there was an effect of pair feeding on the proliferation of the intestinal epithelium within the jejunum post-PNS denervation. The decrease in proliferation in the pair fed group was seen even though at the time of euthanization, all three PNS groups were eating equal kilocalories of food. This may be the result of how these animals were fed each day. They were provided the same amount of food consumed by the corresponding denervated group at the same time every day and ate all of the food within a few hours, instead of freely feeding throughout the day/night cycle. This may have conditioned the animals to anticipate and ingest food at regularly scheduled meals and set a circadian rhythm. We found that pair-feeding within the jejunum decreased intestinal epithelial proliferation and that PNS denervation attenuated this decrease in proliferation. This difference is seen even though at the time of euthanization, all three groups were eating similar kilocalories of food. Meal feeding has been shown to alter the circadian rhythm of intestinal epithelial proliferation (Lakatua *et al.*, 1983). Given that this only occurred in the PNS pair fed group and not the SNS pair fed group, there was likely an interaction between meal feeding and the amount (in kcals) provided over days or weeks. This is because the PNS denervated, and not the SNS denervated group, decreased their food intake post-surgery. Thus, only the PNS pair fed group was fed lesser kcals than they may have eaten ad libitum and less than the SNS pair fed group was eating. These data support the idea that the kcal amount of food alters intestinal epithelial proliferation and that there can be lasting effects of the amount of food eaten on the proliferative capacity of the intestinal epithelium (Brown *et al.*, 1963; Mah *et al.*, 2014; Beyaz *et al.*, 2016).

Compensatory mechanisms occur after ANS denervation in order to reestablish intestinal function under a variety of conditions and include (1) an upregulation of gastrointestinal (GI) receptor expression, (2) compensation by the non-denervated ANS branch and (3) enteric nervous system modulation. For example, PNS denervation initially decreases intestinal motility (Ridolfi *et al.*, 2009), a process which is heavily mediated by serotonin (Kendig & Grider, 2015). PNS denervation has also been shown to reduce

the amount of 5-HT-3 positive serotonergic nerve fibers in the GI tract (Glatzle *et al.*, 2002). As gene expression of the serotonin receptor 5-HT-3 is upregulated in the intestinal epithelium, motility recovers (Tong *et al.*, 2011). This restored motility can be blocked with administration of a 5-HT3 antagonist (Tong *et al.*, 2011). Therefore, upregulation of serotonin receptors in the epithelium is thought to be driving the recovery of intestinal motility. Since serotonin receptors have also been found to be involved in intestinal epithelial proliferation, upregulation of the receptors after PNS denervation may contribute to the recovery of cell turnover (Gross *et al.*, 2012; Dong *et al.*, 2016). Changes in the specific primary neurotransmitter receptors of the denervated ANS branch are also likely to undergo changes to facilitate recovery of the intestinal epithelial turnover. PNS denervation upregulates the amount of muscarinic acetycholinergic gene expression in the stomach (Keshavarzian *et al.*, 1990) and downregulates the expression in the small intestine (Higuchi *et al.*, 1985). The intact branch of the ANS may also participate in the compensation to recover function after denervation. PNS denervation decreases the concentration of norepinephrine, the main SNS neurotransmitter, in the stomach (Graffner *et al.*, 1985; Orloff *et al.*, 1985). Therefore, changes in aspects of both the denervated and intact branches of the ANS may be driving the recovery of function after ANS denervation. The enteric nervous system (ENS), a network of neurons intrinsic to the GI tract, modulates specific intestinal epithelial progenitors to control regeneration (Bjerknes & Cheng, 2001). Given that the ENS makes synaptic connections to both the PNS and the SNS (Costa *et al.*, 2000), it is likely that the ENS may also contribute to the recovery of tissue regeneration after the loss of ANS input as it does in other intestinal functions (Nakao *et al.*, 1998). Taken together, varied compensatory mechanisms after ANS denervation may collectively contribute to the recovery of intestinal function, including proliferation and apoptosis.

We found that the regenerative capacity of the intestinal epithelium is not chronically disrupted by denervation of either branch of the ANS. Our data support the narrative that compensatory mechanisms recover a variety of physiological functions to homeostatic levels after autonomic injury. This finding is important because autonomic denervation is currently utilized in human patients to treat a

variety of diseases. PNS denervation is used for the treatment of gastric ulcers (Olbe, 1994), and also may occur as a consequence of gastric bypass surgery (Okafor *et al.*, 2015). SNS denervation is currently used to treat hyperhidrosis (Dumont *et al.*, 2004), facial blushing (Girish *et al.*, 2017), and a variety of other conditions (Hashmonai *et al.*, 2016). New treatments involving autonomic denervation may also be implemented in the future for other diseases involving autonomic imbalance, such as rheumatoid arthritis (Koopman *et al.*, 2011) or chronic pain (Xie *et al.*, 2016). Disruptions to the intestinal epithelial turnover process as a side effect of ANS denervation procedures could result in improper intestinal epithelial function. For example, chronic decreases in proliferation might lead to mucosal atrophy, a severe reduction in absorptive surface area of the intestine. Mucosal atrophy can lead to intestinal failure, which causes diarrhea, malabsorption, and progressive malnutrition (Shaw *et al.*, 2012). In contrast, chronic increases in proliferation may lead to increased epithelial cell numbers, resulting in excessive increases in nutrient absorption (Singh *et al.*, 1972; Ferraris & Vinnakota, 1995). Uncontrolled increases in intestinal epithelial cell proliferation may also lead to the development of cancer (Krausova & Korinek, 2014). However, based on our findings that intestinal epithelial turnover is able to recover after autonomic injury, ANS denervation may be used as treatment for certain diseases without affecting intestinal epithelial tissue regeneration.

6.6 Figures and captions

Figure 16

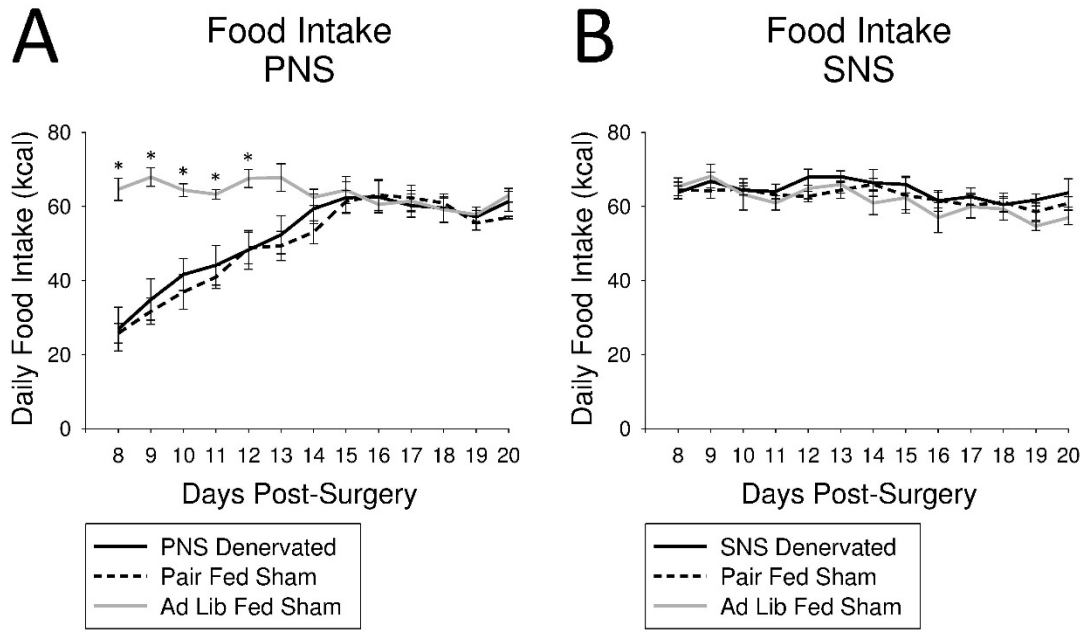

Figure 16. **Influence of PNS or SNS denervation on daily food intake.** (A) Average daily food intake was decreased in PNS denervated animals and pair fed sham animals compared with *ad lib* fed sham surgical controls on days 8 through 12 post-surgery ($p < 0.05$; *). (B) SNS denervation did not significantly alter average daily food intake.

Figure 17

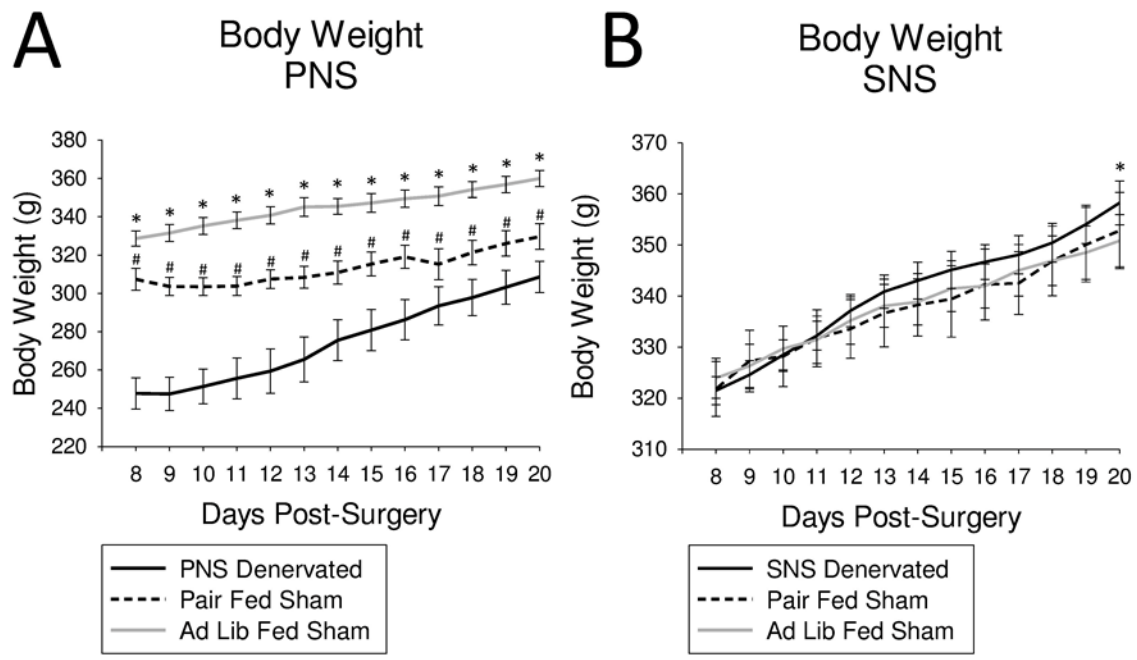

Figure 17. **Influence of PNS or SNS denervation on body weight.** (A) Average body weight was decreased in PNS denervated animals and pair fed sham animals compared with *ad lib* fed sham animals across all time points ($p < 0.05$; *). Average body weight was decreased in PNS denervated animals compared with pair fed sham days across all time points ($p < 0.05$; #). (B) Average body weight of SNS denervated animals was increased compared with *ad lib* fed sham animals on day 20 post-surgery ($p < 0.05$; *).

Figure 18

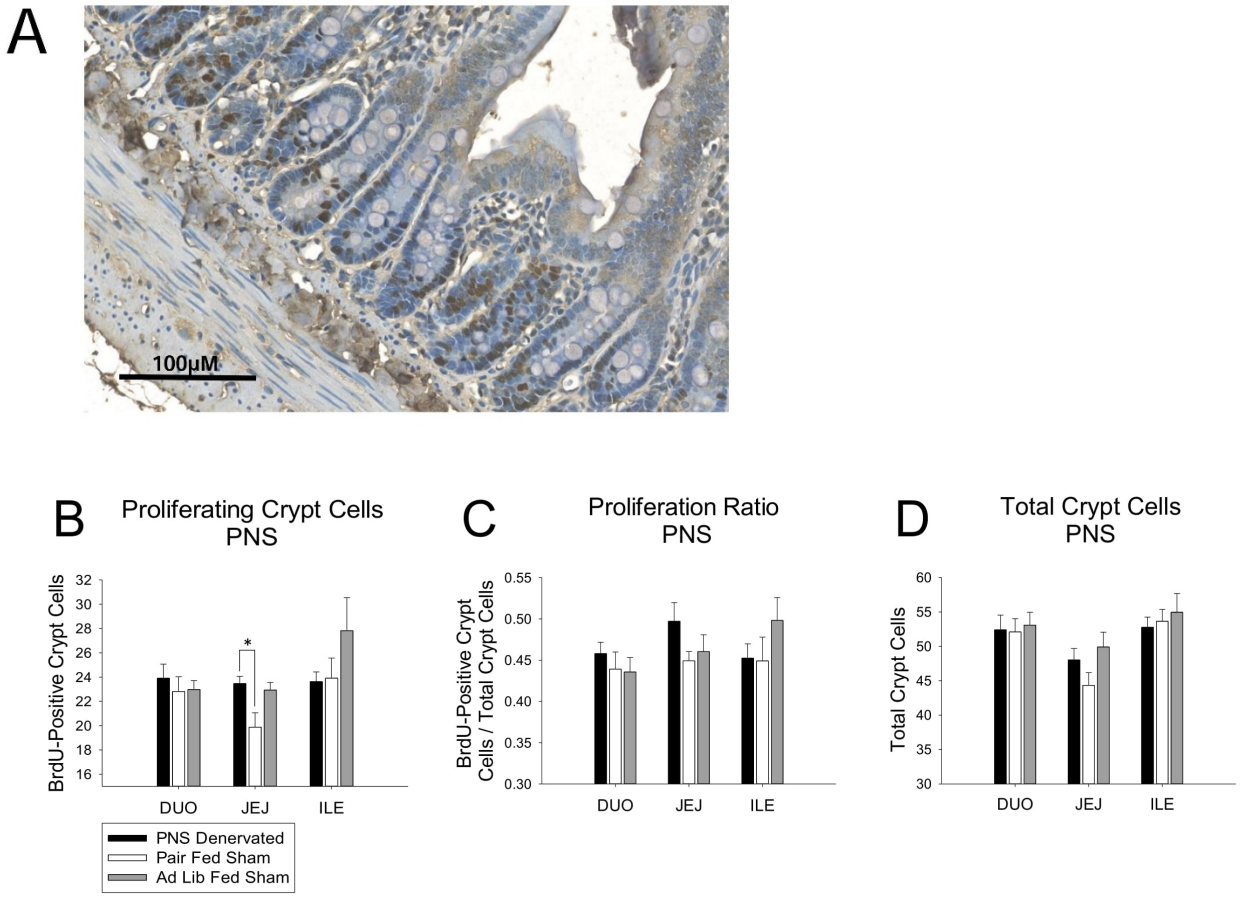

Figure 18. **Effect of PNS denervation on intestinal epithelial crypt cell proliferation.** (A) Intestinal tissue immunohistochemically processed with an anti-BrdU antibody to visualize intestinal epithelial crypt cell proliferation. Tissue counterstained with hematoxylin. (B) Average proliferating crypt cell number in the jejunum was increased in PNS denervated animals compared with pair fed sham animals ($p < 0.05$). (C) There were no differences between groups in average proliferation ratio in the duodenum, jejunum, or ileum. (D) There were no differences between groups in average total crypt cell number in the duodenum, jejunum, or ileum.

Figure 19

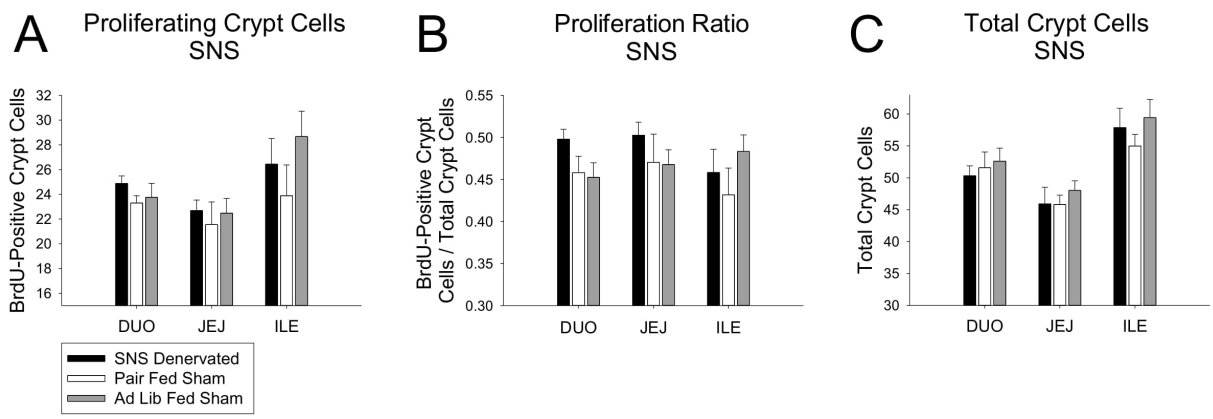

Figure 19. **Effect of SNS denervation on intestinal epithelial crypt cell proliferation.** (A) There were no differences between groups in average apoptotic villus cell number in the duodenum, jejunum, or ileum. (B) There were no differences between groups in average apoptotic ratio in the duodenum, jejunum, or ileum. (C) There were no differences between groups in average total crypt cell number in the duodenum, jejunum, or ileum.

Figure 20

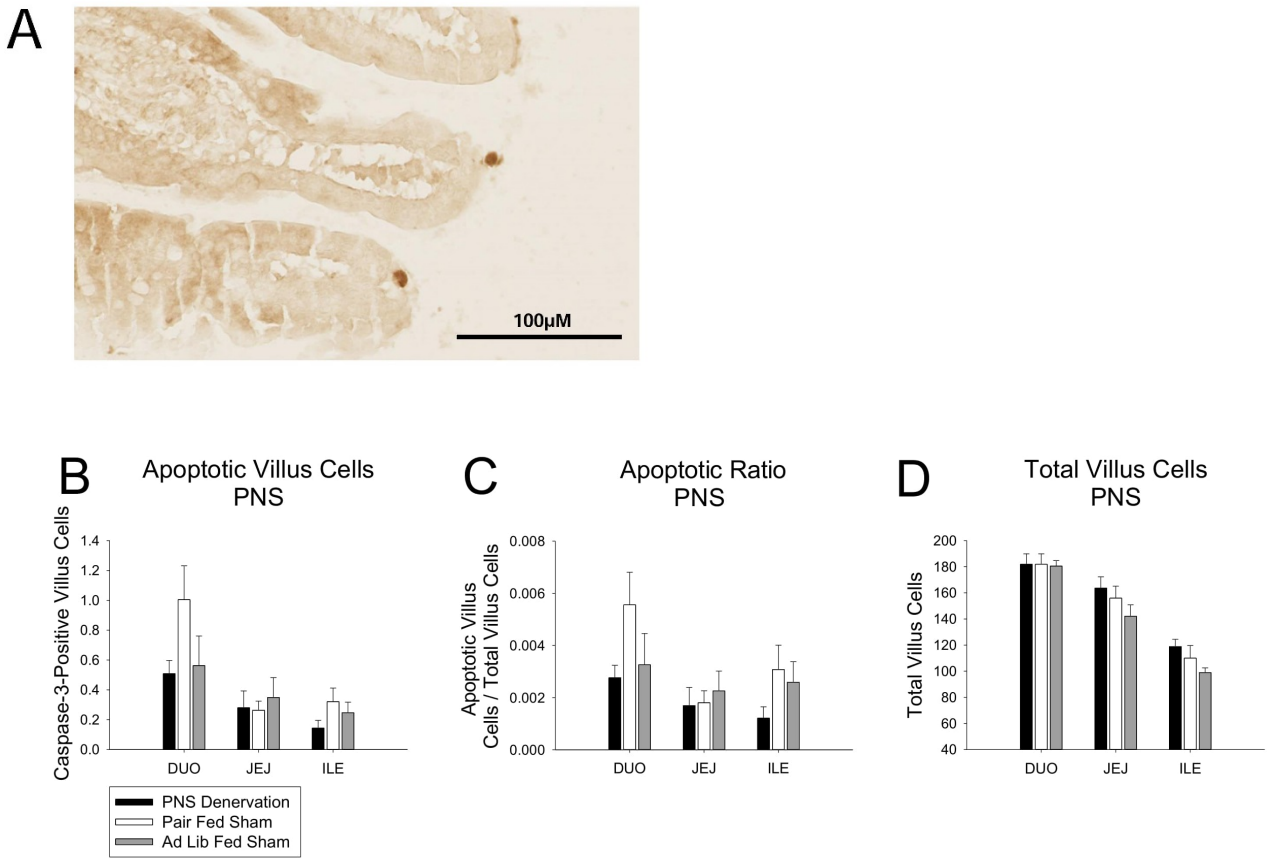

Figure 20. **Effect of PNS denervation on intestinal epithelial cell apoptosis.** (A) Intestinal tissue immunohistochemically processed with an anti-caspase 3 antibody to visualize intestinal epithelial cells undergoing apoptosis. (B) There were no differences between groups in average apoptotic villus cell number in the duodenum, jejunum, or ileum. (C) There were no differences between groups in average apoptotic ratio in the duodenum, jejunum, or ileum. (D) There were no differences between groups in average total villus cell number in the duodenum, jejunum, or ileum.

Figure 21

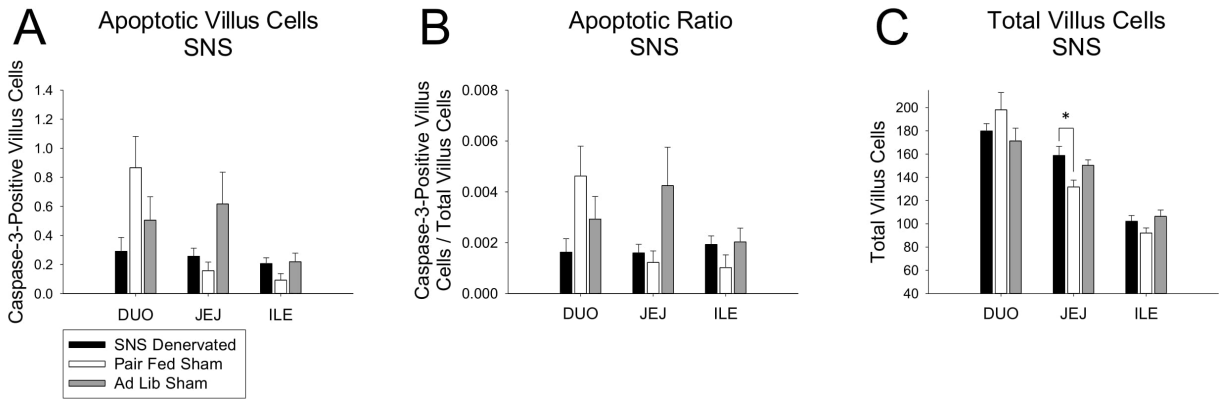

Figure 21. **Effect of SNS denervation on intestinal epithelial cell apoptosis.** (A) There were no differences between groups in average apoptotic villus cell number in the duodenum, jejunum, or ileum. (B) There were no differences between groups in average apoptotic ratio in the duodenum, jejunum, or ileum. (C) Average total villus cell number was increased in SNS denervated animals compared with pair fed sham animals ($p < 0.05$).

6.7 References

Andrews PL & Bingham S (1990). Adaptation of the mechanisms controlling gastric motility following chronic vagotomy in the ferret. *Exp Physiol* **75,** 811-825.

Bejar J, Broitman SA & Zamcheck N (1968). Effect of vagotomy upon the small intestine. *Gut* **9,** 87-90.

Beyaz S, Mana MD, Roper J, Kedrin D, Saadatpour A, Hong SJ, Bauer-Rowe KE, Xifaras ME, Akkad A, Arias E, Pinello L, Katz Y, Shinagare S, Abu-Remaileh M, Mihaylova MM, Lamming DW, Dogum R, Guo G, Bell GW, Selig M, Nielsen GP, Gupta N, Ferrone CR, Deshpande V, Yuan GC, Orkin SH, Sabatini DM & Yilmaz OH (2016). High-fat diet enhances stemness and tumorigenicity of intestinal progenitors. *Nature* **531,** 53-58.

Bjerknes M & Cheng H (2001). Modulation of specific intestinal epithelial progenitors by enteric neurons. *Proc Natl Acad Sci U S A* **98,** 12497-12502.

Brown HO, Levine ML & Lipkin M (1963). Inhibition of intestinal epithelial cell renewal and migration induced by starvation. *Am J Physiol* **205,** 868-872.

Brown TA, Washington MC, Metcalf SA & Sayegh AI (2011). The feeding responses evoked by cholecystokinin are mediated by vagus and splanchnic nerves. *Peptides* **32,** 1581-1586.

Callaghan BD (1991). The effect of pinealectomy and autonomic denervation on crypt cell proliferation in the rat small intestine. *J Pineal Res* **10,** 180-185.

Costa M, Brookes SJ & Hennig GW (2000). Anatomy and physiology of the enteric nervous system. *Gut* **47 Suppl 4,** iv15-19; discussion iv26.

Cruise JL, Houck KA & Michalopoulos GK (1985). Induction of DNA synthesis in cultured rat hepatocytes through stimulation of alpha 1 adrenoreceptor by norepinephrine. *Science* **227,** 749-751.

Dong Y, Yang C, Wang Z, Qin Z, Cao J & Chen Y (2016). The Injury of Serotonin on Intestinal Epithelium Cell Renewal of Weaned Diarrhoea Mice. *European Journal of Histochemistry : EJH* **60,** 2689.

Dumont P, Denoyer A & Robin P (2004). Long-term results of thoracoscopic sympathectomy for hyperhidrosis. *Ann Thorac Surg* **78,** 1801-1807.

Edvell A & Lindstrom P (1998). Vagotomy in young obese hyperglycemic mice: effects on syndrome development and islet proliferation. *Am J Physiol* **274,** E1034-1039.

Ellis H & Pryse-Davies J (1967). Vagotomy in the rat. A study of its effects on stomach and small intestine. *Br J Exp Pathol* **48,** 135-141.

Girish G, D'Souza R E, D'Souza P, Lewis MG & Baker DM (2017). Role of surgical thoracic sympathetic interruption in treatment of facial blushing: a systematic review. *Postgrad Med* **129,** 267-275.

Glatzle J, Sternini C, Robin C, Zittel TT, Wong H, Reeve JR, Jr. & Raybould HE (2002). Expression of 5-HT3 receptors in the rat gastrointestinal tract. *Gastroenterology* **123,** 217-226.

Graffner H, Ekelund M, Håkanson R & Rosengren E (1985). Effect of Different Denervation Procedures on Catecholamines in the Gut. *Scand J Gastroenterol* **20,** 1276-1280.

Gross ER, Gershon MD, Margolis KG, Gertsberg ZV, Li Z & Cowles RA (2012). Neuronal serotonin regulates growth of the intestinal mucosa in mice. *Gastroenterology* **143,** 408-417.e402.

Hansen OH, Larsen JK & Svendsen LB (1978). Changes in gastric mucosal cell proliferation after antrectomy or vagotomy in man. *Scand J Gastroenterol* **13,** 947-952.

Hashmonai M, Cameron AEP, Licht PB, Hensman C & Schick CH (2016). Thoracic sympathectomy: a review of current indications. *Surg Endosc* **30,** 1255-1269.

Higuchi H, Murata M, Uchida S & Yoshida H (1985). Changes in density of muscarinic cholinergic receptor by adrenergic denervation with guanethidine. *Jpn J Pharmacol* **37,** 207-211.

Hunt JV, Washington MC & Sayegh AI (2012). Exenatide and feeding: possible peripheral neuronal pathways. *Peptides* **33,** 285-290.

Kalia M & Sullivan JM (1982). Brainstem projections of sensory and motor components of the vagus nerve in the rat. *J Comp Neurol* **211,** 248-265.

Kato H & Shimazu T (1983). Effect of autonomic denervation on DNA synthesis during liver regeneration after partial hepatectomy. *Eur J Biochem* **134,** 473-478.

Kendig DM & Grider JR (2015). Serotonin and colonic motility. *Neurogastroenterol Motil* **27,** 899-905.

Kennedy MF, Tutton PJ & Barkla DH (1983). Adrenergic factors involved in the control of crypt cell proliferation in jejunum and descending colon of mouse. *Clin Exp Pharmacol Physiol* **10,** 577-586.

Keshavarzian A, Steck TB, Conway D, Gordon JH & Fields JZ (1990). Canine gastric muscarinic receptors up-regulate after vagotomy. *Dig Dis Sci* **35,** 449-452.

Koopman FA, Stoof SP, Straub RH, Van Maanen MA, Vervoordeldonk MJ & Tak PP (2011). Restoring the balance of the autonomic nervous system as an innovative approach to the treatment of rheumatoid arthritis. *Mol Med* **17,** 937-948.

Lachat JJ & Goncalves RP (1978). Influence of autonomic denervation upon the kinetics of the ileal epithelium of the rat. *Cell Tissue Res* **192,** 285-297.

Lakatua DJ, White M, Sackett-Lundeen LL & Haus E (1983). Change in phase relations of circadian rhythms in cell proliferation induced by time-limited feeding in BALB/c X DBA/2F1 mice bearing a transplantable Harding-Passey tumor. *Cancer Res* **43,** 4068-4072.

Mackie DB & Turner MD (1971). The effect of truncal vagotomy on jejunal and ileal blood flow. *J Surg Res* **11,** 356-363.

Mah AT, Van Landeghem L, Gavin HE, Magness ST & Lund PK (2014). Impact of diet-induced obesity on intestinal stem cells: hyperproliferation but impaired intrinsic function that requires insulin/IGF1. *Endocrinology* **155,** 3302-3314.

Musso F, Lachat J-J, Cruz AR & Gonçalves RP (1975). Effect of denervation on the mitotic index of the intestinal epithelium of the rat. *Cell and Tissue Research* **163,** 395-402.

Nakao K, Takahashi T, Utsunomiya J & Owyang C (1998). Extrinsic neural control of nitric oxide synthase expression in the myenteric plexus of rat jejunum. *J Physiol* **507,** 549-560.

Okafor PN, Lien C, Bairdain S, Simonson DC, Halperin F, Vernon AH, Linden BC & Lautz DB (2015). Effect of vagotomy during Roux-en-Y gastric bypass surgery on weight loss outcomes. *Obes Res Clin Pract* **9,** 274-280.

Olbe L (1994). Therapeutic applications of vagotomy. *Yale J Biol Med* **67,** 153-157.

Orloff LA, Orloff MS, Bunnett NW & Walsh JH (1985). Dopamine and norepinephrine in the alimentary tract changes after chemical sympathectomy and surgical vagotomy. *Life Sci* **36,** 1625-1631.

Rezek M, Vanderweele DA & Novin D (1975). Stages in the recovery of feeding following vagotomy in rabbits. *Behav Biol* **14,** 75-84.

Ridolfi TJ, Tong WD, Takahashi T, Kosinski L & Ludwig KA (2009). Sympathetic and parasympathetic regulation of rectal motility in rats. *J Gastrointest Surg* **13,** 2027-2033; discussion 2033.

Schneider K, Rezek M & Novin D (1976). Effects of visceral sympathectomy on 2-deoxy-d-glucose induced eating. *Physiol Behav* **16,** 55-58.

Sullivan CN, Raboin SJ, Gulley S, Sinzobahamvya NT, Green GM, Reeve JR, Jr. & Sayegh AI (2007). Endogenous cholecystokinin reduces food intake and increases Fos-like immunoreactivity in the dorsal vagal complex but not in the myenteric plexus by CCK1 receptor in the adult rat. *Am J Physiol Regul Integr Comp Physiol* **292,** R1071-1080.

Tanaka K, Ohkawa S, Nishino T, Niijima A & Inoue S (1987). Role of the hepatic branch of the vagus nerve in liver regeneration in rats. *Am J Physiol* **253,** G439-444.

Tong W, Kamiyama Y, Ridolfi TJ, Zietlow A, Zheng J, Kosinski L, Ludwig K & Takahashi T (2011). The role of 5-HT3 and 5-HT4 receptors in the adaptive mechanism of colonic transit following the parasympathetic denervation in rats. *J Surg Res* **171,** 510-516.

Tsibulevskii A & Orlova EN (1976). [Physiologic regeneration of jejunal epithelium following bilateral subdiaphragmatic vagotomy in rats]. *Biull Eksp Biol Med* **81,** 236-237.

Tutton PJ & Helme RD (1974). The influence of adrenoreceptor activity on crypt cell proliferation in the rat jejunum. *Cell Tissue Kinet* **7,** 125-136.

van der Flier LG & Clevers H (2009). Stem cells, self-renewal, and differentiation in the intestinal epithelium. *Annu Rev Physiol* **71,** 241-260.

Wright SA, Washington MC, Garcia C & Sayegh AI (2012). Gastrin releasing peptide-29 requires vagal and splanchnic neurons to evoke satiation and satiety. *Peptides* **33,** 125-131.

Xie W, Chen S, Strong JA, Li AL, Lewkowich IP & Zhang JM (2016). Localized Sympathectomy Reduces Mechanical Hypersensitivity by Restoring Normal Immune Homeostasis in Rat Models of Inflammatory Pain. *J Neurosci* **36,** 8712-8725.

Yox DP, Stokesberry H & Ritter RC (1991). Vagotomy attenuates suppression of sham feeding induced by intestinal nutrients. *Am J Physiol* **260,** R503-508.

6.8 Supplemental material: Brief discussion of surgical verification methodology

We collaborated with a laboratory that routinely performs both bilateral subdiaphragmatic vagotomies and celicaomesenteric ganglionectomies (Sullivan *et al.*, 2007; Brown *et al.*, 2011; Hunt *et al.*, 2012; Wright *et al.*, 2012). For vagotomy confirmation, we confirmed that during death, all vagotomized rats showed severely distended stomachs, which is an accepted verification of vagotomy (Sullivan *et al.*, 2007). Due to the expertise of the surgeon who routinely performs this procedure, we chose not to verify vagotomies using a second method. If desired, anatomical methods of verification include immediate hematoxylin and eosin (H&E) staining of removed vagal tissue and confirmed identification of a circular bundle of axons characteristic of the vagus nerve (Brown *et al.*, 2011; Hunt *et al.*, 2012; Wright *et al.*, 2012). Furthermore, postmortem verification can be achieved by confirming a lack of the vagus nerve (Brown *et al.*, 2011; Hunt *et al.*, 2012; Wright *et al.*, 2012). Functional methods of vagotomy verification include measuring cumulative food intake in response to intraperitoneal administration of cholecystokinin, which fails to reduce food intake in vagotomized animals compared with sham surgeries (Hunt *et al.*, 2012; Wright *et al.*, 2012), or measurement of decreased gastric emptying by phenol red (Lee *et al.*, 2012).

Celiacomesenteric ganglionectomies were verified by observation of increased defecation, which is indicative of increased gastric empyting and intestinal transit time (Rosa-e-Silva *et al.*, 1996). We did not choose to further verify these surgeries due to the expertise of the surgeon, who routinely performs this procedure. If desired, additional methods of verification include immediate H&E staining of the removed tissue and confirmation of distinct neuronal tissue with extensive number of cell bodies that is characteristic of the celiacomesenteric ganglion (Brown *et al.*, 2011; Hunt *et al.*, 2012; Wright *et al.*, 2012). Postmortem anatomical verification may include confirmation of the lack of a celiacomesenteric ganglion (Brown *et al.*, 2011; Hunt *et al.*, 2012) or immunohistochemical staining of intestinal

wholemounts that are absent of tyrosine hydroxylase staining, which is indicative of sympathetic denervation (Liu *et al.*, 2015a).

6.9 Supplemental material references

Brown TA, Washington MC, Metcalf SA & Sayegh AI (2011). The feeding responses evoked by cholecystokinin are mediated by vagus and splanchnic nerves. *Peptides* **32,** 1581-1586.

Hunt JV, Washington MC & Sayegh AI (2012). Exenatide and feeding: possible peripheral neuronal pathways. *Peptides* **33,** 285-290.

Lee JH, Kwon OD, Ahn SH, Choi KH, Park JH, Lee S, Choi BK & Jung KY (2012). Reduction of gastrointestinal motility by unilateral thyroparathyroidectomy plus subdiaphragmatic vagotomy in rats. *World J Gastroenterol* **18,** 4570-4577.

Sullivan CN, Raboin SJ, Gulley S, Sinzobahamvya NT, Green GM, Reeve JR, Jr. & Sayegh AI (2007). Endogenous cholecystokinin reduces food intake and increases Fos-like immunoreactivity in the dorsal vagal complex but not in the myenteric plexus by CCK1 receptor in the adult rat. *Am J Physiol Regul Integr Comp Physiol* **292,** R1071-1080.

Wright SA, Washington MC, Garcia C & Sayegh AI (2012). Gastrin releasing peptide-29 requires vagal and splanchnic neurons to evoke satiation and satiety. *Peptides* **33,** 125-131.

Zhuo H & Helke CJ (1996). Presence and localization of neurotrophin receptor tyrosine kinase (TrkA, TrkB, TrkC) mRNAs in visceral afferent neurons of the nodose and petrosal ganglia. *Brain Res Mol Brain Res* **38,** 63-70.

CHAPTER 7: SUMMARY: A DIRECT EFFECT OF THE AUTONOMIC NERVOUS SYSTEM ON SOMATIC STEM CELL PROLIFERATION?

7.1 Summary

Somatic stem cell proliferation is critical for maintaining tissue homeostasis through the regeneration of tissues. Multiple physiological systems modulate somatic stem cell proliferation by altering the rate of renewal, the number of cells produced, or the ratio of differentiated daughter cell types. All of these outcomes ultimately lead to functional changes in the tissue. Studies defining modulators of this process have largely concentrated on nutrients and peptides, but have traditionally neglected to investigate a role for the autonomic nervous system (ANS). It would seem beneficial for the brain to guide somatic stem cell proliferation via ANS signaling, therefore participating in decisions of tissue regeneration such as the replenishment of cells lost due to normal levels of apoptosis, renewal of tissues after injury, and growth of tissues during development or high nutrient availability. Roles for the ANS in controlling tissue regeneration have been identified after tissue injury in the liver (Cihak & Vaptzarova, 1973; Ashrif *et al.*, 1974; Kato & Shimazu, 1983; Cruise *et al.*, 1987) and pancreas (Medina *et al.*, 2013), and following ANS nerve ablation in the intestine and adipose tissue (Tutton & Helme, 1974; Musso *et al.*, 1975b; Tsibulevskii & Orlova, 1976; Lachat & Goncalves, 1978; Kennedy *et al.*, 1983; Callaghan, 1991). However, the direct participation of ANS connections with the somatic stem cells in these effects has been overlooked. Investigation of a possible direct neural influence on somatic stem cell proliferation will allow for further understanding of the mechanisms regulating stem cells and may reveal neurally-driven strategies to therapeutically modulate somatic stem cell proliferation to treat tissue abnormalities.

Limitations in studying the ANS effect on somatic stem cells

Although studying the effect of the ANS on somatic stem cell proliferation is an attractive research topic, there are experimental barriers that have limited the progression of this field. For example,

although the ANS is known to participate in tissue regeneration after injury in the liver and pancreas (Cihak & Vaptzarova, 1973; Ashrif *et al.*, 1974; Kato & Shimazu, 1983; Cruise *et al.*, 1987; Medina *et al.*, 2013), these tissues do not have identified stem cells that can be distinguished and/or isolated from other cell types within the tissue, eliminating the ability to study stem cell behavior in these phenomena. Studies investigating the effect of ANS nerve ablation on cell proliferation *in vivo* have also demonstrated a role for the ANS in tissue regeneration. These studies may have also identified indirect effects on proliferation due to post-surgical changes in food intake, inflammation, or other factors that can alter stem cell proliferation (Dailey, 2014; Slater *et al.*, 2017). Furthermore, it appears that the regeneration process recovers after the initial loss of ANS input (Davis *et al.*, 2017), likely due to adaptive mechanisms from other systems *in vivo*. These confounding variables of post-surgical side effects and eventual recovery mechanisms make it difficult to study the direct effect of the ANS on somatic stem cells *in vivo*. Therefore, a stem cell model that can be readily identified and isolated from its resident tissue and subsequently grown *in vitro* is necessary.

Intestinal epithelial stem cells as a model to investigating ANS influence on somatic stem cells

Intestinal epithelial stem cells (IESCs) are a suitable model to study ANS influence on somatic stem cell proliferation. Biomarkers on IESCs allow these cells to be identified and isolated for further study. IESCs can also be grown into intestinal epithelial organoids *in vitro*. An added advantage of using IESCs is that they undergo rapid proliferation, allowing for experimental measurement and manipulation in short periods of time. Further, the development of transgenic mouse models that express a green fluorescent protein (GFP) tag on an IESC biomarker adds to the relative ease of identifying and isolating IESCs from tissue using methods such as fluorescent activated cell sorting (FACS). Although ANS-induced changes in somatic stem cell proliferation may not use the same mechanisms in all tissue types, investigation of this process in IESCs can develop the initial framework for the study of ANS influence on stem cells within other tissues.

To regenerate intestinal epithelial tissue, IESCs divide to produce proliferating progenitor cells called transit-amplifying (TA) cells. These progenitor cells, in turn, differentiate into mature intestinal

epithelial cell types (*e.g*. enterocytes, goblet cells, enteroendocrine cells, and Paneth cells) as they migrate up the crypt-villus axis or to the crypt base. During differentiation, all of these mature cell types with the exception of the Paneth cells continue to migrate toward the tip of the villus in the small intestine or the surface epithelium in the large intestine, where they will undergo apoptosis. The apoptotic cells are then extruded into the lumen, and subsequently replaced by the new differentiated cells. By modulating the number and makeup of cells in the intestinal epithelium, putative ANS influence on IESCs may have the potential to influence intestinal epithelial functions such as nutrient absorption.

Evidence in support of an autonomic influence on somatic stem cell proliferation: The intestinal epithelium

The ANS participates regulating functions of the intestinal epithelium, the innermost layer of the intestinal mucosa. Examples include direct ANS modulation of functions such as fluid transport (Greenwood *et al.*, 1987) and hormone release (Rocca & Brubaker, 1999). A growing body of anatomical and functional evidence suggests that the ANS can also directly modulate proliferation of the intestinal epithelial stem cells (IESCs) located within the crypts of the tissue. SNS nerve terminals are densely concentrated at the base of the crypt where the IESCs are located (Norberg, 1964; Gabella & Costa, 1968), while PNS nerves make direct synaptic contact with intestinal epithelial cells (Bohorquez *et al.*, 2015). The SNS-associated alpha2A adrenoreceptor (α_{2A}-AR) and the PNS-associated muscarinic acetylcholine receptor subtypes M1 and M3 are expressed in IESCs and have been functionally linked to a role in controlling proliferation in the intestinal epithelium (Paris *et al.*, 1990; Valet *et al.*, 1993; Schaak *et al.*, 2000; Greig & Cowles, 2017a; Davis *et al.*, 2018). Moreover, the primary autonomic neurotransmitters, norepinephrine (NE) and acetylcholine (ACh), are ligands of these receptors and are able to modulate IESC proliferation *in vitro*. Application of NE or ACh to intestinal epithelial organoids decreases expression of a key cell cycle gene, cyclin D1 (Davis *et al.*, 2018), of which the protein is rate-limiting in proliferation (Ohtsubo & Roberts, 1993; Quelle *et al.*, 1993; Albanese *et al.*, 1995; Watanabe *et al.*, 1996; Resnitzky, 1997; Joyce *et al.*, 1999). Consistent with these results, an ACh agonist decreases intestinal epithelial organoid proliferation (Takahashi *et al.*, 2014). Together, these studies support a role

for ANS in the direct modulation of IESC proliferation and tissue regeneration through classically defined neurotransmitters and receptors.

Denervation studies also support a role for the ANS in controlling IESC proliferation. Ablation of the SNS or PNS nerves innervating the intestine alters intestinal epithelial cell proliferation (Tutton & Helme, 1974; Musso *et al.*, 1975b; Tsibulevskii & Orlova, 1976; Lachat & Goncalves, 1978; Kennedy *et al.*, 1983; Callaghan, 1991). The effect may be due to the loss of the nerves as the *in vivo* source of autonomic neurotransmitters, which have been shown to alter proliferation *in vitro*. However, the experimental design of these studies did not allow changes in proliferation to determine if changes in proliferation could be specifically attributed to stem cells, TA cells, or a combination of both cell types. In addition, the results appear to be confounded by the time point investigated. After SNS denervation, proliferation increases at early time points (Lachat & Goncalves, 1978) and decreases at later time points (Tutton & Helme, 1974; Kennedy *et al.*, 1983; Callaghan, 1991), with several studies demonstrating recovery to control levels of proliferation over time (Musso *et al.*, 1975a; Lachat & Goncalves, 1978; Davis *et al.*, 2017). The opposite effect is seen after PNS denervation, with proliferation decreased at early time points (Musso *et al.*, 1975b; Lachat & Goncalves, 1978), increased at later time points (Tsibulevskii & Orlova, 1976; Callaghan, 1991) and eventually recovering (Musso *et al.*, 1975b; Davis *et al.*, 2017). The exact timing of recovery after SNS or PNS denervation seems to depend on the method of denervation used and which segment of intestine (duodenum, jejunum, ileum or colon) is investigated. As previously discussed, confounding factors may also be influencing these varying results across time points, including post-surgical changes in food intake or inflammation that are known to modulate intestinal epithelial cell proliferation (Dailey, 2014; Slater *et al.*, 2017). Due to these limitations, denervation studies alone cannot be relied on to reveal clear trends in ANS influence on somatic stem cell proliferation under homeostatic conditions. Although these studies do provide valuable insight to this process *in vivo*, chronic loss of ANS input after denervation does not reflect the modus operandi of the ANS, which acts to rapidly modulate organ function under acute conditions. Despite these restrictions, these data demonstrate that there is likely a role of the ANS in intestinal epithelial turnover *in vivo*.

Based on the data outlined above, we propose models for the SNS and the PNS to directly influence IESC proliferation (Fig. 22). If either model were proven to be correct, it would be the first known instance of the nervous system directly regulating non-neuronal somatic stem cell proliferation.

Possible effects of autonomic cotransmitters

These models outline effects of NE and ACh, the primary autonomic neurotransmitters (Davis *et al.,* 2018). However, autonomic cotransmitters are also possible candidates to bind to IESCs to effect changes in proliferation. The neuropeptide cotransmitters neuropeptide Y (NPY) and adenosine triphosphate (ATP) are coreleased with NE from sympathetic terminals (Burnstock, 2013), while ATP and vasoactive peptide (VIP) are coreleased from PNS terminals. All three of these autonomic cotransmitters modulate proliferation in different cell types. NPY alters proliferation of myofibroblastic hepatic stellate cells (Oben *et al.*, 2003b), vascular smooth muscle cells (Erlinge *et al.*, 1994), and preadipocytes (Tang *et al.*, 2015). In vascular smooth muscle cells, NPY acts synergistically with NE to modulate proliferation (Oben *et al.*, 2003b). ATP alters proliferation in vascular smooth muscle cells, and is additive to the effects of NE (Erlinge *et al.*, 1993). VIP alters proliferation of hepatocytes (Kar *et al.*, 1996; Khedr *et al.*, 2018), airway smooth muscle cells (Wang *et al.*, 2018), and keratinocytes (Wollina *et al.*, 1998). Based on these findings, there may also be a direct effect of NPY, ATP, VIP or other autonomic cotransmitters on IESC proliferation, possibly additively or synergistically with the classical neurotransmitters NE or ACh. Overall, investigation of the role of cotransmitters would allow further understanding of the complex mechanisms that the ANS might employ to influence proliferation of IESCs or somatic stem cells in other organs.

Evidence for a role of the autonomic nervous system on IESC proliferation independent of the enteric nervous system

The SNS and PNS make synaptic connections with neurons of the enteric nervous system (ENS), the intrinsic neural system of the gastrointestinal (GI) tract. The ENS is already known to participate in the control of intestinal epithelial cell proliferation (Zucoloto *et al.*, 1988; Zucoloto *et al.*, 1997; Hernandes *et al.*, 2000) and, thus, can serve as a neural liaison to enact SNS- and PNS-driven functions.

Although the ENS is a possible pathway through which SNS and PNS alteration of IESC proliferation might occur, evidence indicates a role for the ANS to alter IESC proliferation independent of ENS participation. As NE is not an enteric neurotransmitter (McConalogue & Furness, 1994), the effect of NE on intestinal epithelial cell proliferation can only occur through SNS signaling, constituting a direct effect. With regard to the PNS, ACh is used by both the PNS and ENS as a neurotransmitter (McConalogue & Furness, 1994), which prohibits the definitive attribution of the effect of ACh on intestinal epithelial cell proliferation to the PNS or the ENS. However, as PNS denervation leaves ENS circuitry intact but still alters intestinal epithelial proliferation (Musso *et al.*, 1975b; Tsibulevskii & Orlova, 1976; Lachat & Goncalves, 1978; Callaghan, 1991), this suggests a role for the PNS in controlling IESC proliferation, for which a direct effect cannot be ruled out.

Autonomic influence on somatic stem cells: Potential applications for human medicine

ANS influence on somatic stem cells may be a valuable tool for applications in human medicine. Targeted manipulation of ANS outflow could be used to increase somatic stem cell proliferation and subsequently regenerate a variety of tissue types that are damaged or defective. For example, this strategy could be used on IESCs to treat short bowel syndrome, which is primarily characterized by a poor absorption of nutrients. Another approach could be used to drive somatic stem cell differentiation to purposely alter the ratio of mature cell types, in this case driving the cells toward an absorptive lineage. Notably, alteration of regeneration or differentiation may be an unintended side effect of ANS modulators currently used to treat other diseases. In addition to modifying tissue regeneration and differentiation, alteration of ANS-driven stem cell therapies might also be useful in the treatment of cancer. Many cancers are believed to be of stem cell origin, including the majority of colon cancers, which originate in IESCs (Barker *et al.*, 2009). Therefore, ANS tone might be modulated to decrease the proliferation of cancer stem cells. Autonomic nerves innervate all solid tumors (39), and ANS denervation alters the growth of certain types of tumors in rodent models *in vivo* (Lackovicova *et al.*, 2011; Zhao *et al.*, 2014; Saloman *et al.*, 2016; Decker *et al.*, 2017). Some cancer cells also express autonomic neurotransmitter receptors and subsequently alter their proliferation in response to application of NE, ACh, or related

agonists/antagonists *in vitro* (Park & Cho, 2008; Liou *et al.*, 2009; Huang *et al.*, 2012; Ferretti *et al.*, 2013; Morelli *et al.*, 2014; Coelho *et al.*, 2015; Wang *et al.*, 2016), an effect that is also seen in certain types of cancer stem cells (Alessandrini *et al.*, 2015; Al-Wadei *et al.*, 2016). Overall, these strategies to modulate stem cell proliferation could add to the current selection of ANS modulators in clinical practice.

There is growing evidence that the ANS can alter somatic stem cell proliferation. Characterization of this understudied phenomenon would allow for better understanding of the complex interface between the nervous system and peripheral tissues, possibly allowing for the development of treatments involving neural manipulation of somatic stem cells for clinical use.

7.2 Figure and caption

Figure 22

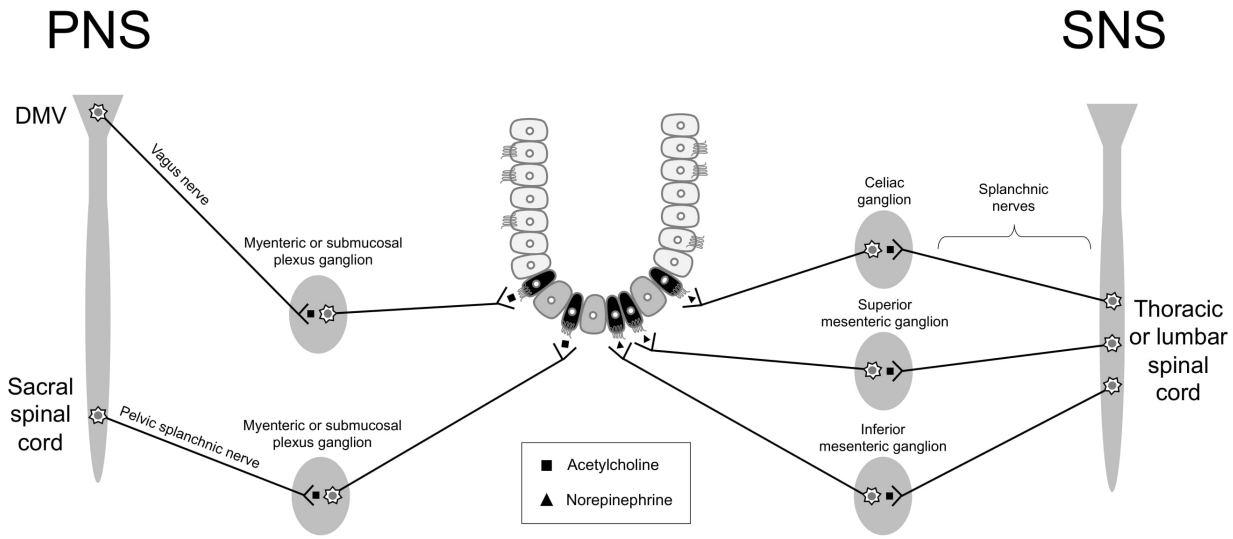

Figure 22. **Proposed model of direct parasympathetic or sympathetic influence on intestinal epithelial stem cell proliferation.**

Parasympathetic model:

When PNS activation occurs, preganglionic PNS neurons become activated. Cell bodies of these postganglionic PNS neurons are located in one of two areas: the dorsal motor nucleus of the vagus (DMV) in the brainstem, or the sacral spinal cord. From these regions, preganglionic PNS neurons project to the one of the two ganglionated plexuses of the enteric nervous system, the myenteric plexus or the submucosal plexus within the small intestine or colon. These neural projections travel via the vagus nerve (supplying the small intestine and proximal colon) or the pelvic splanchnic nerves (supplying the distal colon). Within the enteric plexus ganglia, these preganglionic PNS neurons make synaptic connections with postganglionic PNS neurons, which then project a short distance to make synaptic connections with IESCs. ACh released from the postganglionic PNS nerve terminals binds to M1 and/or M3 AChRs

Figure 22 (cont.)

located on IESCs. This initiates an intracellular signaling cascade that causes a suppression of D1 expression and a downstream decrease in proliferation.

Sympathetic model:

When SNS activation occurs, preganglionic SNS neurons become activated. Preganglionic SNS neurons have cell bodies located in the thoracic or lumbar spinal cord. These neurons project via splanchnic nerves to synapse onto postganglionic SNS neurons located in paravertebral sympathetic ganglia. The paravertebral ganglia include the celiac and superior mesenteric ganglia, which supply the small intestine, and the inferior mesenteric ganglion, which supplies the colon. Postganglionic SNS neurons then project to and make synaptic connections with IESCs. NE is released from the SNS nerve terminals and subsequently binds to α_{2A}-ARs located on IESCs. Activation of the α_{2A}-ARs by NE initiates an intracellular signaling cascade that causes a suppression of cyclin D1 expression and a consequential decrease in proliferation.

7.3 References

Al-Wadei MH, Banerjee J, Al-Wadei HA & Schuller HM (2016). Nicotine induces self-renewal of pancreatic cancer stem cells via neurotransmitter-driven activation of sonic hedgehog signalling. *Eur J Cancer* **52,** 188-196.

Albanese C, Johnson J, Watanabe G, Eklund N, Vu D, Arnold A & Pestell RG (1995). Transforming p21ras mutants and c-Ets-2 activate the cyclin D1 promoter through distinguishable regions. *J Biol Chem* **270,** 23589-23597.

Alessandrini F, Cristofaro I, Di Bari M, Zasso J, Conti L & Tata AM (2015). The activation of M2 muscarinic receptor inhibits cell growth and survival in human glioblastoma cancer stem cells. *Int Immunopharmacol* **29,** 105-109.

Ashrif S, Gillespie JS & Pollock D (1974). The effects of drugs or denervation on thymidine uptake into rat regenerating liver. *Eur J Pharmacol* **29,** 324-327.

Barker N, Ridgway RA, van Es JH, van de Wetering M, Begthel H, van den Born M, Danenberg E, Clarke AR, Sansom OJ & Clevers H (2009). Crypt stem cells as the cells-of-origin of intestinal cancer. *Nature* **457,** 608-611.

Bohorquez DV, Shahid RA, Erdmann A, Kreger AM, Wang Y, Calakos N, Wang F & Liddle RA (2015). Neuroepithelial circuit formed by innervation of sensory enteroendocrine cells. *J Clin Invest* **125,** 782-786.

Burnstock G (2013). Cotransmission in the autonomic nervous system. *Handb Clin Neurol* **117,** 23-35.

Callaghan BD (1991). The effect of pinealectomy and autonomic denervation on crypt cell proliferation in the rat small intestine. *J Pineal Res* **10,** 180-185.

Cihak A & Vaptzarova K (1973). Decreased synthesis of DNA in regenerating rat liver after the administration of reserpine. *Br J Pharmacol* **49,** 253-257.

Coelho M, Moz M, Correia G, Teixeira A, Medeiros R & Ribeiro L (2015). Antiproliferative effects of beta-blockers on human colorectal cancer cells. *Oncol Rep* **33,** 2513-2520.

Cruise JL, Knechtle SJ, Bollinger RR, Kuhn C & Michalopoulos G (1987). Alpha 1-adrenergic effects and liver regeneration. *Hepatology* **7,** 1189-1194.

Dailey MJ (2014). Nutrient-induced intestinal adaption and its effect in obesity. *Physiol Behav* **136,** 74-78.

Davis EA, Washington MC, Yaniz ER, Phillips H, Sayegh AI & Dailey MJ (2017). Long-term effect of parasympathetic or sympathetic denervation on intestinal epithelial cell proliferation and apoptosis. *Exp Biol Med (Maywood)* **242,** 1499-1507.

Davis EA, Zhou W & Dailey MJ (2018). Evidence for a direct effect of the autonomic nervous system on intestinal epithelial stem cell proliferation. *Physiol Rep* **6,** e13745.

Decker AM, Jung Y, Cackowski FC, Yumoto K, Wang J & Taichman RS (2017). Sympathetic Signaling Reactivates Quiescent Disseminated Prostate Cancer Cells in the Bone Marrow. *Mol Cancer Res* **15,** 1644-1655.

Erlinge D, Brunkwall J & Edvinsson L (1994). Neuropeptide Y stimulates proliferation of human vascular smooth muscle cells: cooperation with noradrenaline and ATP. *Regul Pept* **50,** 259-265.

Erlinge D, Yoo H, Edvinsson L, Reis DJ & Wahlestedt C (1993). Mitogenic effects of ATP on vascular smooth muscle cells vs. other growth factors and sympathetic cotransmitters. *Am J Physiol* **265,** H1089-1097.

Ferretti M, Fabbiano C, Di Bari M, Conte C, Castigli E, Sciaccaluga M, Ponti D, Ruggieri P, Raco A, Ricordy R, Calogero A & Tata AM (2013). M2 receptor activation inhibits cell cycle progression and survival in human glioblastoma cells. *J Cell Mol Med* **17,** 552-566.

Gabella G & Costa M (1968). Adrenergic fibres in the mucous membrane of guinea pig alimentary tract. *Experientia* **24,** 706-707.

Greenwood B, Tremblay L & Davison JS (1987). Sympathetic control of motility, fluid transport, and transmural potential difference in the rabbit ileum. *Am J Physiol* **253,** G726-729.

Greig CJ & Cowles RA (2017). Muscarinic acetylcholine receptors participate in small intestinal mucosal homeostasis. *J Pediatr Surg* **52,** 1031-1034.

Hernandes L, Zucoloto S & Alvares EP (2000). Effect of myenteric denervation on intestinal epithelium proliferation and migration of suckling and weanling rats. *Cell Prolif* **33,** 127-138.

Huang XY, Wang HC, Yuan Z, Huang J & Zheng Q (2012). Norepinephrine stimulates pancreatic cancer cell proliferation, migration and invasion via beta-adrenergic receptor-dependent activation of P38/MAPK pathway. *Hepatogastroenterology* **59,** 889-893.

Joyce D, Bouzahzah B, Fu M, Albanese C, D'Amico M, Steer J, Klein JU, Lee RJ, Segall JE, Westwick JK, Der CJ & Pestell RG (1999). Integration of Rac-dependent regulation of cyclin D1 transcription through a nuclear factor-kappaB-dependent pathway. *J Biol Chem* **274,** 25245-25249.

Kar S, Hasegawa K & Carr BI (1996). Comitogenic effects of vasoactive intestinal polypeptide on rat hepatocytes. *J Cell Physiol* **168,** 141-146.

Kato H & Shimazu T (1983). Effect of autonomic denervation on DNA synthesis during liver regeneration after partial hepatectomy. *Eur J Biochem* **134,** 473-478.

Kennedy MF, Tutton PJ & Barkla DH (1983). Adrenergic factors involved in the control of crypt cell proliferation in jejunum and descending colon of mouse. *Clin Exp Pharmacol Physiol* **10,** 577-586.

Khedr M, Abdelmotelb AM, Bedwell TA, Shtaya A, Alzoubi MN, Abu Hilal M & Khakoo SI (2018). Vasoactive intestinal peptide induces proliferation of human hepatocytes. *Cell Prolif***,** e12482.

Lachat JJ & Goncalves RP (1978). Influence of autonomic denervation upon the kinetics of the ileal epithelium of the rat. *Cell Tissue Res* **192,** 285-297.

Lackovicova L, Banovska L, Bundzikova J, Janega P, Bizik J, Kiss A & Mravec B (2011). Chemical sympathectomy suppresses fibrosarcoma development and improves survival of tumor-bearing rats. *Neoplasma* **58,** 424-429.

Liou SF, Lin HH, Liang JC, Chen IJ & Yeh JL (2009). Inhibition of human prostate cancer cells proliferation by a selective alpha1-adrenoceptor antagonist labedipinedilol-A involves cell cycle arrest and apoptosis. *Toxicology* **256,** 13-24.

McConalogue K & Furness JB (1994). Gastrointestinal neurotransmitters. *Baillieres Clin Endocrinol Metab* **8,** 51-76.

Medina A, Yamada S, Hara A, Hamamoto K & Kojima I (2013). Involvement of the parasympathetic nervous system in the initiation of regeneration of pancreatic beta-cells. *Endocr J* **60,** 687-696.

Morelli MB, Amantini C, Nabissi M, Liberati S, Cardinali C, Farfariello V, Tomassoni D, Quaglia W, Piergentili A, Bonifazi A, Del Bello F, Santoni M, Mammana G, Servi L, Filosa A, Gismondi A & Santoni G (2014). Cross-talk between alpha1D-adrenoceptors and transient receptor potential vanilloid type 1 triggers prostate cancer cell proliferation. *BMC Cancer* **14,** 921.

Musso F, Lachat J-J, Cruz AR & Gonçalves RP (1975a). Effect of denervation on the mitotic index of the intestinal epithelium of the rat. *Cell and Tissue Research* **163,** 395-402.

Musso F, Lachat JJ, Cruz AR & Goncalves RP (1975b). Effect of denervation on the mitotic index of the intestinal epithelium of the rat. *Cell Tissue Res* **163,** 395-402.

Norberg KA (1964). Adrenergic innervation of the intestinal wall studied by fluorescence microscopy. *Int J Neuropharmacol* **3,** 379-382.

Oben JA, Yang S, Lin H, Ono M & Diehl AM (2003). Norepinephrine and neuropeptide Y promote proliferation and collagen gene expression of hepatic myofibroblastic stellate cells. *Biochem Biophys Res Commun* **302,** 685-690.

Ohtsubo M & Roberts JM (1993). Cyclin-dependent regulation of G1 in mammalian fibroblasts. *Science* **259,** 1908-1912.

Paris H, Voisin T, Remaury A, Rouyer-Fessard C, Daviaud D, Langin D & Laburthe M (1990). Alpha-2 adrenoceptor in rat jejunum epithelial cells: characterization with [3H]RX821002 and distribution along the villus-crypt axis. *J Pharmacol Exp Ther* **254,** 888-893.

Park YS & Cho NJ (2008). Enhanced proliferation of SNU-407 human colon cancer cells by muscarinic acetylcholine receptors. *BMB Rep* **41,** 803-807.

Quelle DE, Ashmun RA, Shurtleff SA, Kato JY, Bar-Sagi D, Roussel MF & Sherr CJ (1993). Overexpression of mouse D-type cyclins accelerates G1 phase in rodent fibroblasts. *Genes Dev* **7,** 1559-1571.

Resnitzky D (1997). Ectopic expression of cyclin D1 but not cyclin E induces anchorage-independent cell cycle progression. *Mol Cell Biol* **17,** 5640-5647.

Rocca AS & Brubaker PL (1999). Role of the vagus nerve in mediating proximal nutrient-induced glucagon-like peptide-1 secretion. *Endocrinology* **140,** 1687-1694.

Saloman JL, Albers KM, Rhim AD & Davis BM (2016). Can Stopping Nerves, Stop Cancer? *Trends Neurosci* **39,** 880-889.

Schaak S, Cussac D, Cayla C, Devedjian JC, Guyot R, Paris H & Denis C (2000). Alpha(2) adrenoceptors regulate proliferation of human intestinal epithelial cells. *Gut* **47,** 242-250.

Slater TW, Finkielsztein A, Mascarenhas LA, Mehl LC, Butin-Israeli V & Sumagin R (2017). Neutrophil Microparticles Deliver Active Myeloperoxidase to Injured Mucosa To Inhibit Epithelial Wound Healing. *J Immunol* **198,** 2886-2897.

Takahashi T, Ohnishi H, Sugiura Y, Honda K, Suematsu M, Kawasaki T, Deguchi T, Fujii T, Orihashi K, Hippo Y, Watanabe T, Yamagaki T & Yuba S (2014). Non-neuronal acetylcholine as an endogenous regulator of proliferation and differentiation of Lgr5-positive stem cells in mice. *Febs j* **281,** 4672-4690.

Tang HN, Man XF, Liu YQ, Guo Y, Tang AG, Liao EY & Zhou HD (2015). Dose-dependent effects of neuropeptide Y on the regulation of preadipocyte proliferation and adipocyte lipid synthesis via the PPARgamma pathways. *Endocr J* **62,** 835-846.

Tsibulevskii A & Orlova EN (1976). [Physiologic regeneration of jejunal epithelium following bilateral subdiaphragmatic vagotomy in rats]. *Biull Eksp Biol Med* **81,** 236-237.

Tutton PJ & Helme RD (1974). The influence of adrenoreceptor activity on crypt cell proliferation in the rat jejunum. *Cell Tissue Kinet* **7,** 125-136.

Valet P, Senard JM, Devedjian JC, Planat V, Salomon R, Voisin T, Drean G, Couvineau A, Daviaud D, Denis C & et al. (1993). Characterization and distribution of alpha 2-adrenergic receptors in the human intestinal mucosa. *J Clin Invest* **91,** 2049-2057.

Wang J, Shang YX, Cai XX & Liu LY (2018). Vasoactive intestinal peptide inhibits airway smooth muscle cell proliferation in a mouse model of asthma via the ERK1/2 signaling pathway. *Exp Cell Res* **364,** 168-174.

Wang L, Zhi X, Zhang Q, Wei S, Li Z, Zhou J, Jiang J, Zhu Y, Yang L, Xu H & Xu Z (2016). Muscarinic receptor M3 mediates cell proliferation induced by acetylcholine and contributes to apoptosis in gastric cancer. *Tumour Biol* **37,** 2105-2117.

Watanabe G, Lee RJ, Albanese C, Rainey WE, Batlle D & Pestell RG (1996). Angiotensin II activation of cyclin D1-dependent kinase activity. *J Biol Chem* **271,** 22570-22577.

Wollina U, Prochnau D, Hoffmann A, Hipler UC & Wetzker R (1998). Vasoactive intestinal peptide and epidermal growth factor: co-mitogens or inhibitors of keratinocyte proliferation in vitro? *Int J Mol Med* **2,** 725-730.

Zhao CM, Hayakawa Y, Kodama Y, Muthupalani S, Westphalen CB, Andersen GT, Flatberg A, Johannessen H, Friedman RA, Renz BW, Sandvik AK, Beisvag V, Tomita H, Hara A, Quante M, Li Z, Gershon MD, Kaneko K, Fox JG, Wang TC & Chen D (2014). Denervation suppresses gastric tumorigenesis. *Sci Transl Med* **6,** 250ra115.

Zucoloto S, de Deus DA, Martins AA, Muglia VF, Kajiwara JK & Garcia SB (1997). The relationship between myenteric neuronal denervation, smooth muscle thickening and epithelial cell proliferation in the rat colon. *Res Exp Med (Berl)* **197,** 117-124.

Zucoloto S, Diaz JA, Oliveira JS, Muccilo G, Sales Neto VN & Kajiwara JK (1988). Effect of chemical ablation of myenteric neurones on intestinal cell proliferation. *Cell Tissue Kinet* **21,** 213-219

APPENDIX A: FURTHER INVESTIGATION OF THE VAGAL AFFERENT PATHWAY

A.1 Rationale

After developing the methods necessary to isolate and test changes in vagal afferent nerves (presented in Chapter 2), I then began an investigation into the mechanisms underlying nutrient-induced vagal afferent neuroplasticity. I hypothesized that furin, a proprotein convertase that has been implicated in the control of neuroplasiticity in mammalian CNS neurons and peripheral neurons of other species, underlies nutrient-induced changes in vagal afferent fiber density at the level of GI tract and in the NTS. Although fiber density of the vagal afferents in the NTS and the levels of furin in the nodose ganglia (through immunohistochemistry and qPCR methods) were able to be assessed, I was unable to visualize the fiber density of the vagal afferent terminals in the GI tract using multiple methods (i.e., whole mount, CLARITY, frozen tissue on a cryostat, paraffin embedded on a microtome, gelatin embedded on a vibratome, muscularis peel). Because of this methodological issue, I did not pursue additional hypothesis-driven studies.

A.2 Figures and captions

Figure 23

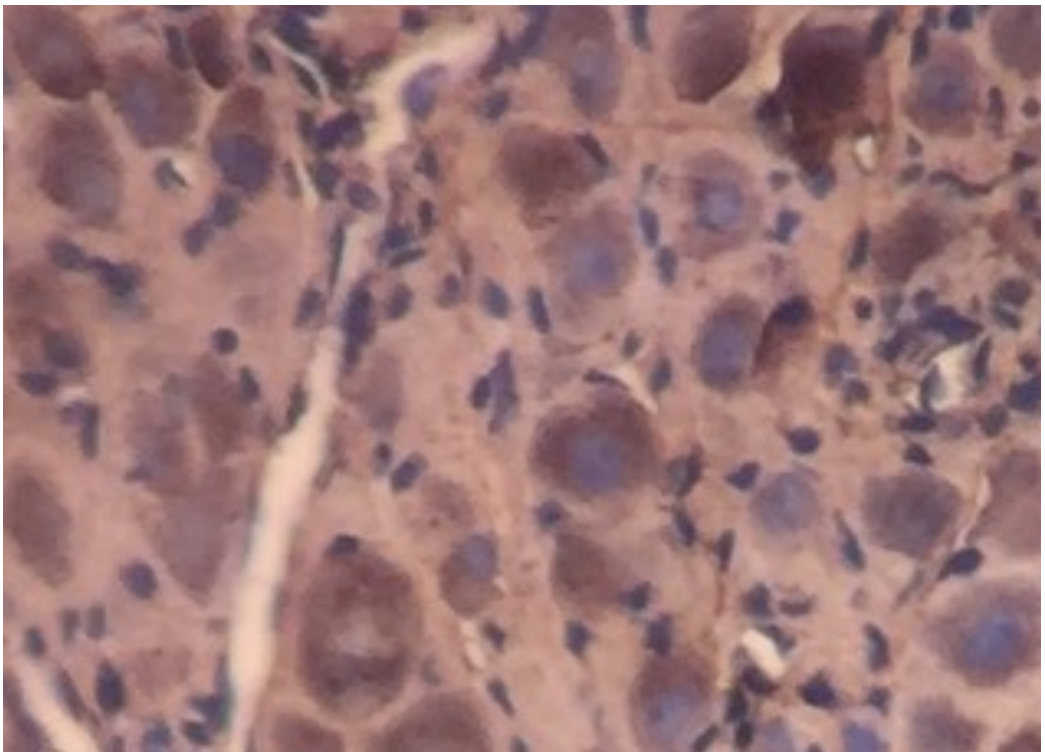

Figure 23. **Evaluation of furin in the rat nodose ganglion.** Representative image of immunohistochemical localization of the furin protein in the rat nodose ganglion (Anti-Furin primary antibody, [1:50, ab183495, Abcam, San Francisco, CA], hematoxylin counterstain.)

Figure 24

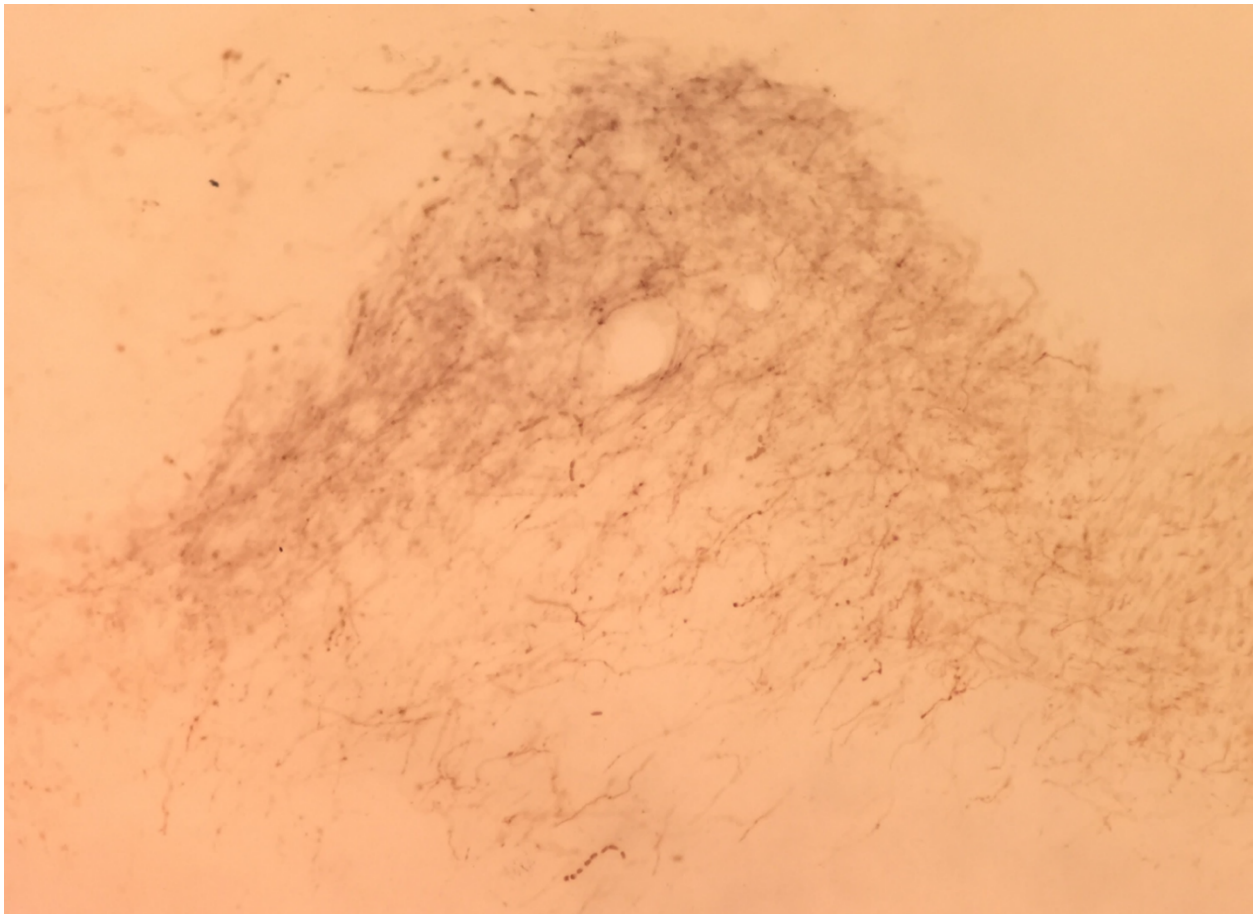

Figure 24. **Visualization of vagal afferent neuron projections to the nucleus of the solitary tract.** I traced vagal afferent neurons using biotinylated dextran amines injected into the nodose ganglion to the nucleus of the solitary tract. Tracer visualized with 3,3'-diaminobenzidine – horseradish peroxidase (DAB-HRP) immunohistochemistry.

APPENDIX B: EXCERPT FROM: OBESITY, INDEPENDENT OF DIET, DRIVES LASTING EFFECTS ON INTESTINAL EPITHELIAL STEM CELL PROLIFERATION IN MICE

(Full manuscript published in Experimental Biology and Medicine; Citation: Zhou W, Davis EA, & Dailey MJ. (2018). Obesity, independent of diet, drives lasting effects on intestinal epithelial stem cell proliferation in mice. Experimental Biology and Medicine, 243(10), 826-835.)

B.1 Abstract

The intestinal epithelium plays an essential role in nutrient absorption, hormone release and barrier function. Maintenance of the epithelium is driven by continuous cell renewal by intestinal epithelial stem cells (IESCs) located in the intestinal crypts. Obesity affects this process and results in changes in the size and function of the tissue. Because both the amount of food intake and the composition of the diet are contributing factors to developing and maintaining obesity, it is necessary to tease apart the separate contributions of obesity versus the type/amount of diet in driving the epithelial changes. C57BL/6J mice were fed a 60% high-fat diet (HFD) versus a 10% low-fat diet (LFD) for 3 months. A pair fed (PF) group was included (mice were fed with HFD, but in equal kcal as that eaten by the LFD fed mice to keep them lean). We investigated the differences in crypt-villus morphology and the number of differentiated epithelial cell types *in vivo*. We found that HFD-induced obesity, independent of the HFD, increased crypt depth, villus height, and the number of IESCs and goblet cells *in vivo*.

B.2 Materials and methods

Animals

Male C57BL/6J mice at 10-weeks-old were obtained from the Jackson Laboratory (Bar Harbor, ME; N=24). Mice were individually housed in modified shoebox cages with a raised woven wire platform and lined with brown kraft paper for collection and measurement of food spillage. Mice were acclimated to the housing for 1 week with *ad libitum* access to tap water and laboratory chow (Tecklad 22/5, Tecklad Diets, Madison, WI) on a 12:12 light:dark cycle in a climate-controlled room (22 ± 1 °C and 60% relative

humidity). All procedures were approved by the Institutional Animal Care and Use Committee at the University of Illinois at Urbana-Champaign.

Following the 1 week acclimation, mice were fed a HFD or a LFD for 3 months. The HFD and control groups were as follows: 1) 60% HFD *ad libitum* fed (Research Diets D12492), 2) 10% LFD *ad libitum* fed (Research Diets D12450J), and 3) 60% HFD PF group (fed a HFD, but in equal kcal as that eaten by the LFD fed animals to keep them lean), n=8 per group. It is not possible to include a LFD that eats the same kcal amount as the HFD ad libitum group without using a transgenic mouse or lesioning the hypothalamus to induce hyperphagia of the LFD. Mice were weighed weekly and food intake was measured daily. Mice in HFD PF group were given an equal kcal of the food eaten by the LFD fed mice a day later than other groups.

After 3 months, mice were killed by decapitation under isoflurane anesthesia (Henry Schein Animal Health, Dublin, OH). A subset of the mice (n=5 per group) were used for histology. A power analysis (G*Power 3.1.9.2) based on previously published data investigating epithelial changes *in vivo* show that to achieve a power = 0.8 and a type I error of 0.05, an n=5 per group for *in vivo* analysis is needed (Mah *et al.*, 2014; Beyaz *et al.*, 2016). The intestine was exposed, and tissue was collected from the duodenum, jejunum, ileum and colon as previously described (Blackmore *et al.*, 2017). Briefly, to ensure that we are collecting similar segments of the intestine for analysis between animals, we measured from the pyloric sphincter, discarded the first 1 cm and then collected two 5 mm samples to be processed for histology. We then measured from the cecum, discarded the first 1 cm and then collected two 5 mm segments of the ileum or colon. From the remaining jejunal segment, we measured from the middle and collected two 5 mm segments to be processed similarly to the duodenal and ileal segments. Each of the 5 mm intestinal segments were fixed in 10% neutral buffered formalin for 24 h at RT and then stored in 70% ETOH at RT prior to paraffin embedding.

Formalin fixed tissue sections were embedded using paraffin and cut on a microtome at 5 µm thickness and mounted onto charged glass microscope slides. For crypt-villus morphology, tissue sections were deparaffinized in xylenes followed by a series of graded ethanol, then rinsed in deionized water.

Intestinal sections were counterstained in hematoxylin (Fisher HealthCare, Houston, TX) and dehydrated in a series of graded ethanol followed by xylenes. Slides were mounted with Permount mounting media (Fisher Scientific, Pittsburgh, PA) and stored at RT.

For immunohistochemical processing for Olfactomedin-4 (Olmf4; an IESC marker) and Chromogranin A (an enteroendocrine cell marker), after deparaffinizing slides as described above, antigen retrieval was performed by immersing the slides in the sodium citrate buffer (10 mM sodium citrate hydrochloride [Fisher Scientific, Pittsburgh, PA] and 0.05% Tween 20 [Sigma- Aldrich, St. Louis, MO] diluted in distilled water, pH 6.0) for 20 min in a water bath at 95°C, then allowed to cool while still immersed in the sodium citrate buffer solution for 30 min at RT. Slides were rinsed between each step in 1x PBS. Slides were incubated in blocking solution (3% Normal Donkey Serum [Jackson ImmunoResearch, West Grove, PA] and 0.3% Triton X-100 [Sigma-Aldrich, St. Louis, MO] diluted in 1x PBS) for 1 h at RT. Sections were incubated overnight at 4 °C in the following primary antibodies diluted in the blocking solution: Olmf4 (1:400; Cell Signaling Technology, Danvers, MA), Chromogranin A (1:1,000; Abcam, Cambridge, United Kingdom). Sections were incubated in a donkey anti-rabbit biotin-conjugated IgG (H&L) secondary antibody (1:500, Jackson ImmunoResearch, West Grove, PA) diluted in 1x PBS for 1 h at RT. Sections were then incubated in an avidin-biotin complex (Vector Laboratories, Burlingame, CA) for 30 min at RT. A diaminobenzidine-hydrogen peroxidase reaction was performed using a substrate kit (Vector Laboratories, Burlingame, CA). Slides were dehydrated and mounted as described above.

For Periodic Acid Schiff staining of mucins (a goblet cell marker) and Paneth cell granules (a Paneth cell marker), after deparaffinizing slides as described above, slides were immersed in 0.5% Periodic Acid (Newcomer Supply, Middleton, WI) for 10 min at RT and washed in distilled water. Sides were then immersed in Schiff reagent (Newcomer Supply, Middleton, WI) for 30 min at RT, and rinsed in 0.55% potassium metabisulfite (Fisher Scientific, Pittsburgh, PA) for 30 sec and followed by washing in warm running tap water for 10 min. Slides were counterstained in hematoxylin, dehydrated and mounted as described above.

For staining of alkaline phosphatase (an enterocyte marker), after deparaffinizing slides as described above, slides were immersed in alkaline phosphatase substrate working solution (Vector Laboratories, Burlingame, CA) for 25 min. Slides were then washed in 100 mM Tris hydrochloride (PH 8.2; Fisher Scientific, Pittsburgh, PA) for 5 min and followed by washing in running distilled water for 5 min. Slides were dehydrated and mounted as described above.

Intestinal tissues sections were visualized using a NanoZoomer Digital Pathology (NDP) System (Hamamatsu, Hamamatsu City, Japan) using a 40× objective and NDP Scan software. Crypt depth and villus height of 3 intestinal cross sections (4 crypts or villi per section) from each segment of the intestine (duodenum, jejunum, ileum and colon) per mouse were measured using NDP View 2 software. The number of Olmf4-postive IESCs, Chromogranin A-positive enteroendocrine cells, Periodic Acid Schiff-positive goblet cells and Periodic Acid Schiff-positive Paneth cells of 3 intestinal cross sections (3 crypts or villi per section) from the jejunum per mouse were measured using NDP View 2 software. The expression of alkaline phosphatase was determined by measuring relative intensity of alkaline phosphatase staining of 3 intestinal cross sections (3 villi per section) from the jejunum per mouse were measured using ImageJ software.

Data analysis

Data are expressed as Mean ± SEM. For measurements of crypt depth, villus height, number of different intestinal cell types, and the relative intensity of alkaline phosphatase staining, differences between groups for each segment were analyzed using a one-way ANOVA. Fisher's LSD post-hoc tests were used where appropriate. $p<0.05$ was considered statistically significant.

B.3 Results

Body weight and food intake

Body weight and food intake were increased in the HFD fed mice compared with the LFD and HFD PF groups (Fig. 25A, B&C; $p<0.05$).

Intestinal crypt and villus morphometry

Crypt depth and villus height in the duodenum and jejunum were increased in the HFD fed mice compared with the LFD and HFD PF groups (Fig. 26B&C; $p<0.05$), but no differences were found in the ileum and colon (Fig. 26B&C).

Number of intestinal epithelial cell types

The number of Olmf4-positive IESCs and Periodic Acid Schiff-positive goblet cells in the jejunum was increased in the HFD fed mice compared with the LFD and HFD PF groups (Fig. 27B&H; $p<0.05$). There were no differences in the number of Periodic Acid Schiff-positive Paneth cells and Chromogranin A-positive enteroendocrine cells in the jejunum between the HFD, HFD PF or LFD groups (Fig. 27D&F).

Expression of intestinal enzymes or secretory proteins

The protein levels of alkaline phosphatase (a marker for enterocytes) was highest in the HFD PF group in the jejunum (Fig. 28B; $p<0.05$). Specifically, alkaline phosphatase levels in the HFD PF group were increased compared with the HFD and LFD groups (Fig. 28B; $p<0.05$). Alkaline phosphatase levels were also increased in the HFD compared with the LFD group (Fig. 28B; $p<0.05$).

B.4 Figures and captions

Figure 25

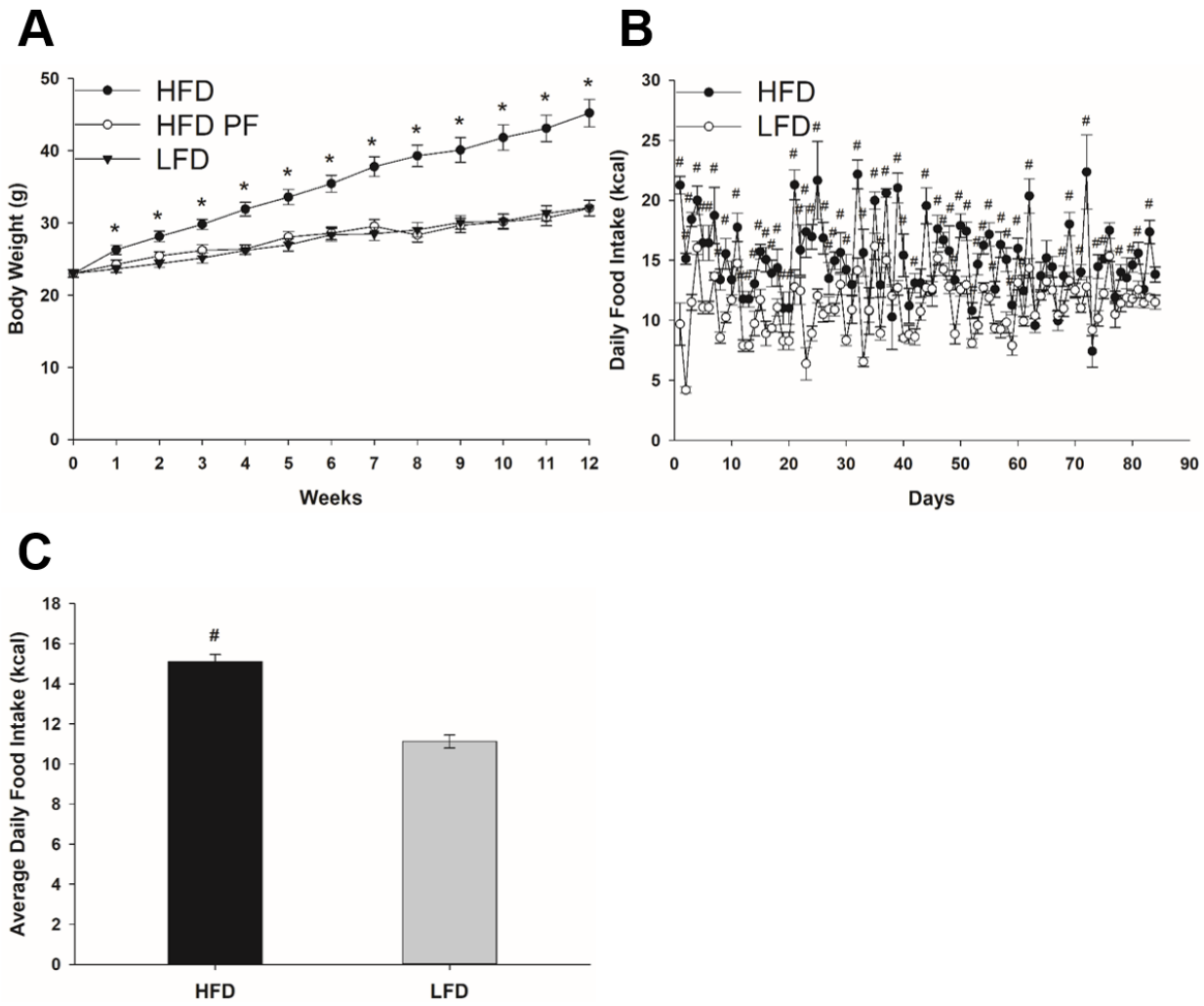

Figure 25. Body weight (A), daily food intake (B) and average daily food intake (C) of mice fed with HFD or LFD for 3 months. Data are expressed as Mean ± SEM (n=8). * indicates significant different between HFD and HFD PF groups and between HFD and LFD groups at that time point, $p<0.05$. # indicates significantly different between HFD and LFD groups at that time point, $p<0.05$.

Figure 26

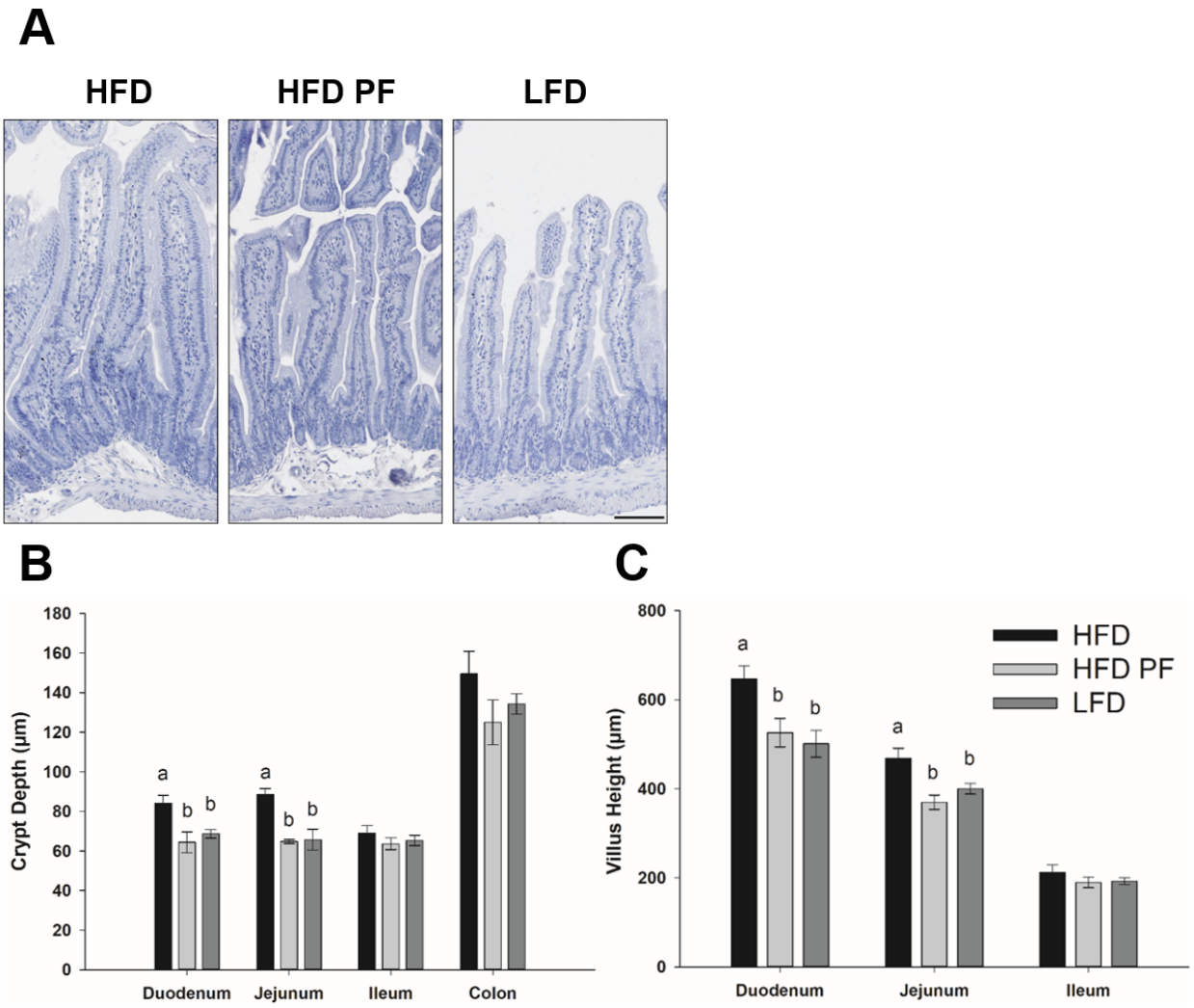

Figure 26. Representative images of hematoxylin stained crypt-villus morphology in the jejunum (A), and quantification of crypt depth and villus height in intestinal segments (duodenum, jejunum, ileum and colon) (B) collected from mice fed with HFD or LFD. Scale bar, 100 μm. Data are expressed as Mean ± SEM (n=5). Means with different letters indicate significantly different in each intestinal segment, $p < 0.05$.

Figure 27

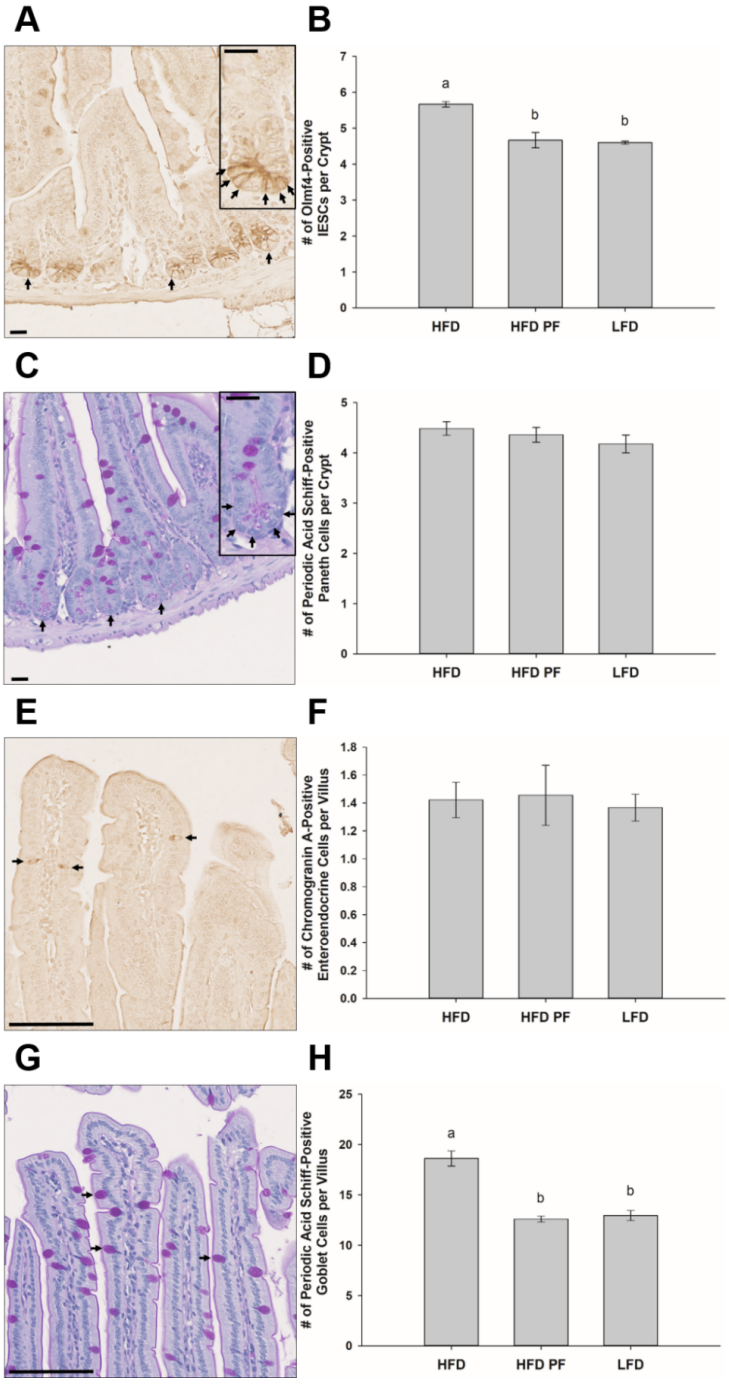

Figure 27. Representative images of the jejunal sections stained with Olmf4 (IESC marker), Scale bar, 20 µm (A), Paneth cell granules (Paneth cell marker), Scale bar, 20 µm (C), Chromogranin A (enteroendocrine cell maker), Scale bar, 100 µm (E), and mucins (goblet cell marker), Scale, 100 µm (G).

Figure 27 (cont.)

Quantification of the number of Olmf4-positive IESCs (B), Periodic Acid Schiff-positive Paneth cells (D), Chromogranin A-positive enteroendocrine cells (F), and Periodic Acid Schiff-positive goblet cells (H) in the jejunum. Data are expressed as Mean ± SEM (n=5). Means with different letters indicate significantly different, $p < 0.05$.

Figure 28

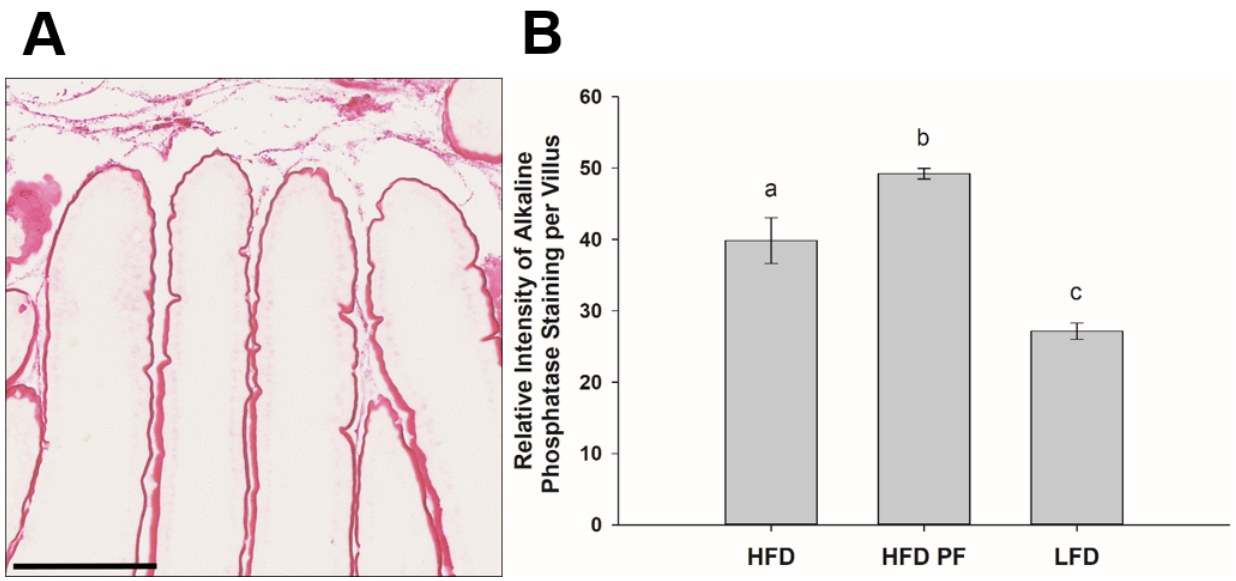

Figure 28. Representative images of the jejunal sections stained with alkaline phosphatase (enterocyte marker), Scale bar, 100 µm (A), and quantification of relative intensity of alkaline phosphatase staining (B). Data are expressed as Mean ± SEM (n=5). Means with different letters indicate significantly different, $p < 0.05$.

B.5 References

Beyaz S, Mana MD, Roper J, Kedrin D, Saadatpour A, Hong SJ, Bauer-Rowe KE, Xifaras ME, Akkad A, Arias E, Pinello L, Katz Y, Shinagare S, Abu-Remaileh M, Mihaylova MM, Lamming DW, Dogum R, Guo G, Bell GW, Selig M, Nielsen GP, Gupta N, Ferrone CR, Deshpande V, Yuan GC, Orkin SH, Sabatini DM & Yilmaz OH (2016). High-fat diet enhances stemness and tumorigenicity of intestinal progenitors. *Nature* **531,** 53-58.

Blackmore K, Zhou W & Dailey MJ (2017). LKB1-AMPK modulates nutrient-induced changes in the mode of division of intestinal epithelial crypt cells in mice. *Exp Biol Med (Maywood)* **242,** 1490-1498.

Mah AT, Van Landeghem L, Gavin HE, Magness ST & Lund PK (2014). Impact of diet-induced obesity on intestinal stem cells: hyperproliferation but impaired intrinsic function that requires insulin/IGF1. *Endocrinology* **155,** 3302-3314.

APPENDIX C: EXCERPT FROM: SEX DIFFERENCES INFLUENCE INTESTINAL EPITHELIAL STEM CELL PROLIFERATION INDEPENDENT OF OBESITY

(Full manuscript published in Physiological Reports; Citation: Zhou W, Davis EA, Li K, Nowak RA, & Dailey MJ. (2018). Sex differences influence intestinal epithelial stem cell proliferation independent of obesity. *Physiological reports*, 6(13), e13746.)

C1. Abstract

The intestinal epithelium is continuously regenerated by cell renewal of intestinal epithelial stem cells (IESCs) located in the intestinal crypts. Obesity affects this process and results in changes in the size and cellular make-up of the tissue, but it is unknown if there are sex differences in obesity-induced alterations in IESC differentiation. We fed male and female mice a 60% high-fat diet (HFD) or a 10% low-fat diet (LFD) for 3 months and investigated the differences in intestinal epithelial morphology *in vivo*.

C2. Materials and methods

Male (n=24) and female (n=20) Lgr5-EGFP-ires-CreERT2 mice at 10- to 12-weeks-old were used. These mice were bred at the Division of Animal Resources facility at the University of Illinois at Urbana-Champaign from original breeding pairs obtained from the Jackson Laboratory (Bar Harbor, ME). Mice were individually housed in modified shoebox cages with a raised woven wire platform and lined with brown kraft paper for collection and measurement of food spillage. Mice were acclimated to the housing for 1 week with *ad libitum* access to tap water and laboratory chow (Teklad 22/5, Teklad Diets, Madison, WI) on a 12:12 light:dark cycle in a climate-controlled room (22 ± 1 °C and 60% relative humidity). All procedures were approved by the Institutional Animal Care and Use Committee at the University of Illinois at Urbana-Champaign.

Following 1 week acclimation, mice were fed a HFD or LFD for 3 months. Male and female mice were divided into groups based on average body weight as follows: 1) 60% HFD fed (Research Diets

D12492; n=13 males; n=11 females), and 2) 10% LFD fed (Research Diets D12450J; n=11 males; n=9 females). After 3 months, mice were killed by decapitation under isoflurane anesthesia (Henry Schein Animal Health, Dublin, OH). The mice were killed in the middle of the light cycle following a 6 h food deprivation. A subset of mice (n = 6-10 per group) were used for histology. A power analysis (G*Power 3.1.9.2) based on previously published data investigating the lasting effect of diet-induced obesity on epithelial changes *in vivo* show that to achieve a power = 0.8 and a type I error of 0.05, an n=5 per group for analysis is needed (Beyaz *et al.*, 2016; Lee *et al.*, 2018). To harvest tissue for histology, we exposed the intestine and collected the mid-small intestinal tissue (i.e., jejunum) as previously described (Blackmore *et al.*, 2017). Briefly, to ensure that we were collecting similar segments of the intestine for analysis between animals, we measured from the pyloric sphincter and ileocecal valve to isolate the middle of jejunum and collected a 5 mm segment to be processed for histology. Each of the 5 mm intestinal segments were fixed in 10% neutral buffered formalin for 24 h at room temperature (RT) and then stored in 70% ethanol at RT prior to paraffin embedding.

Morphometric analyses were performed on formalin fixed, paraffin embedded, and hematoxylin stained cross sections. Briefly, intestinal sections (5 mm) were fixed in 10% neutral buffered formalin for 24 h at RT and then stored in 70% ethanol at RT until later processing. In order to paraffin embed the tissue, sections were dehydrated in a series of graded ethanols, cleared in xylene and infiltrated with paraffin in a Tissue Tek VIP 1000 tissue processor (Miles, Elkhart, IN). Paraffin blocks of tissue were cut on a microtome at 5 μm thickness and mounted onto charged glass microscope slides. Tissue sections were then deparaffinized in xylenes, hydrated in a series of graded ethanols, and rinsed in deionized water. Sections were stained in hematoxylin (Fisher HealthCare, Houston, TX) followed by dehydration in a series of graded ethanols and cleared in xylene. Slides were coverslipped with Permount mounting media (Fisher Scientific, Fair Lawn, NJ). Intestinal tissue sections were visualized using a NanoZoomer Digital Pathology (NDP) System (Hamamatsu, Hamamatsu City, Japan) using a 40× objective and NDP Scan software. Nine crypts or villi from the jejunal sections per mouse were chosen based on intact

morphology of the intestine (Argenzio *et al.*, 1990; Heise *et al.*, 1991; Liu *et al.*, 2015; Jinga *et al.*, 2017). Crypt depth and villus height were measured using NDP View 2 software.

Data are expressed as Mean ± SEM. Differences between groups at each time point were analyzed using a two-way ANOVA. Fisher's LSD post-hoc tests were used where appropriate. Assumptions of normality, homogeneity of variance, and independence were met.

C.3 Results

Intestinal crypt and villus morphometry

Crypt depth and villus height were greater in HFD fed mice than LFD group (Fig. 29A, B&C; $p<0.05$), but there was no sex effect or interaction between diet and sex (Fig. 29B, C).

C.4 Figure and caption

Figure 29

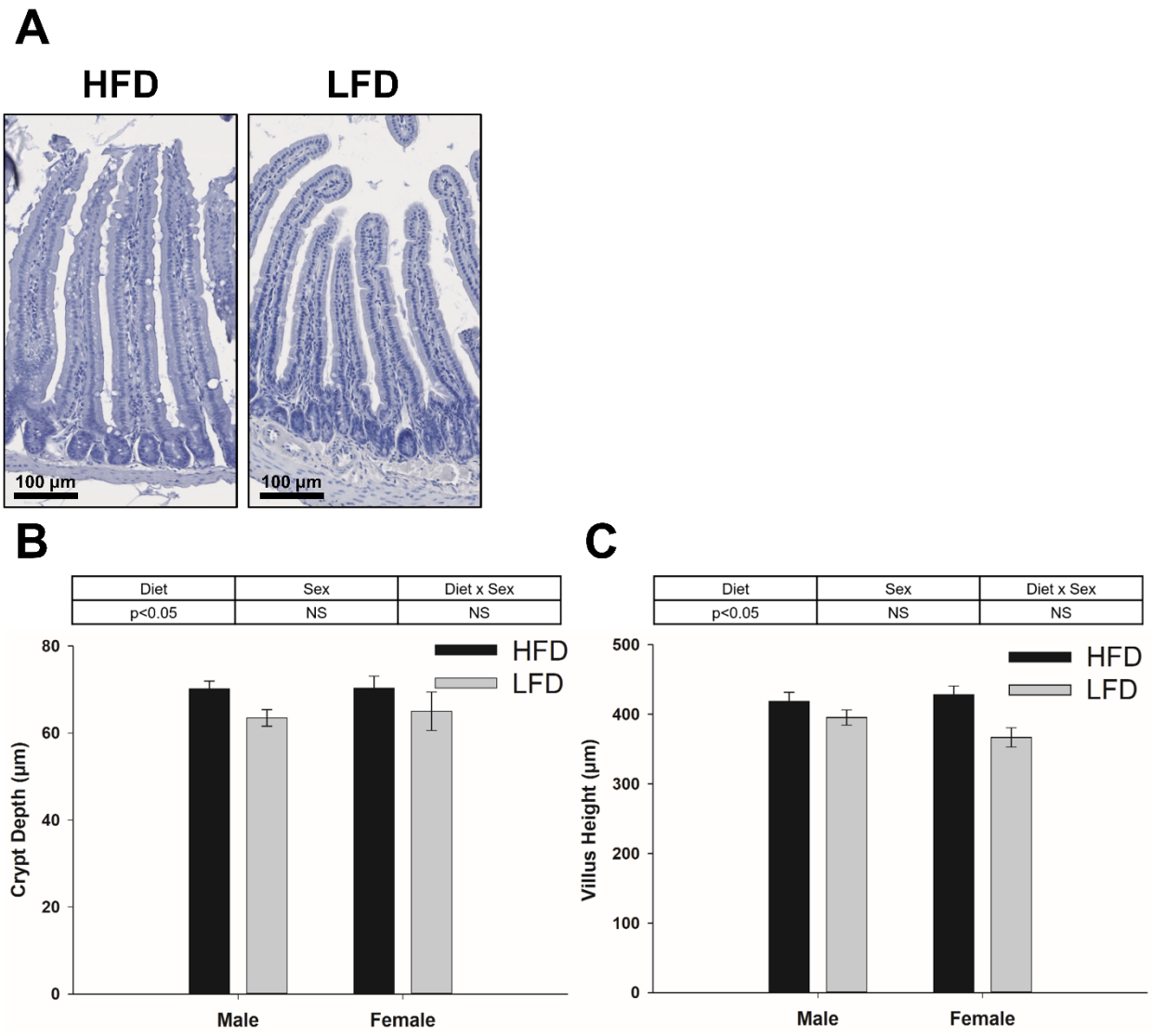

Figure 29. Representative image of hematoxylin stained crypt-villus morphology (A) and quantification of crypt depth (B) and villus height (C) in the jejunum collected from mice fed with HFD or LFD using diet and sex as two factors (two-way ANOVA). Data are expressed as Mean ± SEM (n=6-10). Scale bar, 100 µm.

C.5 References

Argenzio RA, Liacos JA, Levy ML, Meuten DJ, Lecce JG & Powell DW (1990). Villous atrophy, crypt hyperplasia, cellular infiltration, and impaired glucose-Na absorption in enteric cryptosporidiosis of pigs. *Gastroenterology* **98,** 1129-1140.

Beyaz S, Mana MD, Roper J, Kedrin D, Saadatpour A, Hong SJ, Bauer-Rowe KE, Xifaras ME, Akkad A, Arias E, Pinello L, Katz Y, Shinagare S, Abu-Remaileh M, Mihaylova MM, Lamming DW, Dogum R, Guo G, Bell GW, Selig M, Nielsen GP, Gupta N, Ferrone CR, Deshpande V, Yuan GC, Orkin SH, Sabatini DM & Yilmaz OH (2016). High-fat diet enhances stemness and tumorigenicity of intestinal progenitors. *Nature* **531,** 53-58.

Blackmore K, Zhou W & Dailey MJ (2017). LKB1-AMPK modulates nutrient-induced changes in the mode of division of intestinal epithelial crypt cells in mice. *Exp Biol Med (Maywood)* **242,** 1490-1498.

Heise C, Dandekar S, Kumar P, Duplantier R, Donovan RM & Halsted CH (1991). Human immunodeficiency virus infection of enterocytes and mononuclear cells in human jejunal mucosa. *Gastroenterology* **100,** 1521-1527.

Jinga M, Balaban DV, Peride I, Niculae A, DuTescu IM, Vasilescu F, Maki M & Popp AM (2017). Crypt hyperplastic enteropathy in distal duodenum in Helicobacter pylori infection - report of two cases without evidence of celiac disease. *Rom J Morphol Embryol* **58,** 685-688.

Lee JM, Govindarajah V, Goddard B, Hinge A, Muench DE, Filippi MD, Aronow B, Cancelas JA, Salomonis N, Grimes HL & Reynaud D (2018). Obesity alters the long-term fitness of the hematopoietic stem cell compartment through modulation of Gfi1 expression. *J Exp Med* **215,** 627-644.

Liu WF, Wen SH, Zhan JH, Li YS, Shen JT, Yang WJ, Zhou XW & Liu KX (2015). Treatment with Recombinant Trichinella spiralis Cathepsin B-like Protein Ameliorates Intestinal Ischemia/Reperfusion Injury in Mice by Promoting a Switch from M1 to M2 Macrophages. *J Immunol* **195,** 317-328.

Mah AT, Van Landeghem L, Gavin HE, Magness ST & Lund PK (2014). Impact of diet-induced obesity on intestinal stem cells: hyperproliferation but impaired intrinsic function that requires insulin/IGF1. *Endocrinology* **155,** 3302-3314.

APPENDIX D: EXCERPT FROM: CENTRAL SENSORY-MOTOR CROSSTALK IN THE NEURAL GUT-BRAIN AXIS

(Full manuscript submitted to Journal of Comparative Neurology. Citation: Parker CG, Davis EA, & Dailey MJ.)

D.1 Abstract

The neural gut-brain axis consists of viscerosensory and autonomic motor neurons innervating the gastrointestinal (GI) tract. Sensory neurons transmit nutrient-related and non-nutrient-related information to the brain, while motor neurons regulate GI motility and secretion. Previous research provides an incomplete picture of the brain nuclei that are directly connected with the neural gut-brain axis, and no studies have thoroughly assessed sensory-motor overlap in those nuclei. Our goal in this study was to comprehensively characterize the central sensory and motor circuitry associated with the neural gut-brain axis linked to a segment of the small intestine. We injected a retrograde (pseudorabies; PRV) and anterograde (herpes simplex virus 1; HSV) transsynaptic viral tracer into the duodenal wall of adult male rats. Immunohistochemical processing revealed single- and double-labeled cells that were quantified per nucleus. We found that across nearly all brain regions assessed, PRV+HSV immunoreactive neurons comprised the greatest percentage of labeled cells compared with single-labeled PRV or HSV neurons. These results indicate that even though sensory and motor information can be processed by separate neuronal populations, there is neuroanatomical evidence of direct sensory-motor feedback in the neural gut-brain axis throughout the entire caudal-rostral extent of the brain. This is the first study to exhaustively investigate the sensory-motor organization of the neural gut-brain axis, and is a step toward phenotyping the many central neuronal populations involved in GI control.

D.2 Materials and methods

Parker CG performed all handling of animals, injections and tissue processing. I participated in data and statistical analysis.

Data analysis

The entire caudal-rostral extent of the brain was analyzed for PRV and HSV immunoreactive neurons. For each section of each nuclei, the total number cells of each type (PRV+, HSV+, PRV+/HSV+) were counted. The average number of labeled cells of any type was calculated for each labeled nuclei across animals, and the percent of the total number of labeled cells in a given nuclei that were either PRV+, HSV+, or PRV+/HSV+ were calculated. One-way ANOVAs were performed to determine differences between groups. Assumptions of normality and homogeneity of variance were met. Data are presented as mean ± SEM.

D.3 Results

Across nearly all brain regions assessed, there was a majority of PRV+/HSV+ cells (Fig. 32b). Note that despite the consistent ratios of PRV+ or HSV+ to PRV+/HSV+ cells across nuclei, the actual number of neurons labeled in different brain nuclei varied greatly (Fig. 32a). Regions in the medulla and pons tended to have a greater percentage of HSV+ cells compared to PRV+ cells, while regions in the midbrain and forebrain tended to have a greater percentage of PRV+ cells compared to HSV+ cells (Fig. 32b; see also Figs. 33-35).

Hindbrain

At the level of the hindbrain, there was labeling in a number of nuclei throughout both the medulla and pons. In the medulla (Fig. 33), labeling was prominent in the nucleus of the solitary tract (NTS), dorsal motor nucleus of the vagus (DMV), and the rostral ventrolateral reticular formation (RVL). This finding is consistent with the established functions of these nuclei, as the NTS receives first-order visceral sensory input via the afferent vagus nerve, the DMV contains preganglionic parasympathetic neurons and receives sensory relays from the NTS along with visceral spinal input, and the RVL innervates preganglionic sympathetic neurons in the intermediolateral cell column (IML). Labeling was also seen throughout the caudal raphe nuclei (e.g. RMg, ROb, RPa), which also send direct projections to the preganglionic sympathetic neurons. Labeled neurons were found in a number of other reticular nuclei as well. These nuclei are a relay for ascending pathways to the cortex in the ascending reticular activating

system and descending pathways to the spinal cord via the reticulospinal tracts. Both of these pathways are involved in multiple ANS functions.

At the level of the pons, labeling was observed in a similarly wide variety of brain regions (Fig. 32). Labeling continued to be observed in pontine reticular nuclei, including the specific noradrenergic cell groups NA5 and NA7, and the locus coeruleus (LC). The Barrington's nucleus (Bar) and the parabrachial nucleus (PB) also showed labeling. Whereas the PB acts as an interface between medullary reflexes and forebrain action, the LC and Bar project to parasympathetic preganglionic neurons in the IML of the sacral spinal cord.

Midbrain

Midbrain labeling was observed in a more modest number of brain regions (Fig. 32). This again included a number of reticular nuclei, and also the dorsal raphe nucleus (DR) and the periaqueductal gray (PAG). The DR contains serotonergic neurons that innervate nuclei throughout the brain, including projections to the RVL in the hindbrain and many forebrain areas. The PAG, on the other hand, is known for its role in pain and receives peripheral information through the spinomesencephalic tract and sends descending information to multiple autonomic tracts. Labeling was also seen in the red nucleus (Red), which appeared to have a relatively higher percentage of single labeled PRV+ neurons than other labeled regions. Red is the origin of the rubrospinal tract and has multisynaptic projections to the cerebellum.

Forebrain

Labeling in the forebrain was observed in a number of hypothalamic nuclei and limbic nuclei. Labeled hypothalamic nuclei included the paraventricular nucleus (PVN), lateral hypothalamus (LH), and dorsal hypothalamic area (DH; Fig. 33). Limbic brain regions labeled were the central amygdala (CeA), bed nucleus of the stria terminalis (BNST), and insular cortex (Ins; Fig. 34).

D.4 Conclusions

Although a number of studies have examined the broader communication network of viscerosensory and autonomic motor connections within the gut-brain axis [for review, see (Loewy & Spyer, 1990)], this is the first study to demonstrate the extent of sensory-motor overlap within the same

neurons at each node of the network. Roughly half of the gut-brain axis neurons at each nuclei in the central autonomic network include overlap of the sensory inputs and motor outputs, creating direct feedback loops. These direct feedback loops throughout the brainstem and forebrain have previously been described when outlining the viscerosensory and autonomic connections in other tissues [i.e. white and brown adipose tissue; (Ryu & Bartness, 2014; Ryu et al., 2015]. In fact, the neural circuits connected to white adipose tissue demonstrate the same ~50% overlap of sensory-motor neurons at each node of the autonomic network when using the same tracing methods as the present study (Ryu & Bartness, 2014). This suggests that the overlap in sensory-motor neuronal communication is not organ specific, but is a general characteristic of how the central viscerosensory and autonomic networks are organized.

D.5 Figures and captions

Figure 30

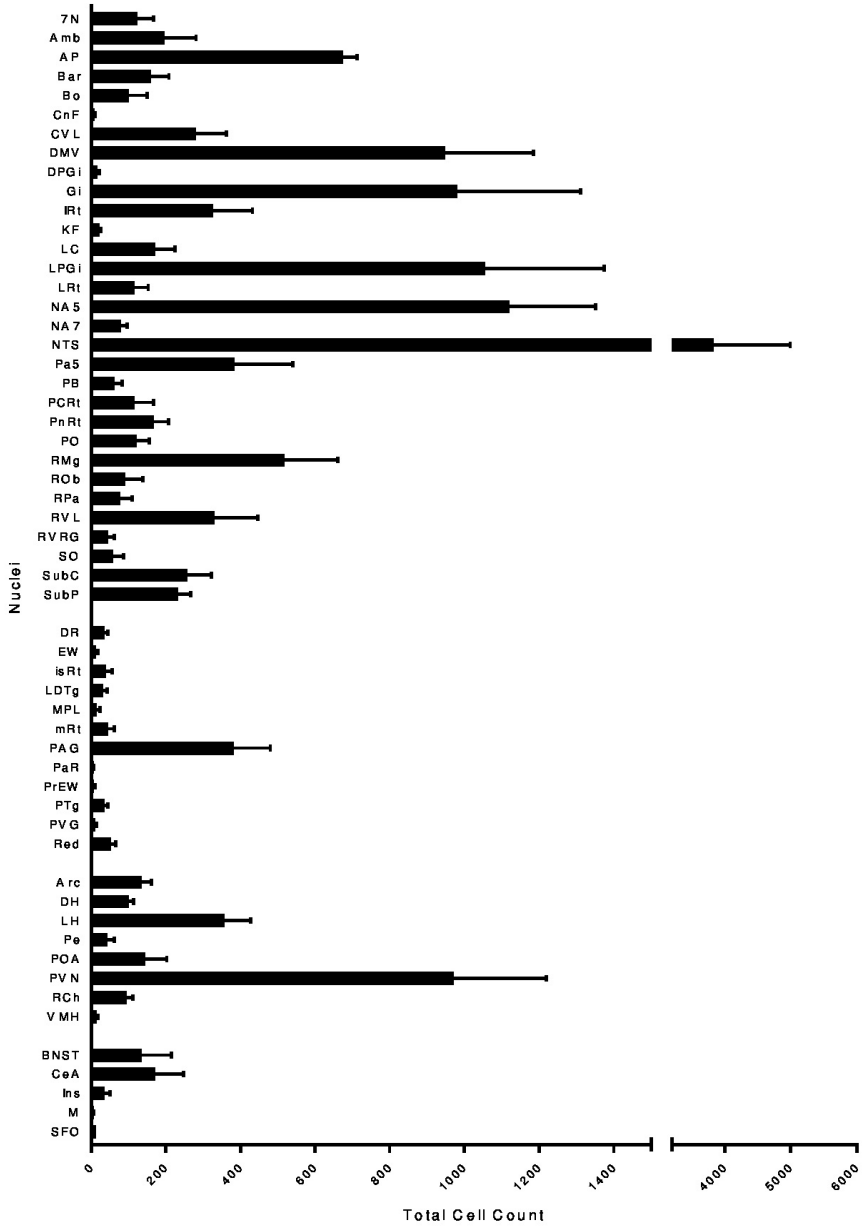

Figure 30. **Total number of labeled cells (PRV+, HSV+, and PRV+/HSV+) per nuclei.** Nuclei are arranged alphabetically in clusters corresponding to hindbrain, midbrain, hypothalamus, and other forebrain nuclei. Mean ± SEM.

Figure 31

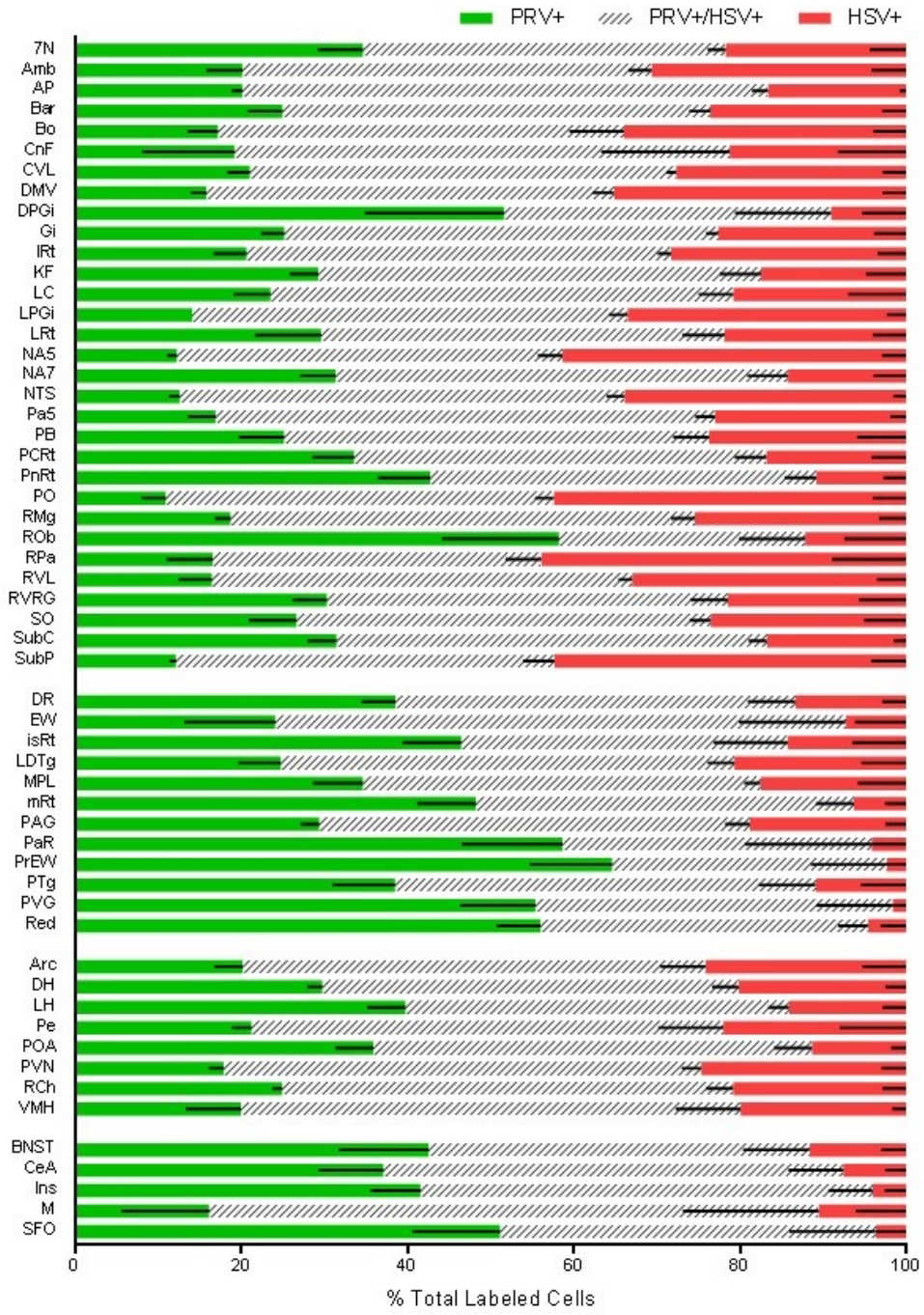

Figure 31. **Percent of the total number of labeled cells per nuclei that were PRV+, HSV+, or PRV+/HSV+.** Nuclei are arranged alphabetically in clusters corresponding to hindbrain, midbrain, hypothalamus, and other forebrain nuclei. Mean ± SEM.

Figure 32

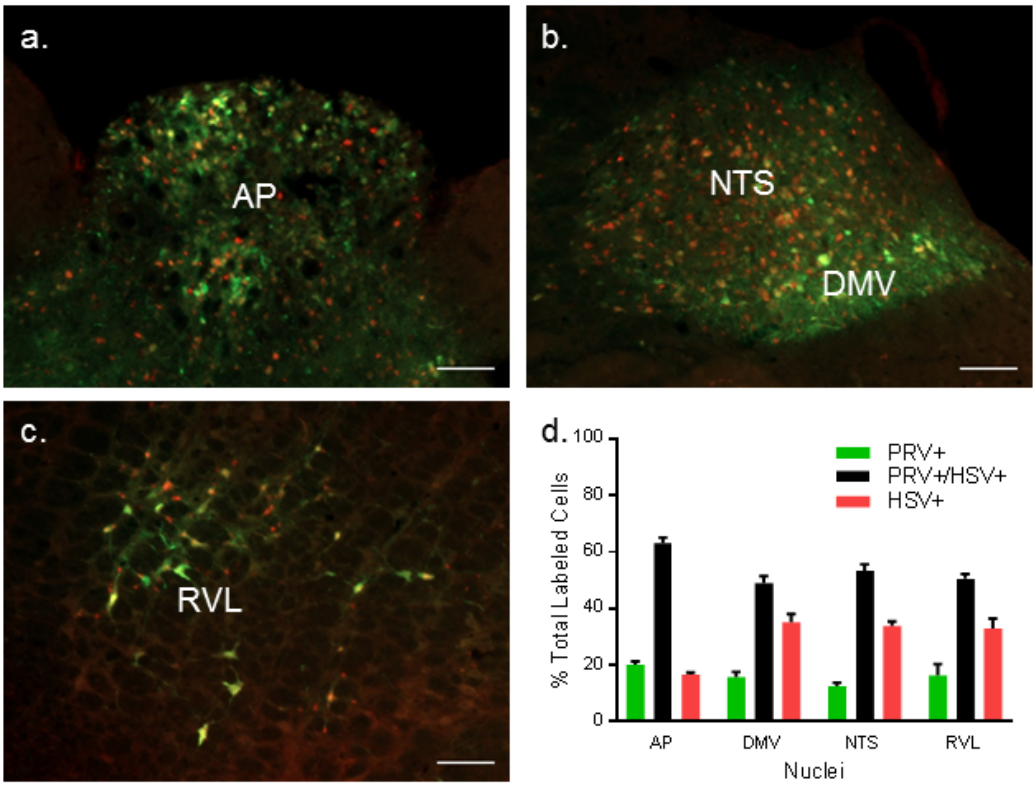

Figure 32. **Viral tracer labeling in select brainstem nuclei.** a) Representative image showing dense labeling in the AP. b) Representative image showing labeling in the NTS and DMV. c) Representative image showing labeling in the RVL. d) Relative proportions of PRV+, HSV+, and PRV+/HSV+ cells in select nuclei. Mean ± SEM. Scale bars indicate 100 um.

Figure 33

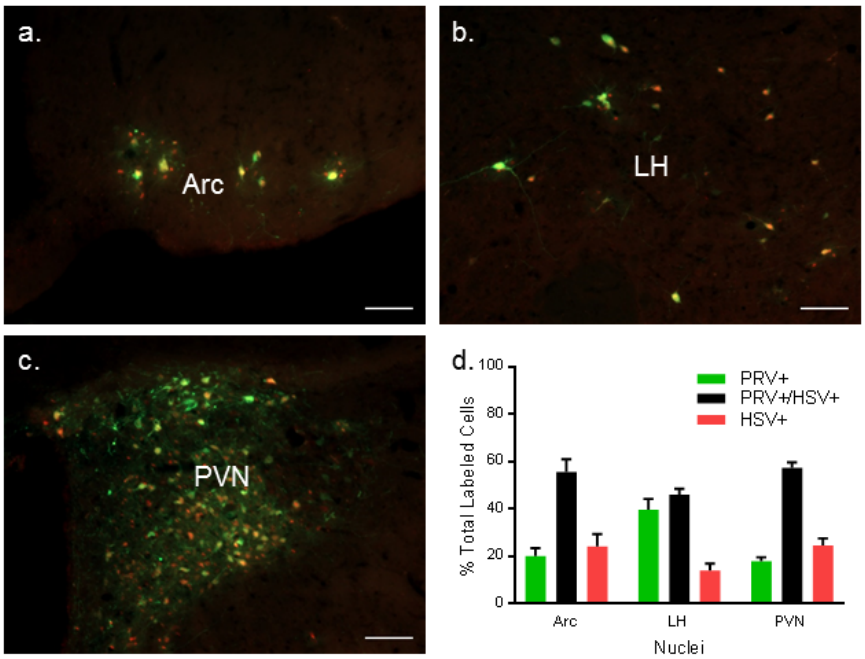

Figure 33. **Viral tracer labeling in select hypothalamic nuclei.** a) Representative image showing labeling in the Arc. b) Representative image showing labeling in the LH. c) Representative image showing dense labeling in the PVH. d) Relative proportions of PRV+, HSV+, and PRV+/HSV+ cells in select nuclei. Mean ± SEM. Scale bars indicate 100 um.

Figure 34

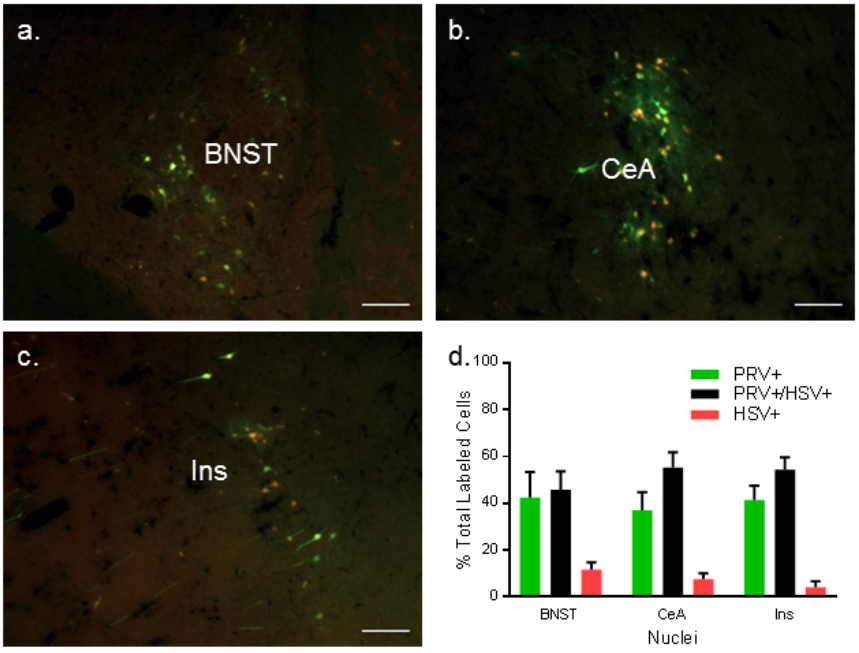

Figure 34. **Viral tracer labeling in select forebrain nuclei.** a) Representative image showing labeling in the BNST. b) Representative image showing labeling in the CeA. c) Representative image showing dense labeling in the Ins. d) Relative proportions of PRV+, HSV+, and PRV+/HSV+ cells in select nuclei. Mean ± SEM. Scale bars indicate 100 um.

D.6 References

Loewy, A. D., & Spyer, K. M. (1990). *Central regulation of autonomic functions*: Oxford University Press.

Ryu, V., & Bartness, T. J. (2014). Short and long sympathetic-sensory feedback loops in white fat. *American Journal of Physiology-Regulatory, Integrative and Comparative Physiology, 306*(12), R886-R900.

Ryu, V., Garretson, J. T., Liu, Y., Vaughan, C. H., & Bartness, T. J. (2015). Brown adipose tissue has sympathetic-sensory feedback circuits. *J Neurosci, 35*(5), 2181-2190. doi:10.1523/jneurosci.3306-14.2015